

2019

# Advancement of the Hybrid Ion Exchange Nitrogen and Phosphate (HIX-NP) Recovery from Waste Water and a New Approach to Brine-Free Nitrate Removal

Chelsey Shepsko  
Lehigh University

Follow this and additional works at: <https://preserve.lehigh.edu/etd>

 Part of the [Environmental Engineering Commons](#)

---

## Recommended Citation

Shepsko, Chelsey, "Advancement of the Hybrid Ion Exchange Nitrogen and Phosphate (HIX-NP) Recovery from Waste Water and a New Approach to Brine-Free Nitrate Removal" (2019). *Theses and Dissertations*. 5572.  
<https://preserve.lehigh.edu/etd/5572>

This Dissertation is brought to you for free and open access by Lehigh Preserve. It has been accepted for inclusion in Theses and Dissertations by an authorized administrator of Lehigh Preserve. For more information, please contact [preserve@lehigh.edu](mailto:preserve@lehigh.edu).

**Advancement of the Hybrid Ion Exchange Nitrogen and Phosphate (HIX-NP)  
Recovery from Waste Water and a New Approach to Brine-Free Nitrate Removal**

by

Chelsey Shepsko

Presented to the Graduate and Research Committee  
of Lehigh University  
in Candidacy for the Degree of  
Doctor of Philosophy

in

Environmental Engineering

Lehigh University

May 2019

**Copyright by Chelsey Shepsko**

**2019**

## DISSERTATION APPROVAL BY THE DOCTORAL COMMITTEE

Approved and recommended for acceptance as a dissertation in partial fulfillment of the requirements for the degree of Doctor of Philosophy in Environmental Engineering on

\_\_\_\_\_  
DATE

\_\_\_\_\_  
**John T. Fox, Ph.D.**

*Committee Chairperson*

Department of Civil and  
Environmental Engineering  
Lehigh University

\_\_\_\_\_  
**Arup K. SenGupta, Ph.D.**

*Dissertation Advisor*

Department of Civil and  
Environmental Engineering  
Lehigh University

\_\_\_\_\_  
**Derick G. Brown, Ph.D.**

*Co-Dissertation Advisor*

Department of Civil and  
Environmental Engineering  
Lehigh University

\_\_\_\_\_  
**Kristen Jellison, Ph.D.**

*Committee Member*

Department of Civil and  
Environmental Engineering  
Lehigh University

\_\_\_\_\_  
**Sabrina S. Jedlicka, Ph.D.**

*External Committee Member*

Department of Materials Science  
& Engineering  
Lehigh University

## Acknowledgements

As a student at Lehigh University, my journey began in the semester of Fall 2010 as an undergraduate student and continued through to the semester of Spring 2019 as a Ph.D graduate. During those nine years, I have had many people inspire and support me through this long journey. I would like to start by thanking my family (my parents Sue and Billy, and my sister Shannon) first and foremost for being there for me every single day of these nine years (and the 18 years before that also). There were many weekday phone calls and weekend visits that were necessary to recharge, push through the hard work, and remember that there is so much more to life than stress and graduate school. This accomplishment is a testament to your unconditional love, guidance, and teachings. Without you, this accomplishment as well as the successful person I have become today would not be possible.

Another important thank you goes to Dr. Arup SenGupta, my dissertation advisor. You have challenged me to think beyond simple answers since junior year of my undergraduate career, encouraged me to pursue this passion for environmental engineering to the fullest, and show that academics need to be balanced by excitement for other endeavors in life. I am a better professional, academic, and person because of you. I would also like to thank my Ph.D Committee: Dr. Brown (who encouraged me to pursue research as an undergraduate student), Dr. Fox (the Chair of my Committee), Dr. Jellison (a role model for young women in the STEM field), and Dr. Jedlicka (an external Committee Member who has provided and challenged me with an outside perspective of my work).

An enormous appreciation goes out to the Office of Residence Life at Lehigh University who have funded my tuition for the past three years. Not only did they provide

the necessity for me to attend and finish my degree at Lehigh, they also gave me opportunities for personal growth and learning in all topics that range from creative thinking to equity and diversity. Every professional staff member has individually supported my priority of completing this degree with deep understanding during my Graduate Assistantship since 2016 until now.

Finally, I want to thank the Environmental Engineering Department's graduate students past and present (especially from Dr. SenGupta's research group), who have been able to support each other in the classroom, laboratory research, and in our personal lives. This journey is long on paper but felt like a brief moment in time because of everyone listed above, so thank you from the bottom of my heart.

# Table of Contents

Abstract.....	1
<b>CHAPTER 1: Introduction.....</b>	<b>4</b>
<b>1.1 Water reuse and recovery .....</b>	<b>4</b>
<i>1.1.1 Water reuse in practice .....</i>	<i>6</i>
<i>1.1.2 N and P concentrates from water reuse technology .....</i>	<i>7</i>
<i>1.1.3 Co-contaminants to consider prior to RO.....</i>	<i>9</i>
<b>1.2 Groundwater supply contamination .....</b>	<b>11</b>
<i>1.2.1 A focus on nitrate-contaminated groundwater .....</i>	<i>11</i>
<i>1.2.2 Selenium contamination of water resources .....</i>	<i>14</i>
<b>1.3 A review of current water treatment technologies.....</b>	<b>15</b>
<i>1.3.1 Water reuse technologies: reverse osmosis (RO) and ion exchange (IX).....</i>	<i>15</i>
<i>1.3.2 Nutrient removal and recovery technologies .....</i>	<i>18</i>
<i>1.3.3 Emerging contaminant technology .....</i>	<i>18</i>
<i>1.3.4 Nitrate removal from drinking water .....</i>	<i>19</i>
<i>1.3.5 Selenium characteristics that provide parallels to nitrate removal.....</i>	<i>20</i>
<b>1.4 Objectives .....</b>	<b>22</b>
<b>CHAPTER 2: Scientific Concepts of HIX-NP, BIO-NIX, and BIO-RNIX .....</b>	<b>24</b>
<b>2.1 HIX-NP as a pretreatment to RO.....</b>	<b>24</b>
<i>2.1.1 Nitrate-selective HAIX-NanoZr .....</i>	<i>24</i>
<i>2.1.2 pH dependency of HAIX-NanoZr for selective P removal .....</i>	<i>26</i>
<i>2.1.3 WAC for hardness removal and partial desalination .....</i>	<i>30</i>
<i>2.1.4 PPCPs (a co-contaminant) simultaneous removal in HAIX-NanoZr .....</i>	<i>33</i>
<i>2.1.5 Summary of the HIX-NP process .....</i>	<i>35</i>
<b>2.2 BIO-NIX for nitrate removal from groundwater .....</b>	<b>37</b>
<i>2.2.1 Fixed-film biological denitrification.....</i>	<i>38</i>
<i>2.2.2 Citric acid slow release for carbon dosing .....</i>	<i>40</i>
<i>2.2.3 Ion exchange polishing .....</i>	<i>43</i>
<i>2.2.4 Modification of BIO-NIX for ion exchange brine regeneration.....</i>	<i>45</i>
<b>CHAPTER 3: Experimental Materials and Methods.....</b>	<b>48</b>
<b>3.1 Sources of influent water for column runs .....</b>	<b>48</b>
<i>3.1.1 Bethlehem secondary wastewater .....</i>	<i>48</i>

3.1.2 Manheim nitrate-contaminated groundwater .....	49
<b>3.2 Experimental set-up</b> .....	50
3.2.1 HIX-NP column runs.....	50
3.2.2 BIO-NIX groundwater system.....	52
3.2.3 BIO-RNIX brine regeneration runs.....	54
<b>3.3 Materials</b> .....	56
3.3.1 HAIX-NanoZr synthesis .....	56
3.3.2 SS-WAC.....	57
3.3.3 Citric acid-loaded resins.....	57
3.3.4 Metamateria for fixed-film media .....	58
<b>3.4 Analytical methods</b> .....	59
3.4.1 Influent and effluent composition analysis.....	59
3.4.2 Zeta potential .....	59
3.4.3 Scanning electron microscopy .....	60
<b>CHAPTER 4: Results and Discussion of HIX-NP and its Effectiveness as a Pretreatment to RO</b> .....	61
<b>4.1 Validation of pH dependency for P removal by HAIX-NanoZr</b> .....	61
<b>4.2 Nutrient removal and recovery by HAIX-NanoZr</b> .....	63
4.2.1 Multiple runs of HAIX-NanoZr.....	63
4.2.2 Regeneration and recovery of N and P .....	65
4.2.3 Precipitation of N-P-K regenerant .....	67
<b>4.3 SS-WAC performance</b> .....	70
4.3.1 Hardness removal by SS-WAC.....	70
4.3.2 CO <sub>2</sub> regeneration of SS-WAC .....	71
<b>4.4 Potential for co-contaminant removal</b> .....	75
<b>CHAPTER 5 BIO-NIX and its Effectiveness for Groundwater Remediation</b> .....	77
<b>5.1 Validation of the complete BIO-NIX system</b> .....	77
<b>5.2 Resiliency tests</b> .....	82
5.2.1 Carbon source interruption .....	83
5.2.2 Influent nitrate surge.....	85
5.2.3 Flow increase.....	87
5.2.4 Summary of resiliency.....	89
<b>5.3 Selenate removal using BIO-NIX</b> .....	91



<b>5.4 Citric acid-loaded anion exchanger design</b> .....	94
<b>5.5 Regeneration of the nitrate-selective ion exchange column</b> .....	96
<b>5.6 Cost comparison to Manheim’s water treatment facility</b> .....	97
<b>5.7 BIO-RNIX, modification for ion exchange regeneration from wastewater removal</b> ... 98	
5.7.1 Nitrate analysis of the regeneration process .....	98
5.7.2 BIO-RNIX comparison to other brine reuse processes .....	101
5.7.3 Application for selenate regeneration.....	102
<b>CHAPTER 6: Conclusions</b> .....	105
<b>6.1 Process summary conclusions</b> .....	105
<b>6.2 Future work and potential for scale-up</b> .....	108
6.2.1 HIX-NP scale-up.....	108
6.2.2 BIO-NIX future work.....	109
<b>References</b> .....	111
<b>Vita</b> .....	127

## List of Tables

<b>Table 2-1.</b> Nitrate Selectivity of a SBA as a Function of Alkyl Groups within the Matrix.....	<b>24</b>
<b>Table 2-2.</b> Examples of HIOCs and their Structures.....	<b>34</b>
<b>Table 3-1.</b> Purolite A520E Characteristics.....	<b>56</b>
<b>Table 3-2.</b> SS-WAC Resin Characteristics.....	<b>57</b>
<b>Table 3-3.</b> Purolite A400 Characteristics.....	<b>58</b>
<b>Table 3-4.</b> Metamateria Properties.....	<b>58</b>
<b>Table 6-1.</b> Phosphorus Data from the George Barley Water Prize.....	<b>108</b>

## List of Figures

<b>Figure 1-1.</b> A map of the world depicting locations that are nearing and facing water scarcity in shades of red.....	4
<b>Figure 1-2.</b> A map of the 10 largest wastewater treatment plants in the world and their respective influent flow rates.....	5
<b>Figure 1-3.</b> A simplified RO schematic for desalination (left) and a close-up of what occurs at the membrane boundary (right).....	7
<b>Figure 1-4.</b> Projected quantities of P rock reserves over time based on increased P recovery and sustainable P utilization efforts.....	9
<b>Figure 1-5.</b> The brine to influent concentration ratio ( $C_B/C_F$ ) as a function of the recovery rate (Y) in a RO system.....	10
<b>Figure 1-6.</b> Nitrate contamination of groundwater sources located in the United States (left) and three countries in Africa (right).....	12
<b>Figure 1-7.</b> Flue gas desulfurization process.....	14
<b>Figure 1-8.</b> Singapore’s NEWater treatment process for water reclamation.....	16
<b>Figure 1-9.</b> Components of a cation exchange resin.....	17
<b>Figure 1-10.</b> Selenium pE-pH diagram at 25°C and 1 bar.....	21
<b>Figure 2-1.</b> LAB interactions between phosphate ( $H_2PO_4^-$ ) and $ZrO_2$ .....	26
<b>Figure 2-2.</b> The distribution of hydrated zirconium oxide surface functional groups (top) and phosphate species (bottom) illustrating the pH range of sorption and desorption of phosphate.....	27
<b>Figure 2-3.</b> Sorption and desorption processes of a HAIX-NanoZr resin as a function of pH.....	28
<b>Figure 2-4.</b> Phosphate capacity curve as a function of varying influent concentrations modeled as a Langmuir isotherm.....	30
<b>Figure 2-5.</b> A demonstration of the WAC resin bed’s ability to remove hardness in exchange for hydrogen ions.....	31
<b>Figure 2-6.</b> Representations of the SS-WAC resin with the carboxylic functional groups and by SEM-EDX.....	32
<b>Figure 2-7.</b> A schematic depicting the enhancement of phosphate and nitrate removal capacities by the two-bed HIX-NP system with concurrent reduction in hardness aided by $CO_2$ .....	36
<b>Figure 2-8.</b> Schematic of the BIO-NIX system for removal of nitrate.....	37
<b>Figure 2-9.</b> Steps for self-regeneration of the nitrate-selective ion exchange resin.....	44

<b>Figure 2-10.</b> BIO-RNIX regeneration system schematic.....	<b>46</b>
<b>Figure 3-1.</b> Satellite view of the Bethlehem WWTP in Bethlehem, PA (40°37'03.5"N 75°20'00.2"W).....	<b>48</b>
<b>Figure 3-2.</b> A satellite view of the water treatment facility's location in Manheim, Pennsylvania (306 Doe Run Road) surrounded by farmland.....	<b>49</b>
<b>Figure 3-3.</b> Two column bench-top stainless-steel setup for the HIX-NP process with a CO <sub>2</sub> regeneration system.....	<b>51</b>
<b>Figure 3-4.</b> A diffuser (left) placed within the regeneration tank to sparge carbon dioxide efficiently in water as the regenerant solution.....	<b>52</b>
<b>Figure 3-5.</b> BIO-NIX system set-up.....	<b>53</b>
<b>Figure 3-6.</b> BIO-RNIX system set-up.....	<b>55</b>
<b>Figure 4-1.</b> (A) Phosphorus removal capacity of HAIX-NanoZr and zeta potential of the hydrated zirconium oxide particles as a function of pH; (B) Comparison of phosphate effluent histories and (C) pH effluent values from i) HAIX-NanoZr column alone and ii) SS-WAC column followed by HAIX-NanoZr fed with Bethlehem secondary wastewater. (Influent composition: 5 mg/L P, 65 mg/L NO <sub>3</sub> <sup>-</sup> , 32 mg/L SO <sub>4</sub> <sup>2-</sup> , 83 mg/L Cl <sup>-</sup> , 48 mg/L Ca <sup>2+</sup> , 487 mg/L TDS, pH 7.1.).....	<b>61</b>
<b>Figure 4-2.</b> Three successive effluent history plots of (A) phosphorus and (B) nitrate- with one sulfate effluent history curve for comparison- using secondary wastewater from the Bethlehem Wastewater Treatment Plant in Bethlehem, PA. (Influent composition: 2.4 mg/L P, 100 mg/L NO <sub>3</sub> <sup>-</sup> , 32 mg/L SO <sub>4</sub> <sup>2-</sup> , 69 mg/L Cl <sup>-</sup> , 50 mg/L Ca <sup>2+</sup> , 466 mg/L TDS, pH 7.0.).....	<b>63</b>
<b>Figure 4-3.</b> A comparison of nitrate and phosphorus in the influent (left) to their effluent concentrations at 200 bed volumes (right).....	<b>64</b>
<b>Figure 4-4.</b> Three successive regeneration elution curves of (A) phosphorus and (B) nitrate using KOH as the regenerant solution. (C) Recovery factors of N, P and Cl in the spent regenerant.....	<b>65</b>
<b>Figure 4-5.</b> SEM-EDX maps of Zr from a parent HAIX-NanoZr resin bead and of P and Cl from an exhausted bead.....	<b>67</b>
<b>Figure 4-6.</b> (A) Imhoff cone of precipitated N, P, K fertilizer by MgCl <sub>2</sub> addition. (B) SEM-EDX analysis of the solid formed in the Imhoff cone (SEM conditions: FOV at 153 μm, 15kV Point, BSD Full detector).....	<b>68</b>
<b>Figure 4-7.</b> (A) SEM-EDX mapping of the solid formed in the Imhoff cone at (A) pH 9 and (B) pH 6.5. (SEM conditions: FOV at 153 μm, 15kV Point, BSD Full detector).....	<b>69</b>
<b>Figure 4-8.</b> Three successive effluent history plots of (A) calcium and (B) pH using secondary wastewater from the Bethlehem Wastewater Treatment Plant in Bethlehem,	

PA. (C) Calcium in the influent (left) compared to the effluent concentrations at 200 bed volumes (right). (Influent composition: 2.4 mg/L P, 100 mg/L NO <sub>3</sub> <sup>-</sup> , 32 mg/L SO <sub>4</sub> <sup>2-</sup> , 69 mg/L Cl <sup>-</sup> , 50 mg/L Ca <sup>2+</sup> , 466 mg/L TDS, pH 7.0.).....	70
<b>Figure 4-9.</b> (A) Calcium recovery (R <sub>Ca</sub> ) during regeneration with CO <sub>2</sub> as the sole regenerant at 3.4 atm, 6.8 atm, and 10.2 atm; (B) Delayed precipitation of CaCO <sub>3</sub> in the SS-WAC spent regenerant over time.....	71
<b>Figure 4-10.</b> SEM-EDX analysis of Ca from an exhausted SS-WAC resin bead (left) and from a regenerated bead (right).....	72
<b>Figure 4-11.</b> Log-log plot of eluted calcium concentrations versus partial pressures of CO <sub>2</sub> from the experimental data.....	75
<b>Figure 4-12.</b> (A) Ibuprofen effluent history plots using secondary wastewater from the Bethlehem Wastewater Treatment Plant in Bethlehem, PA. (B) Regeneration effluent curves of ibuprofen using 4% NaOH versus 4% NaCl. (Influent composition: 2.4 mg/L P, 100 mg/L NO <sub>3</sub> <sup>-</sup> , 32 mg/L SO <sub>4</sub> <sup>2-</sup> , 69 mg/L Cl <sup>-</sup> , 50 mg/L Ca <sup>2+</sup> , 466 mg/L TDS, pH 7.0.).....	76
<b>Figure 5-1.</b> Nitrate effluent results of the BIO-NIX system through 500 BV (A) after the Metamateria column and (B) after the entire BIO-NIX system. (C) Nitrate effluent results from a nitrate-selective ion exchange column only run.....	77
<b>Figure 5-2.</b> Ion chromatograph of the influent samples (left) and effluent samples (right) after 200 BV of service during the BIO-NIX run.....	79
<b>Figure 5-3.</b> (A) pH values exiting the Metamateria column during the run shown in Figures 5-1A,B. (B) pE-pH diagram of nitrogen species in aqueous solution overlaid with ORP values during the BIO-NIX run and a close-up of the pe points plotted.....	80
<b>Figure 5-4.</b> Agar-loaded petri dishes to show bacterial presence on the Metamateria (left) and ion exchangers (right) after 24 hours.....	81
<b>Figure 5-5.</b> Nitrate effluent history following a shut-down of the citric acid bypass line at 500 BV (designated by circles) (A) after the Metamateria column and (B) after the ion exchange column.....	83
<b>Figure 5-6.</b> Nitrate effluent histories (A) between and (B) after the two columns from the time citric acid was interrupted (500BV) and after citric acid was reintroduced (1000 BV).....	84
<b>Figure 5-7.</b> Nitrate effluent histories (A) between and (B) after the two columns during the transition to a sudden spike of influent nitrate to 120 mg/L NO <sub>3</sub> <sup>-</sup> . (C) Image of the Metamateria column that highlights bubbles trapped within the column during the nitrate spike.....	86

- Figure 5-8.** Nitrate effluent history as a result of a decreased detention time from 15 minutes to 10 minutes from 150 BV to 350 BV (A) after the Metamateria column and (B) after the ion exchange column.....87
- Figure 5-9.** A summary of the nitrate effluent histories (A) leaving the Metamateria column (red line) and (B) leaving the ion exchange column (black line) as a result of various interruptions of the BIO-NIX system. (C) A comparison of both effluent histories overlapped.....89-90
- Figure 5-10.** Nitrate and selenate effluent results of the BIO-NIX system through 500 BV (A) after the Metamateria column and before the ion exchange column and (B) after the entire BIO-NIX system. (C) pE-pH diagram of selenium species in aqueous solution overlaid with ORP values during the BIO-NIX run with a close-up of the plotted pe-pH points on the right.....92
- Figure 5-11.** (A) Effluent history of citric acid (diluted to 20%), nitrate, and sulfate leaving the citric acid-loaded column. (B) Comparison of citrate effluent histories between the Metamateria column and the BIO-NIX effluent.....94
- Figure 5-12.** (A) Three successive effluent history plots of nitrate using secondary wastewater from the Bethlehem Wastewater Treatment Plant in Bethlehem, PA. (B) Three successive regeneration effluent history plots of nitrate using the BIO-RNIX process. (C) pE-pH diagram of aqueous nitrogen species with overlapping plotted pE points during each regeneration run and a close-up of the plotted pe-pH points on the right. (Influent composition: 1 mg/L Se as  $\text{SeO}_4^{2-}$ , 2.4 mg/L P, 100 mg/L  $\text{NO}_3^-$ , 32 mg/L  $\text{SO}_4^{2-}$ , 69 mg/L  $\text{Cl}^-$ , 50 mg/L  $\text{Ca}^{2+}$ , 466 mg/L TDS, pH 7.0.).....99
- Figure 5-13.** (A) Schematic of the SBR regeneration system by Lehman et al., 2008. (B) Regeneration effluent profiles of nitrate (among perchlorate as well) in the SBR following the draw stage.....101
- Figure 5-14.** (A) Three successive effluent history plots of selenate using secondary wastewater from the Bethlehem Wastewater Treatment Plant in Bethlehem, PA. (B) Three successive regeneration effluent history plots of selenate using the BIO-RNIX process. (C) pE-pH diagram of aqueous selenium species with overlapping plotted pE points during each regeneration run and a close-up of the plotted pe-pH points on the right. (D) Visual representation of the bacteria present on the Metamateria pieces after three runs. (Influent composition: 1 mg/L Se as  $\text{SeO}_4^{2-}$ , 2.4 mg/L P, 100 mg/L  $\text{NO}_3^-$ , 32 mg/L  $\text{SO}_4^{2-}$ , 69 mg/L  $\text{Cl}^-$ , 50 mg/L  $\text{Ca}^{2+}$ , 466 mg/L TDS, pH 7.0.).....103
- Figure 6-1.** A collection of photos from the BIO-NIX pilot tests conducted in China...110

## Abstract

Due to rapid declining freshwater reserves worldwide, societies are reexamining approaches to maintain potable and industrial water supplies to meet the current and future demands. By utilizing wastewater, an impaired water resource that is large, resilient, and near consumption centers, societies can reuse and recover potable water through treatment via reverse osmosis (RO). However, RO generates a reject brine that must be disposed, and for societies that live inland and far away from the ocean (a dumping ground for such reject streams), disposal poses eutrophication of surface and groundwater sources as high concentrations of N and P compounds contaminate the environment with harmful algal blooms.

In this study, we present a Hybrid Ion Exchange nitrogen and phosphate (HIX-NP) recovery process that also reduces hardness at the same time. Thus, the treated wastewater does not warrant any pretreatment or dosing of anti-scaling agents for RO to avoid membrane fouling. One shallow shell weak-acid cation exchanger (SS-WAC) and a hybrid anion exchanger (HAIX-NanoZr) with specific affinity for nitrate and phosphate form the heart of the HIX-NP process. Studies were conducted using secondary wastewater from the Bethlehem, PA plant and CO<sub>2</sub> was the only regenerant used in the process. The HIX-NP process accomplished near complete removal of phosphate, nitrate and hardness compared to influent values for multiple cycles with more than 90% of phosphate and nitrate recovered without the presence of competing anions. SS-WAC was efficiently regenerated with CO<sub>2</sub> at 10.2 atm, and calcium desorbed was stoichiometrically sequestered by CO<sub>2</sub> as CaCO<sub>3</sub>(s).

Nitrate is also considered a contaminant for drinking water when concentrations exceed the maximum contaminant level (MCL) of 10 mg/L NO<sub>3</sub>-N. Nitrate contamination of groundwater occurs frequently due to overuse of fertilizer application and excess manure, in which ammonium species are oxidized to nitrate in the soil subsurface and mobile nitrate transports to groundwater sources. Ion exchange provides kinetically fast removal of nitrates but employs a 10-15% brine solution for regeneration that needs to be disposed. Biological denitrification is a more sustainable process that removes nitrate to nitrogen gas but is kinetically slow.

In this second study, we present a BIO-NIX system that combines the sustainability of biological denitrification with the fast kinetics of ion exchange. BIO-NIX consists of three columns: (i) a bypass line to a citric-acid loaded column that slow releases citric acid as the carbon source; (ii) a fixed-film media column that removes nitrate through biological denitrification; (iii) a nitrate-selective anion exchanger that polishes any nitrate removal required following the fixed-film column. Studies were conducted using synthetic wastewater designed from a real nitrate-contaminated groundwater source in Manheim, PA and tested for its resiliency against varying parameters. The BIO-NIX process provided high nitrate removal with effluent nitrate remaining below the MCL for over 3000 BV, where the fixed-film column provided majority of the nitrate removal and the ion exchange column provided polishing and emergency removal during times of interruption. The ion exchange column did not need to be regenerated throughout the entire run and no chemicals were used in the process. This process can be applicable to selenate removal.

Finally, the BIO-NIX system was modified to address the issue of 10-15% brine used to regenerate a nitrate-loaded ion exchanger, known as the BIO-RNIX system. BIO-



RNIX utilizes a recirculation process of  $MgCl_2$  to kick nitrate off the anion exchanger and the high concentration nitrate stream is carried to the fixed-film column to biologically reduce nitrate to nitrogen gas. Studies were completed following exhaustion of a nitrate-selective anion exchanger with secondary wastewater from the Bethlehem plant. Nitrate was reduced  $>75\%$  in the brine within 8 hours of recirculation for multiple runs, and co-contaminant selenate showed similar results.

## CHAPTER 1: Introduction

### 1.1 Water reuse and recovery

As population, urbanization, and environmental pollution increases with a gradual decrease in the fresh water supply, societies worldwide are reevaluating strategies to sustain potable and industrial water supplies to meet the current and future demands. Climate change effects have aggravated the crisis further by adversely impacting the reliability of existing fresh water resources.<sup>1</sup> A study completed in 2007 shows half of the world approaching and already facing water scarcity, with that number only expected to rise, as shown below in **Figure 1-1**.

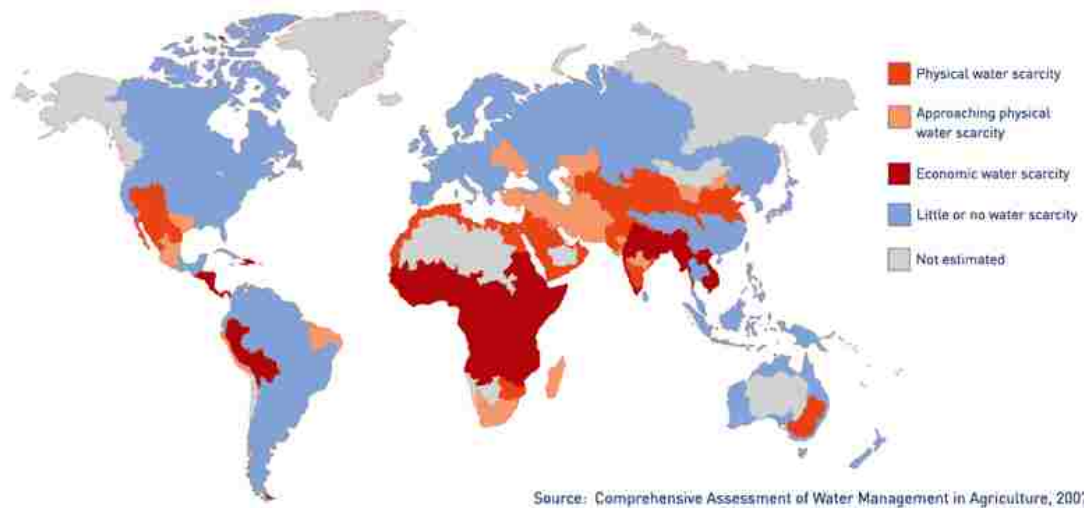


**Figure 1-1.** A map of the world depicting locations that are nearing and facing water scarcity in shades of red.<sup>2</sup>

Due to these increasing conditions, large metropolitan areas are looking towards impaired water resources to treat and reuse. Impaired water resources that are available include ocean and brackish water, which are large volume water supplies with total dissolved solids (TDS) concentrations ranging from 3,000 (brackish) to 35,000 (ocean) mg/L TDS. Treating

high TDS waters down to the consumable water limit of 500 mg/L TDS is expensive and difficult.<sup>3</sup> A more suitable, impaired resource is treated municipal wastewater due to its overall resiliency in that it is a large resource, near to the consumption centers, and relatively insulated from climate change effects. **Figure 1-2** shows the largest wastewater treatment facilities in the world and their daily total flow rates.

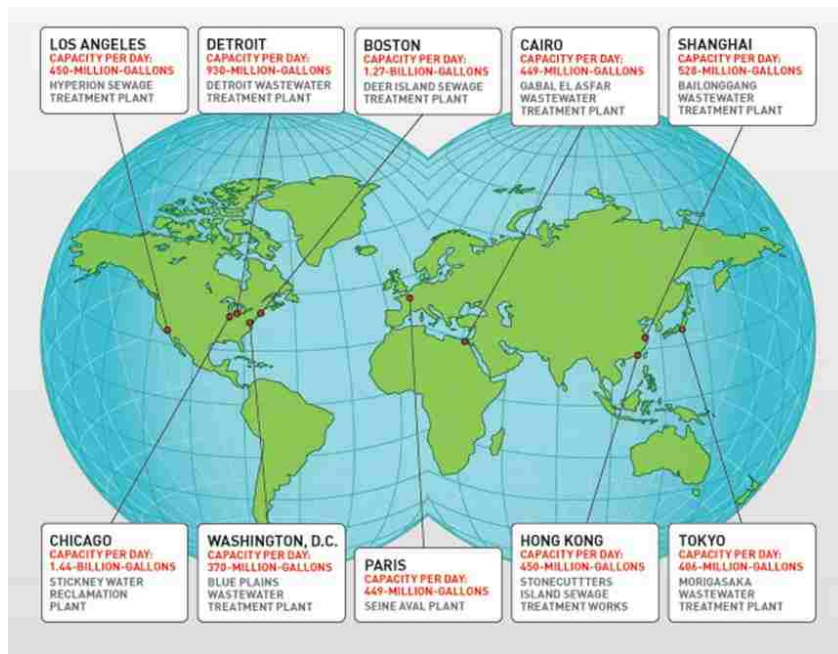


**Figure 1-2.** A map of the 10 largest wastewater treatment plants in the world and their respective influent flow rates.<sup>4</sup>

The water intake ranges from 370 million gallons of treated water per day (Washington D.C.) to 1.44 billion gallons per day (Chicago). This volume of discharge approximately meets the water demands for its locale. Such municipal wastewaters everywhere are further misconceived as impracticable for reuse when in reality more than 99% is pure water. Reconditioning this misconception of a huge ‘wastewater’ body into ‘usable’ water offers opportunities to mitigate water shortages especially in arid regions.<sup>5</sup>

### *1.1.1 Water reuse in practice*

In water-starved regions including California and Singapore, engineered processes have been underway to recover a bulk of wastewater sources for indirect/direct reuse and groundwater recharge. For example, San Diego, California imports 80% to 90% of its water from hundreds of miles away because of dry weather conditions, i.e. ten inches of rain each year and unsustainable stored local runoff. To reduce the demand for imported water, San Diego created the North City Water Reclamation Plant to provide water reuse options for groundwater recharge, agricultural irrigation, commercial uses (including firefighting and cooling), etc. The plant's main treatment technology is reverse osmosis (RO) with added demineralization to meet TDS standards. Reuse strategies allow the plant to take 30 million gallons per day (MGD) and redistribute it after treatment throughout over 79 miles of pipeline for reuse.<sup>6</sup>

California also produced the Orange County Water District (OCWD), where 45 to 70 MGD of reclaimed water can be recharged back into the groundwater basin from their water reclamation plant. The reclaimed water provides a new water supply at less than 40% of the cost for imported water and also prevents seawater intrusion, improves groundwater quality, and reduces ocean discharge.<sup>7</sup> Internationally, countries like Singapore have also turned toward water reclamation plants for water resources and have conducted extensive studies to validate its safe use. Singapore's water reclamation plant NEWater conducted a two-year study where the water product was deemed safe for potable use (based on a comprehensive physical, chemical, and microbiological analysis by an expert panel) that meets the U.S. Environmental Protection Agency's National Primary and Secondary Drinking Water Standards as well as the World Health Organization's Drinking Water

Quality Guidelines.<sup>8</sup> Thanks to the innovation and efforts of places like San Diego, OCWD, and Singapore, water reclamation plants have shown that water reuse is a safe and adequate water supply to meet future demands.

### 1.1.2 *N and P concentrates from water reuse technology*

The most significant treatment technology used for water reclamation is reverse osmosis (RO), a treatment technology that applies a pressure across a membrane, allowing pure water through the membrane and expelling all other components (ions, organics, microbial cells, etc.) for an overall reduction in TDS. The expelled components are concentrated in a reject waste stream due to the smaller volume of the brine as compared to the influent as seen in **Figure 1-3**.

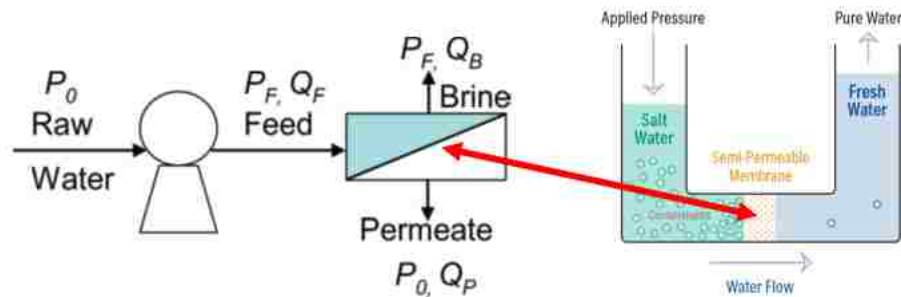


**Figure 1-3.** A simplified RO schematic for desalination (left) and a close-up of what occurs at the membrane boundary (right).<sup>9</sup>

For example, a RO system with 80% recovery and an influent of 100L would have 20L of brine (the  $P_B$ ,  $Q_B$  stream in Figure 1-3), thereby concentrating the compounds five times compared to the influent. In places like California and Singapore, brine streams can be directly deposited to the nearby ocean waters without harm, but the fate of water reuse facilities inland (i.e. far away from the ocean) is undetermined.

When inland desalination plants need solutions to their reject streams, their choices are deep-well injection, landfills or evaporation ponds, which can lead to contamination of nearby groundwater and surface water sources, reduction of soil fertility, and high expenses. Deep-well injection specifically faces restrictions in many states that make it a nonviable option.<sup>10</sup> Nitrogen and phosphorus-containing compounds are particularly of interest during disposal of reject, as they are always present in municipal wastewater streams. By concentrating them even further and disposing them near water resources, we face eutrophication effects. Eutrophication occurs when N and P-laden water is discharged to water resources at levels that produce algal blooms, which leads to dissolved oxygen levels plummeting and detrimental effects on the water ecosystem (hypoxia, toxicity, loss of habitat, etc.).<sup>11-13</sup> In addition, N and P are essential to all living things and applied as the top two components present in fertilizer worldwide. Phosphorus compounds are more difficult to come by than our nitrogen-loaded planet, so in response, phosphate rock reserves have been mined and are depleting at an unsustainable rate to keep up with the demand for P in fertilizer with a growing population as shown in **Figure 1-4**.

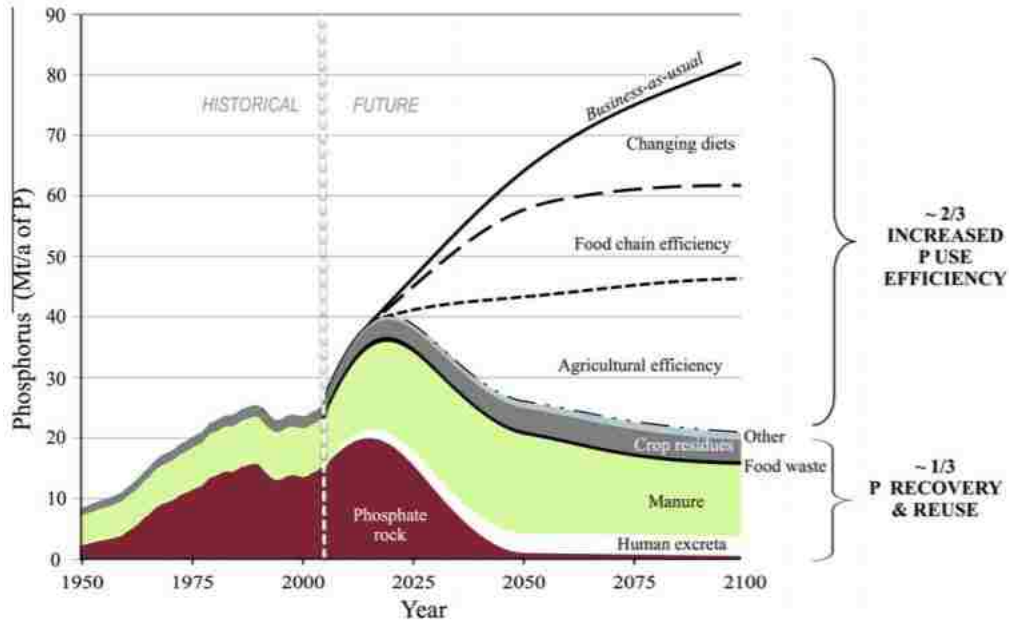


**Figure 1-4.** Projected quantities of P rock reserves over time based on increased P recovery and sustainable P utilization efforts.<sup>14</sup>

As phosphorus mines are depleting (and projected to be depleted within decades), Figure 1-4 shows that a significant portion of future actions will be dedicated to P recovery and reuse efforts in order to keep up with the demand for P and the sustenance for a growing population. This call to action is more realistic than the idea of the “increased P use efficiency option” also shown in the figure that calls for human behavior changes. Removing and recovering P (as well as N) from wastewater effluent prior to its treatment during RO will provide a sustainable solution to eutrophication and P recovery.

### 1.1.3 Co-contaminants to consider prior to RO

In addition to N and P removal prior to RO, hardness removal should also be considered during a pretreatment schematic. As an increase in concentration of electrolytes at the membrane interface occurs and at a high recovery rate, concentration polarization greatly enhances scaling potential.<sup>15-17</sup> Scaling occurs when hardness (divalent cations such as  $\text{Ca}^{2+}$  and  $\text{Mg}^{2+}$ ) precipitates on the membrane surface and

inhibits high recovery due to blockage of the membrane. The ratio of brine concentration to the influent concentration as a function of the recovery rate is displayed in **Figure 1-5** below.

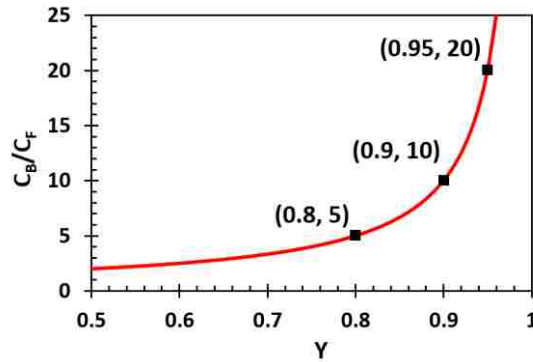


**Figure 1-5.** The brine to influent concentration ratio ( $C_B/C_F$ ) as a function of the recovery rate ( $Y$ ) in a RO system.<sup>18</sup>

Figure 1-5 shows that as the percent recovery ( $Y$ ), also known as the amount of water recovered for reuse over the amount of inflow, increases in correspondence to the concentration of the brine and is validated by the following **Equation 1-1**.

$$C_B/C_F = 1/(1-Y) \quad \text{Equation 1-1}$$

Achievement of greater percent recovery signifies a higher brine concentration especially at the membrane interface. Removal of hardness prior to RO would allow membranes to mitigate scaling potential and in return maintain high recovery rates.

Other co-contaminants to focus on are emerging contaminants that are commonly found in the effluent of wastewater treatment known as pharmaceuticals and personal care products (PPCPs). PPCPs (e.g. prescription drugs, supplements, cosmetics) are discharged to wastewater treatment plants from residential wastewater from human consumption. The concentrations of PPCPs discharged are very low at  $\mu\text{g/L}$  levels and



below, however, there is not much information collected on the adverse impacts of these PPCPs and at what concentrations. Some water bodies have noticed adverse impacts on species due to trace amounts of PPCPs, for example, rapid changes in female to male ratios, and further research is being completed on potential impacts such as antibiotic resistance and blood pressure effects.<sup>19,20</sup> Water quality standards are impending for certain PPCPs for these reasons. Regarding RO pretreatment, removing these compounds prior to concentrating them in a RO reject stream would mitigate potential disposal impacts on species and the overall environment.

## **1.2 Groundwater supply contamination**

Even though communities are searching to reuse impaired water sources, the groundwater supply has always been a resource for consumable water and must be safeguarded against contamination. This section will focus on one main contaminant, nitrate, and a co-contaminant, selenate, that contaminate groundwater resources around the world and impact human health when consumed.

### *1.2.1 A focus on nitrate-contaminated groundwater*

Nitrate has been designated as a drinking water contaminant by the U.S Environmental Protection Agency to a maximum contaminant level (MCL) of 10 mg/L  $\text{NO}_3^-$ -N. Ingestion of nitrate at concentrations above the MCL leaves select groups of people (most commonly infants as well immuno-compromised people) vulnerable to a condition known as blue baby syndrome. This syndrome leaves blood cells to become de-oxygenated and restricts breathing.<sup>21</sup> Nitrate treatment is regulated throughout water

treatment plants, however, groundwater sources, the primary domestic water supply for over 90% of the rural population and 50% of the total population of North America<sup>22</sup>, are not as controlled. Nitrate contamination of groundwater is considered widespread (Figure 1-6) and can be found within the United States, South Africa, India, Australia, and many more.

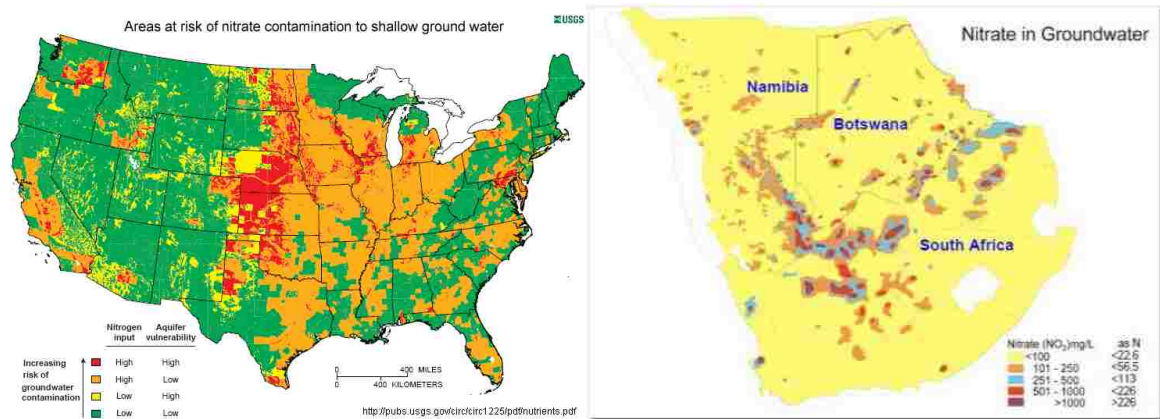
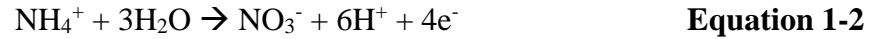


**Figure 1-6.** Nitrate contamination of groundwater sources located in the United States (left)<sup>23</sup> and three countries in Africa (right)<sup>24</sup>.

As Figure 1-6 shows, the detected nitrate contaminated sources are not centralized to one location within these countries but is spread throughout. Some of the groundwater sources located throughout South Africa, Botswana, and Namibia are so high (over 10 times the MCL in purple) that no humans should be consuming the water. With groundwater sources being the only viable drinking source for many of these locations, simple and sustainable treatment technology needs to be in place to mitigate the contamination.

The widespread nitrate contamination of groundwater stems from the overuse of fertilizers in agriculture. When urea (and other ammonia-based compounds) is dispensed throughout soil, excess ammonia trickles down into the subsurface. The nitrifying

bacteria present in the subsurface reduce ammonium ions to nitrate as seen in the following oxidation reaction in **Equation 1-2**:



Nitrate can then transport to nearby groundwater wells and contaminate drinking water sources. Excess use of fertilizer is a global issue and is the main cause for nitrate-contaminated groundwater. Best practices for fertilizer use would mitigate this issue significantly, but to address the situation now, a focus on nitrate remediation technologies is a must.<sup>25</sup>

Nitrate presence in groundwater is also an accomplice to uranium contamination of groundwater. Uranium (U) contamination is also present in groundwater where activities such as mining, nuclear testing, and spent nuclear fuel are exercised. Non-soluble, reduced U(IV) in the presence of oxidizing groundwater produces soluble U(VI) species, which is mobile. At a pH range of 6 to 10, U(VI) will strongly adsorb to dissolved carbonate concentrations, favoring formation of soluble U(VI)-carbonate species and a resulting mobile component. When nitrate is present in the groundwater system as well and undergoes biological denitrification, alkalinity is produced and carries out the oxidation of U(IV), the non-soluble form of uranium, to U(VI)-carbonate species complex. Nitrate-driven Fe(II) reactions (and even intermediate compounds formed during denitrification such as nitrite) can further oxidize U(IV) to U(VI). With nitrate and iron commonly present in groundwater, the probability of U(VI) contamination in these locations is highly likely and reduction of nitrate in the groundwater can reduce uranium contamination.<sup>26</sup>

### 1.2.2 Selenium contamination of water resources

Selenium is an essential trace element in all living things and is present in natural deposits as ores. Although it is necessary for survival, a drinking water standard of 0.05 mg/L selenium has been established by the U.S. E.P.A. due to a range of acute health effects at concentrations higher than the standard. Contamination of wastewater or groundwater sources mostly stems from the overuse of fertilizers containing high selenium as well as the burning of ores, which result in their subsequent release of selenium into the environment. For surface waters and groundwater, contamination occurs as selenium is wasted with flue gas plumes or runoff from agricultural lands and deposited into nearby water sources.<sup>27</sup> For wastewater contamination of selenium, it is a more complicated process. Coal burning power plants, in addition to other ore-burning plants, need to rid flue gas of sulfur dioxide, which is necessary for air quality compliance. Flue gas desulfurization uses an alkaline solution that is rinsed through the scrubber converting any  $\text{SO}_{2(g)}$  to  $\text{SO}_{4(aq)}$  in an aqueous solution as seen in **Figure 1-7**.

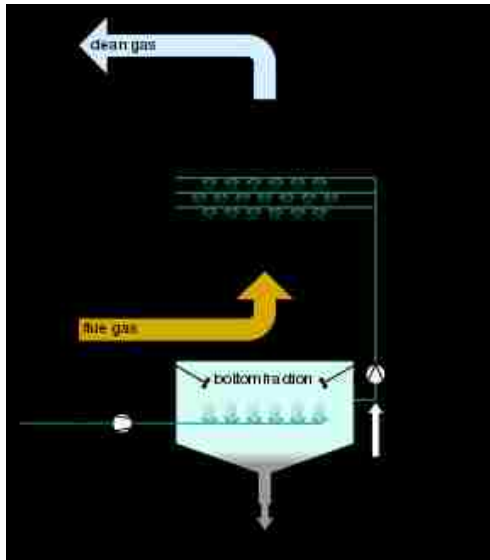


**Figure 1-7.** Flue gas desulfurization process.<sup>28</sup>

As the alkaline solution sprays at the top of the scrubber through the flue gas exiting the plant, any selenium present in the gas will be oxidized to selenate ( $\text{SeO}_4^{2-}$ ) and selenite ( $\text{SeO}_3^{2-}$ ) species that are then discharged to wastewater treatment plants. Selenate is the most toxic species due to its preference for uptake by living organisms and subsequent bioaccumulation in species. The second most toxic is selenite, which forms when selenate (+6 oxidation state) is reduced to selenite (+4 oxidation state).<sup>29</sup> Selenium species are not specifically targeted in wastewater treatment and, therefore, should be considered for RO pretreatment as well.

### 1.3 A review of current water treatment technologies

The purpose of this work is to evaluate the shortcomings of current technology for the contamination issues outlined above and from that, design solutions that can improve upon them regarding efficiency and sustainability. This section outlines the current and most used technology for water reuse, pretreatment, and groundwater treatment from which we will build a foundation for new technology.

#### 1.3.1 Water reuse technologies: reverse osmosis (RO) and ion exchange (IX)

Advanced treatment of recycled water used for indirect potable reuse involves a series of filtration processes. Singapore's NEWater (the brand name given to its reclaimed water) is produced with the following treatment process shown in **Figure 1-8**.

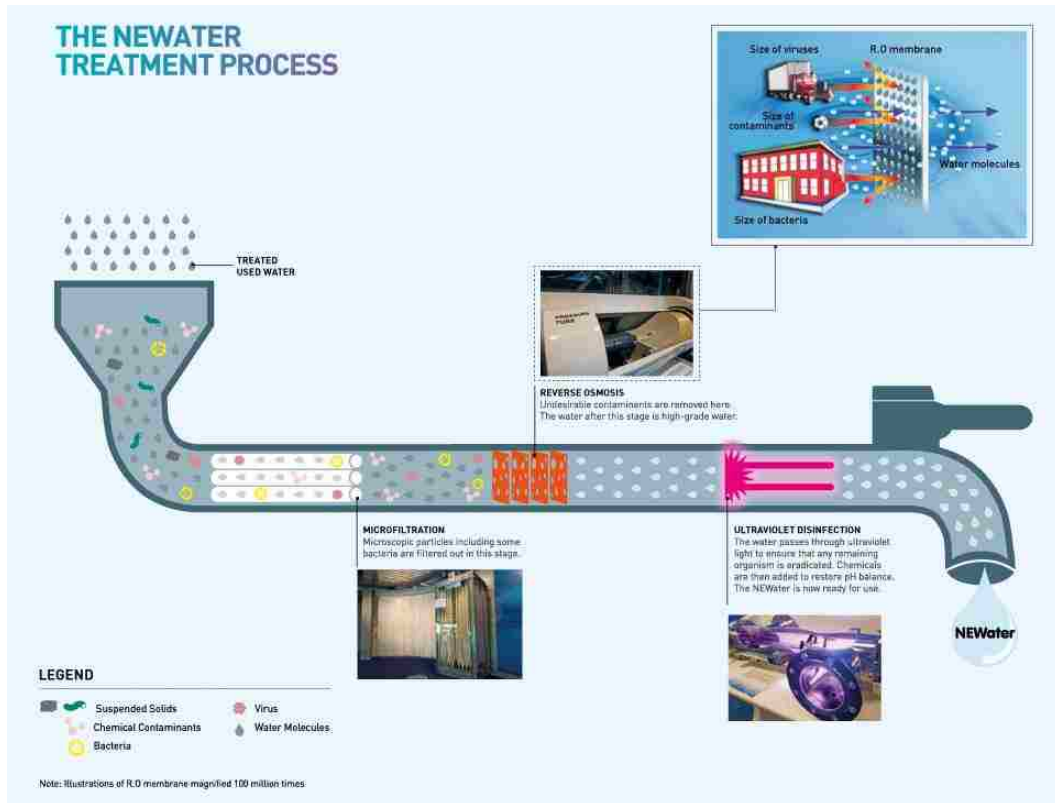


**Figure 1-8.** Singapore’s NEWater treatment process for water reclamation.<sup>30</sup>

The treatment technologies used to produce recycled water include microfiltration (particle exclusion by size, typically in the micron and above range), RO (for TDS removal), and then ultraviolet (UV) treatment (for disinfection of organisms). The main technology in these schematics is RO, and then microfiltration is used for pretreatment to RO and UV disinfection is a polishing step. RO processes for municipal wastewater recovery require extensive pretreatment to protect the semi-permeable membrane from scaling and biofouling. For example, salts of phosphate and sulfate associated with hardness have poor solubility:  $K_{sp}$  or solubility product values of calcium phosphate, calcium sulfate and barium sulfate are respectively  $2.03 \times 10^{-33}$ ,  $4.93 \times 10^{-5}$ , and  $1.08 \times 10^{-10}$ . An increase in concentration of these electrolytes at the membrane interface at high recovery accompanied by concentration polarization greatly enhances scaling potential. Microfiltration will not

exclude these ions in solution, so dosing of anti-scaling agents, polyacrylic or phosphonic acid, is practiced universally in addition. Anti-scaling agents, however, promote biological growth and consequent biofouling on the membrane surface.<sup>16</sup>

Ion exchange is another option for TDS reduction. The ion exchange process involves resin beads comprised of a polymeric matrix with fixed functional groups and freely moving ions of opposite charge that exchange with other like-charge ions in solution, as seen in **Figure 1-9**.

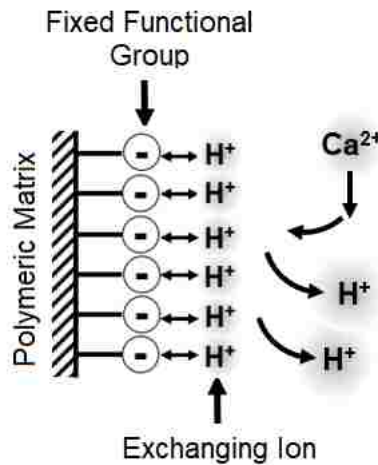


**Figure 1-9.** Components of a cation exchange resin.

By placing a cation exchange column that releases H<sup>+</sup> ions in exchange for other cations in solution followed by an anion exchange column that exchanges OH<sup>-</sup> ions for other anions in solution, total anion removal can be achieved. However, ion exchange does not have the enormity of RO removal or its capability to exclude non-ionized compounds and organisms. Considering cation exchange for pretreatment allows for calcium/hardness removal without dosing chemicals, but this process requires the use of brine or mineral acid as a regenerant to reuse the resin beads, posing disposal problems.<sup>31</sup> Water reuse

demands a pretreatment process to RO that can reduce hardness efficiently to mitigate scaling potential and without resorting to doses of chemicals.

### *1.3.2 Nutrient removal and recovery technologies*

Combined nutrient removal systems present in wastewater treatment schematics are typically biological nutrient removal (BNR) systems. These systems utilize a series of anaerobic and aerobic biological tanks that promote uptake of P and consequent nitrate reduction to nitrogen gas by specific bacteria under anaerobic conditions. Although these systems can achieve high removal rates, requirements include carbon source dosing and high sludge removal. This type of removal technology works for wastewater treatment, however, it does not work as a viable system for pretreatment to RO due to those requirements that would inhibit high recovery.<sup>11,32</sup> In addition to BNR, several studies have been devoted to remove and recover phosphate specifically from municipal wastewater mostly as struvite or  $MgNH_4PO_4$ , a slow release fertilizer.<sup>33-39</sup> For precipitation to occur, the appropriate ratio of each component is required at a high pH. Components that are lacking will be dosed at high concentrations along with a pH adjustment by NaOH or lime. Increased dosing of chemicals and the potential for by-product precipitates (i.e. magnesium sulfate precipitates) makes this an unsustainable treatment for P removal alone. Recovery systems need to concentrate N and P in small volumes with little to no chemical addition to be an efficient and cost-effective treatment technology.

### *1.3.3 Emerging contaminant technology*

Because of the complexity in structure of PPCPs, biological degradation or chemical oxidation have been the preferred methods of PPCP removal from water.

Chemical oxidation utilizes an advanced oxidation process using a combination of highly



reactive oxygen species and energy sources (e.g. ozone, UV, H<sub>2</sub>O<sub>2</sub>). These processes are effective in degrading the initial compound; however, it often leaves even more toxic intermediates. Biological degradation methods apply bacteria and a carbon source to degrade the PPCP compound without excessive toxic intermediates, but the trace concentrations become difficult for bacteria to complete degradation to its non-hazardous form.<sup>19,40</sup> To effectively use biological degradation methods, the PPCPs need to be captured and concentrated before fed to the main biological system.

#### *1.3.4 Nitrate removal from drinking water*

Ion exchange is typically the chosen drinking water treatment for nitrate-contaminated streams. Ion exchange has fast kinetics, high removal, and can be modified to be selective for nitrate over competing anions. However, once the ion exchange bed is completely loaded with nitrate, a regeneration process will occur where nitrate is kicked off the bed with a high concentration brine solution, generally 10-15% NaCl solution.<sup>41</sup> The spent regenerant solution, now highly concentrated in nitrate, other anions, and excess NaCl, needs to be disposed. Again, disposal through landfill and deep-well injection will cause contamination problems such as eutrophication and impairing groundwater sources.

In wastewater treatment, nitrate is biologically reduced to nitrogen gas anaerobically. This process sustainably removes nitrate from the waste stream to an innocuous nitrogen source, no brine needed. One example is the Anammox treatment system where an anaerobic tank that degrades nitrate to nitrogen gas is followed by an aerobic tank that nitrifies any influent ammonia to be recycled back to the front of the anaerobic tank. However, the process is kinetically slow, produces sludge in need of

disposal, and requires the addition of a carbon source to drive the reduction reaction of nitrate.<sup>11,42</sup> The carbon source is added because biological oxygen demand (BOD), a source of biodegradable carbon, is removed in both primary and secondary treatment processes that occur ahead of the denitrification process. Among typical carbon sources that are dosed into the denitrification systems are methanol and acetate, based on their nonhazardous, cost-effective, high yield, and biodegradability characteristics.<sup>43</sup> Based on the advantages explored in ion exchange and biological denitrification for nitrate removal, a groundwater nitrate removal system that can combine to apply fast kinetics of ion exchange with the sustainability of nitrate reduction to nitrogen gas biologically would be an improvement to existing technologies.

#### *1.3.5 Selenium characteristics that provide parallels to nitrate removal*

Selenium can take the form of numerous species in aqueous solutions based on the pH and the oxidation-reduction potential of the solution. **Figure 1-10** demonstrates this speciation with the pE-pH diagram of selenium.

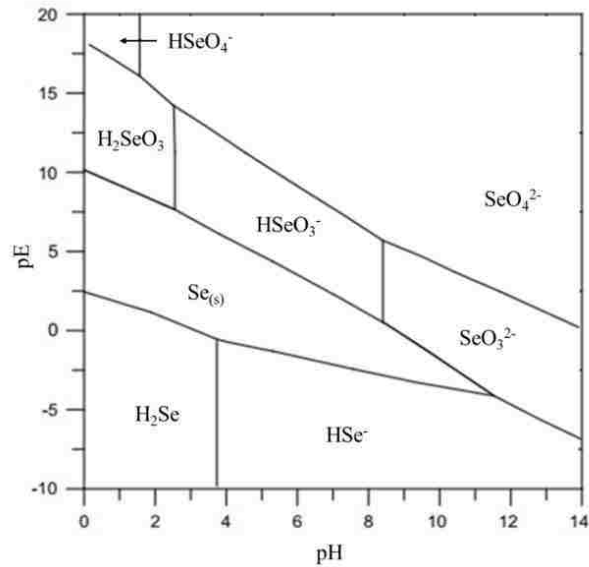


**Figure 1-10.** Selenium pE-pH diagram at 25°C and 1 bar.<sup>44</sup>

As discussed previously, selenium contamination from flue gas desulfurization takes the form of selenate ( $\text{SeO}_4^{2-}$ ) and selenite ( $\text{SeO}_3^{2-}$ ). When selenium takes the form of selenate (which has been noted as the main speciation during contamination of water sources), it has a likeness to a nitrate ion: it is highly soluble and can be anaerobically reduced to elemental selenium. This signifies that selenate can be removed like nitrate, both by ion exchange and anaerobic biological degradation.<sup>45</sup> Selenite is an intermediate component in the biological reduction from selenate to selenium, however, it acts more like a ligand like phosphate than an ion-exchanging compound such as nitrate. For nitrate and selenium removal from contaminated water sources, the speciation of selenium must be considered for full removal of harmful selenate and selenite to a sustainable recovery of elemental selenium.

## 1.4 Objectives

The objectives of this first study are to design and enhance a treatment system to remove N, P, hardness, and other compounds for RO pretreatment, design and enhance a treatment system for widespread contaminants of groundwater with a focus on nitrate and selenium, and design and enhance a treatment of nitrate-loaded brine from ion exchange regeneration. The first study will outline the design of a treatment system called HIX-NP for nutrient removal and recovery with overall RO pretreatment. This work will address the first research question: can we create reusable water using RO that has a reject free of N and P and retains high recovery? To address this question, goals of the study were established to validate the basic premise of the conceptualized HIX-NP process using secondary wastewater from the Bethlehem Wastewater Plant (BWWP) in Pennsylvania and specifically investigate the following:

1. An enhancement in selective phosphate and nitrate removal with concurrent hardness removal;
2. Simultaneous recovery of phosphate and nitrate using KOH as the sole regenerant;
3. Efficient use of CO<sub>2</sub> as a regenerant and its consequent sequestration.

The second study explores the second research question: can we create a process that combines the fast kinetics of ion exchange with the sustainability of biological denitrification to remove nitrate and selenate from contaminated groundwater without use of brine? This question is addressed by designing a combined biological denitrification and ion exchange system (known as BIO-NIX) to address the contamination of nitrate (and potentially selenate) from groundwater and their sustainable conversion to nonhazardous

species. The goals of the study were to validate the basic premise of the conceptualized BIO-NIX process using synthesized groundwater created from the influent of the Manheim Water Treatment Plant (MWTP) in Pennsylvania and specifically investigate the following:

1. High removal of nitrate (and selenate) from groundwater without chemical addition or brine waste;
2. A resilient nitrate removal system that can handle impulsive fluctuations in influent and system parameters.

The third study explores the question, can we sustainably remove nitrate and selenate from a high concentration regeneration brine from ion exchange processes and continuously reuse the brine to eliminate disposal needs. The BIO-NIX process was modified to design the solution to this question, a new process called BIO-RNIX. The goals of this study were to validate the design of BIO-RNIX using a wastewater exhausted ion exchange column from BWWP secondary wastewater and specifically investigate the following:

1. High removal of nitrate and selenate from regenerant brine within hours timeframe during a regeneration cycle;
2. Reuse of the treated brine for multiple cycles.

## CHAPTER 2: Scientific Concepts of HIX-NP, BIO-NIX, and BIO-RNIX

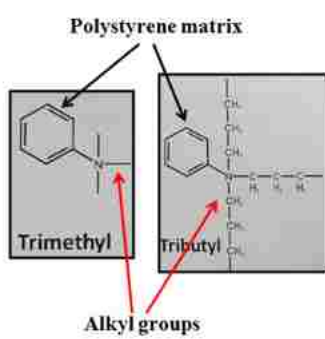
### 2.1 HIX-NP as a pretreatment to RO

The HIX-NP process is comprised of a shallow shell weak acid cation (WAC) exchanger followed by a hybrid anion exchanger loaded with zirconium oxide nanoparticles (HAIX-NanoZr). HIX-NP addresses enhanced nutrient removal and recovery through the HAIX-NanoZr, hardness removal through the WAC, and explores co-contaminant removal in addition.

#### 2.1.1 Nitrate-selective HAIX-NanoZr

The HAIX-NanoZr is comprised of a strong-base anion (SBA) exchange resin with tri-butyl functional groups that prefer monovalent nitrate ( $\text{NO}_3^-$ ) over divalent sulfate ( $\text{SO}_4^{2-}$ ). Typical SBAs with trimethyl functional groups prefer sulfate and other competing anions over nitrate.<sup>41,46</sup> **Table 2-1** below shows how varying alkyl groups that form the matrix of a SBA change the selectivity of nitrate over sulfate.

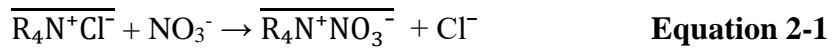
**Table 2-1.** Nitrate Selectivity of a SBA as a Function of Alkyl Groups within the Matrix.<sup>46</sup>



Alkyl Group in Q.A. Functional Group	Moisture Content (%)	Capacity (eq/L)	Selectivity $K_{n/s}$
Methyl	57.0	1.41	100
Ethyl	48.0	1.2	1,000
Propyl	30.4	0.84	1,100
Butyl	33.0	0.66	11,000

As the alkyl group that makes up the matrix becomes bulkier (i.e. from methyl to butyl) the moisture content decreases. These bulkier alkyl groups decrease in moisture content

and begin to resist hydrated, divalent sulfate. A gradual decrease in capacity follows in relation to increased hydrophobicity and a greater charge separation distance between sulfate and the bulkier alkyl chain. The selectivity is now in favor of nitrate over sulfate and increases as the alkyl chains grow bulkier.<sup>47</sup> The SBA's exchange reaction for nitrate with a chloride-loaded resin is shown in **Equation 2-1** below:



where the overbar denotes the exchanger phase. By utilizing a SBA resin with tributyl functional groups, nitrate is more selective than competing sulfate, high nitrate removal can be achieved, and high purity N recovery can be achieved.

Phosphate (the predominant species of phosphorus in aqueous solutions) is a ligand that binds to a central metal atom to form an inner sphere complex; it does not participate in ion exchange (an outer sphere complex).<sup>33</sup> Based on this chemistry, the SBA described above is dosed with zirconium oxide nanoparticles to selectively remove phosphate in addition to nitrate. Zirconium, the 21<sup>st</sup> most abundant element in the world, is stable, chemically innocuous and non-hazardous. Nanoparticles of zirconium oxide (ZrO<sub>2</sub>) have unique sorption properties to bind a variety of anionic trace ligands including phosphate through Lewis acid-base interactions (LAB) as described in **Figure 2-1** below.<sup>48,49</sup>

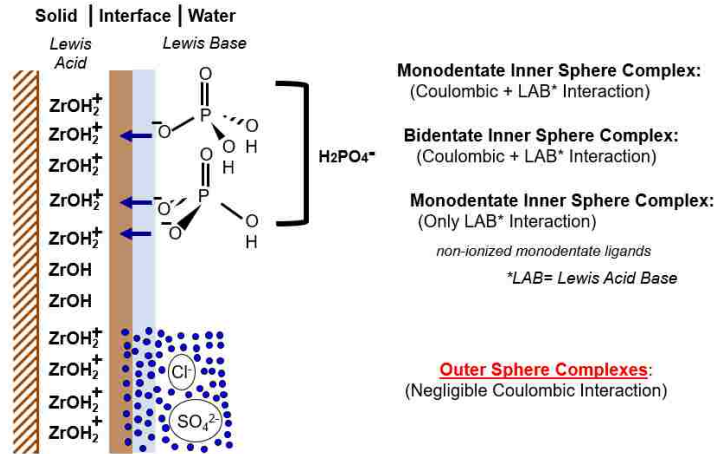


**Figure 2-1.** LAB interactions between phosphate ( $\text{H}_2\text{PO}_4^-$ ) and  $\text{ZrO}_2$ .<sup>33</sup>

The metal oxide ( $\text{ZrO}_2$ ) acts as the strong electron acceptor and phosphate as the strong electron donor for a strong bond. In comparison with other metal oxides such as Al(III) and Fe(III) oxides,  $\text{ZrO}_2$  is more chemically stable over a wide range of pH and varying redox conditions. Recently, a process of synthesis has been developed and refined to disperse  $\text{ZrO}_2$  nanoparticles irreversibly within the macropores and gel phase of anion exchange resins and the technique is easily extended to nitrate-selective anion exchange resins.<sup>50,51</sup> The resulting hybrid ion exchanger, referred to as HAIX-NanoZr, is a robust sorbent material with dual sorption sites: tri-butyl quaternary ammonium functional groups with high affinity toward nitrate and phosphate-selective surface sorption sites of hydrated zirconium oxide (HZrO). Furthermore, HAIX-NanoZr is also amenable to regeneration and reuse for multiple cycles.

### 2.1.2 pH dependency of HAIX-NanoZr for selective P removal

Hydrated zirconium oxide (HZrO) surfaces are amphoteric and their two acid-dissociation constants are presented as follows in **Equation 2-2** and **Equation 2-3**.<sup>50,52</sup>





Figure 2-2A shows the distribution of HZrO surface functional groups as a function of pH.

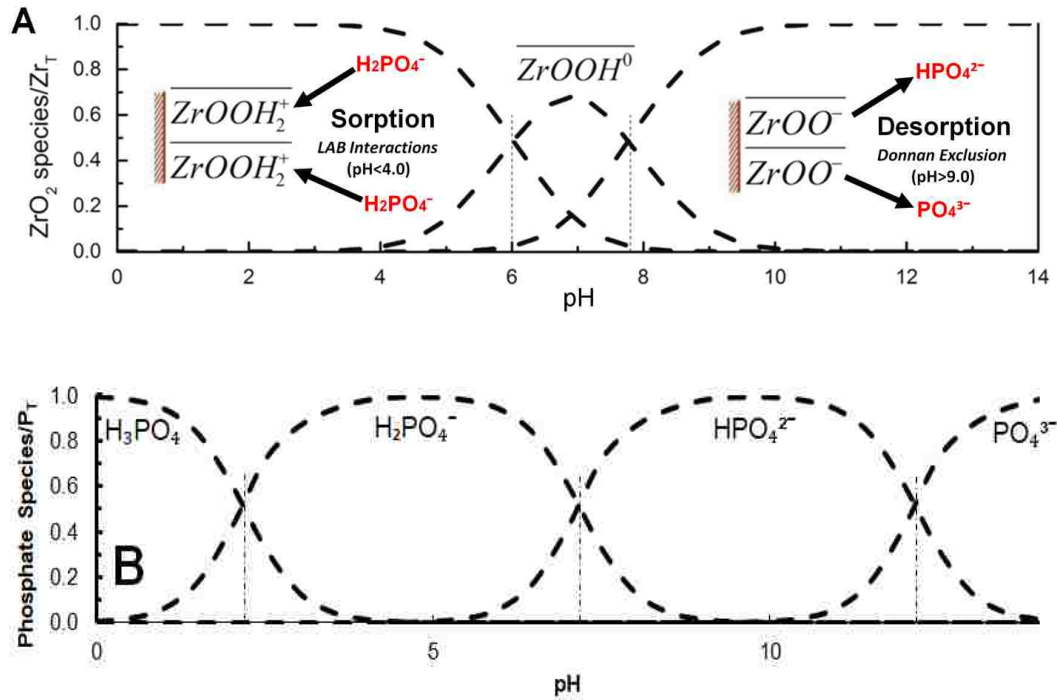
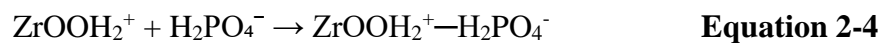
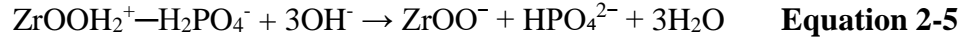


Figure 2-2. The distribution of hydrated zirconium oxide surface functional groups (top) and phosphate species (bottom) illustrating the pH range of sorption and desorption of phosphate.

At  $\text{pH} \leq 5.0$ , HZrO surfaces have residual positive charges exhibiting strong affinity toward anionic ligands.<sup>48,52</sup> Monovalent phosphate ( $\text{H}_2\text{PO}_4^-$ ) seen in Figure 2-2B will be strongly sorbed onto HZrO surfaces under such operating conditions through concurrent electrostatic (EL) and LAB interactions and can be represented by Equation 2-4:



Conversely, at  $\text{pH} \geq 11$ ,  $\text{HZrO}$  surfaces turn negatively charged and will, therefore, desorb phosphate through the Donnan exclusion.<sup>15,53</sup> If an alkaline solution is applied to HAIX-NanoZr,  $\text{OH}^-$  ions from the solution will create this effect as seen in **Equation 2-5**.



Nitrate may also be concurrently desorbed from the quaternary ammonium functional groups along with phosphate even in the presence of sulfate (**Equation 2-6**).

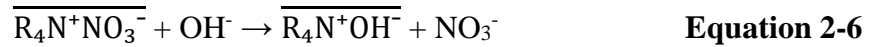


**Figure 2-3** illustrates how phosphate and nitrate can be very selectively sorbed and desorbed through pH swings.

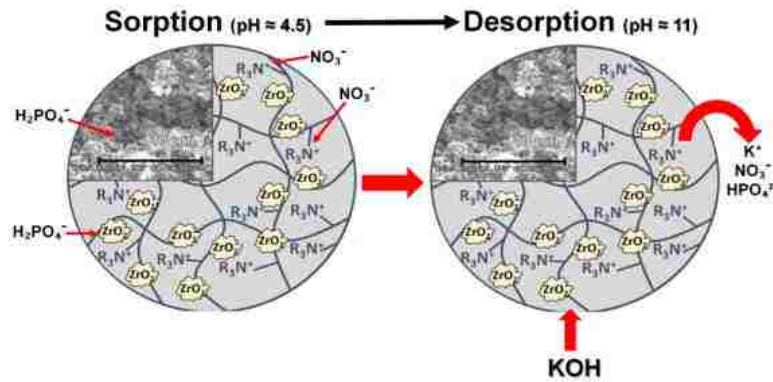


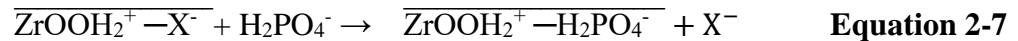
**Figure 2-3.** Sorption and desorption processes of a HAIX-NanoZr resin as a function of pH.

Note that use of  $\text{KOH}$  results in the spent regenerant solution rich in N, P and K, three essential elements of a fertilizer.<sup>54</sup>

Typical wastewater effluent (the influent to the RO system) has a neutral pH around 7.0-7.5. For increased phosphate removal capacity by the HAIX-NanoZr, a decrease in pH to approximately 4.5 is necessary as discussed above. A typical, easy solution to decrease

pH of a solution is to dose with a high concentration acid such as hydrochloric acid or sulfuric acid. These acids are very hazardous due to their corrosive nature and factor into the cost of the system when having to dose large volumes of the acid into the influent. By using a weak acid cation exchanger (WAC), pH can be decreased without dosing the system with hazardous mineral acids.<sup>55,56</sup>

The capacity of the HAIX-NanoZr resin in relation to its high selectivity for phosphate as a result of the WAC can be determined from a modified reaction of Equation 2-4.



Note that **Equation 2-7** is not an ion exchange reaction but modeled as above to show phosphate's selectivity over other anions ( $\text{X}^-$ ) in solution. The K value of this reaction (also known as the selectivity,  $K_{P/X}$ ) can be represented by **Equation 2-8** below.

$$K_{P/X} = \frac{q_p C_X}{q_X C_P} \quad \text{Equation 2-8}$$

where  $q_p$  and  $q_X$  are the phosphate and anion capacities of HAIX-NanoZr respectively, and  $C_P$  and  $C_X$  are the concentrations of phosphate and anions in solution. The total capacity of HAIX-NanoZr ( $Q$ ) and the total aqueous phase concentration ( $C_T$ ) can be shown in **Equations 2-9 and 2-10**.

$$Q = q_p + q_X \quad \text{Equation 2-9}$$

$$C_T = C_P + C_X \quad \text{Equation 2-10}$$

By substituting Equations 2-9 and 2-10 for Equation 2-8 and rearranging for  $q_p$ ,

**Equation 2-11** is generated.

$$q_p = \frac{K_{P/X} Q (C_P/C_T)}{1 + (K_{P/X}-1)(C_P/C_T)} \quad \text{Equation 2-11}$$

Equation 2-11 determines that the phosphate capacity for HAIX-NanoZr can be modeled as a Langmuir isotherm and can be seen in **Figure 2-4** below as completed in the literature.

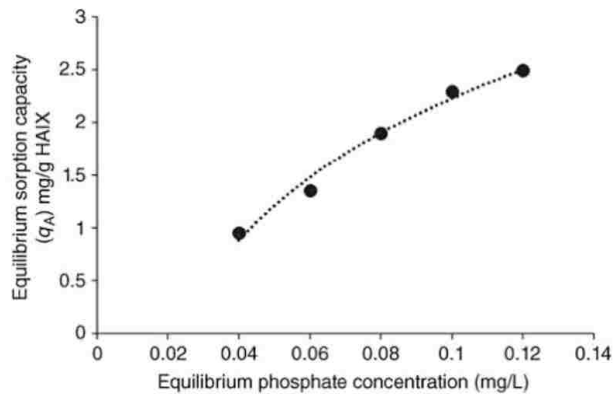


**Figure 2-4.** Phosphate capacity curve as a function of varying influent concentrations modeled as a Langmuir isotherm.<sup>33</sup>

Because this work has already been completed, results of this nature will focus on the capacities found during HAIX-NanoZr runs with secondary wastewater.<sup>46</sup>

### 2.1.3 WAC for hardness removal and partial desalination

Every municipal wastewater invariably contains hardness and alkalinity. By implementing a WAC resin bed ahead of HAIX-NanoZr, we can achieve hardness removal, a pH decrease, and a reduction in TDS. A WAC resin has carboxylic functional groups that exchange hydrogen ions on the carboxylic group with other cations in solution, preferring

hardness over monovalent cations. **Figure 2-5** shows the WAC resin exchange and its carboxylic functional groups.

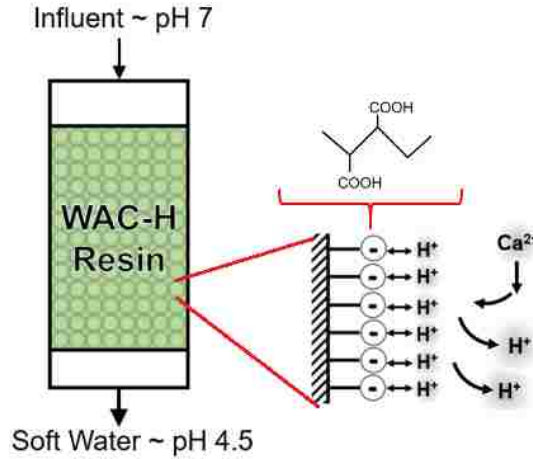
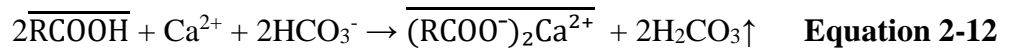


**Figure 2-5.** A demonstration of the WAC resin bed’s ability to remove hardness in exchange for hydrogen ions.

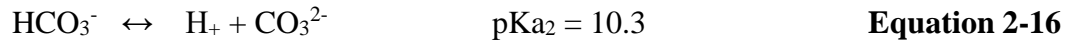
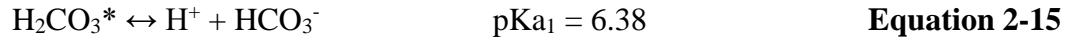
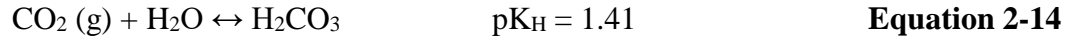
Thus, passage through a weak-acid cation (WAC) exchanger helps reduce and maintain pH in the 4.0-4.5 range, providing the highest phosphate removal capacity by HZrO sorption. Alkalinity constituted by hardness is selectively removed by the WAC resulting in the lowering of pH in the range of 4.0-4.5 and can be demonstrated by **Equation 2-12**:



By combining H<sup>+</sup> ions released from the WAC with alkalinity in solution, carbonic acid is formed (H<sub>2</sub>CO<sub>3</sub>) and can be further dissociated into CO<sub>2</sub>(g) and water for an overall reduction in TDS (**Equation 2-13**).



As carbon dioxide forms and dissociates as both a weak acid (carbonic acid) and a weak base (bicarbonate), which often be referred to as alkalinity, the following K values can be assigned to the equations representing carbon dioxide chemistry.<sup>57</sup>



At a pH between pK<sub>a1</sub> and pK<sub>a2</sub>, bicarbonate is the dominant species and the total concentration merges with bicarbonate for overall TDS reduction. TDS reduction will not be analyzed in this study, but such systems have previously been studied for TDS reduction as an added benefit.<sup>18</sup>

Once the WAC is exhausted, it needs to be intermittently regenerated, which is typically done with a mineral acid to reload H<sup>+</sup> ions. To make the regeneration process more efficient, a shallow shell weak-acid cation (SS-WAC) exchange resin is employed, where the carboxylate functional groups reside primarily in the outer periphery of the spherical beads as seen in **Figure 2-6**.

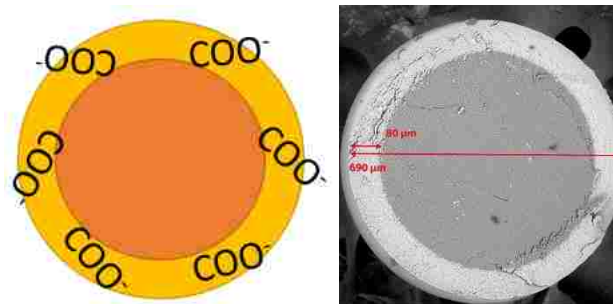
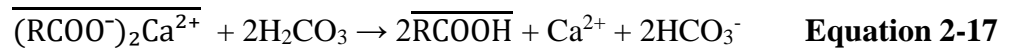


**Figure 2-6.** Representations of the SS-WAC resin with the carboxylic functional groups and by SEM-EDX.

With a traditional diameter size in the range of 500-1200  $\mu\text{m}$ , WAC resins exhibit poor regeneration kinetics and the sorption of  $\text{H}^+$  ions is intra-particle diffusion controlled. The outer shell of the SS-WAC resin contains the functional groups, allowing faster removal and regeneration because the intraparticle diffusion path length is relatively short.<sup>58</sup>

Instead of utilizing a hazardous mineral acid such as HCl, the SS-WAC is amenable to regeneration by pressurized carbon dioxide ( $\text{CO}_2$ ) that forms  $\text{H}_2\text{CO}_3$  once sparged in water and uses dissociated  $\text{H}^+$  ions to reload the bed as seen in **Equation 2-17**.<sup>18,59,60</sup>

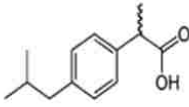
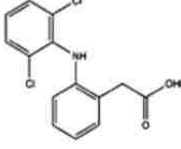
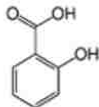
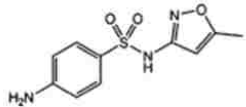


The  $\text{CO}_2(\text{g})$  regenerant is a more sustainable option for regeneration as it is not a hazardous mineral acid and can mitigate greenhouse gas effects with its use. Finally, carbon dioxide is sequestered as  $\text{CaCO}_3(\text{s})$  in the calcium-loaded spent regenerant.

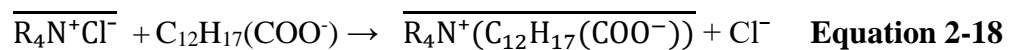
#### 2.1.4 PPCPs (a co-contaminant) simultaneous removal in HAIX-NanoZr

Below is a list of PPCP compounds (also known as hydrophobic ionizable organic compounds, HIOCs) and their structures in **Table 2-2**.

**Table 2-2.** Examples of HIOCs and their Structures<sup>19</sup>

HIOC Name:	Formula:	Structure
Ibuprofen	C <sub>13</sub> H <sub>18</sub> O <sub>2</sub>	
Diclofenac	C <sub>14</sub> H <sub>11</sub> NC <sub>2</sub> O <sub>2</sub>	
Salicylic acid	C <sub>7</sub> H <sub>6</sub> O <sub>3</sub>	
Sulfamethoxazole	C <sub>10</sub> H <sub>11</sub> N <sub>3</sub> O <sub>3</sub> S	

PPCPs as shown in Table 2-2 are essentially weak acids and weak bases that can take ionizable forms, which allows them to be removed through ion exchange processes.<sup>19,46,61</sup> For example, ibuprofen can take the form of C<sub>12</sub>H<sub>17</sub>(COO<sup>-</sup>) with a pK<sub>a</sub> of 4.9. At the pH designed by the WAC in the range of 4.0-4.5, ibuprofen's majority form will be ionized. The quaternary ammonium functional groups of a strong base anion exchanger have high affinity towards hydrophobic anions, such as ionized ibuprofen. Ibuprofen can undergo anion exchange with the HAIX-NanoZr with the following reaction:



Note that the ion exchanger is still more selective towards nitrate, as the bulkier alkyl groups will prefer both monovalent ions, but size exclusion will favor nitrate.



Once the ibuprofen is captured on the ion exchange bed, regeneration will provide a concentrated solution for biological degradation and sustainable removal of the PPCP compound. Regeneration of ibuprofen will also occur using a NaCl or NaOH solution (where a high concentration of  $\text{Cl}^-$  or  $\text{OH}^-$  ions replace ibuprofen on the resins). However, the regenerant solution needs to be amended with a methanol-water mixture for greater efficiency. The methanol presence assists the non-electrostatic interaction between the polymeric resin matrix and the benzene ring present in ibuprofen's structure. Once concentrated, the regenerant stream of NaOH and water-methanol mixture can continue to biological methods for remediation. <sup>62,63</sup>

#### *2.1.5 Summary of the HIX-NP process*

The proposed innovation using the two-bed hybrid ion exchange process for concurrent phosphate and nitrate recovery in conjunction with hardness removal is illustrated in **Figure 2-7**.

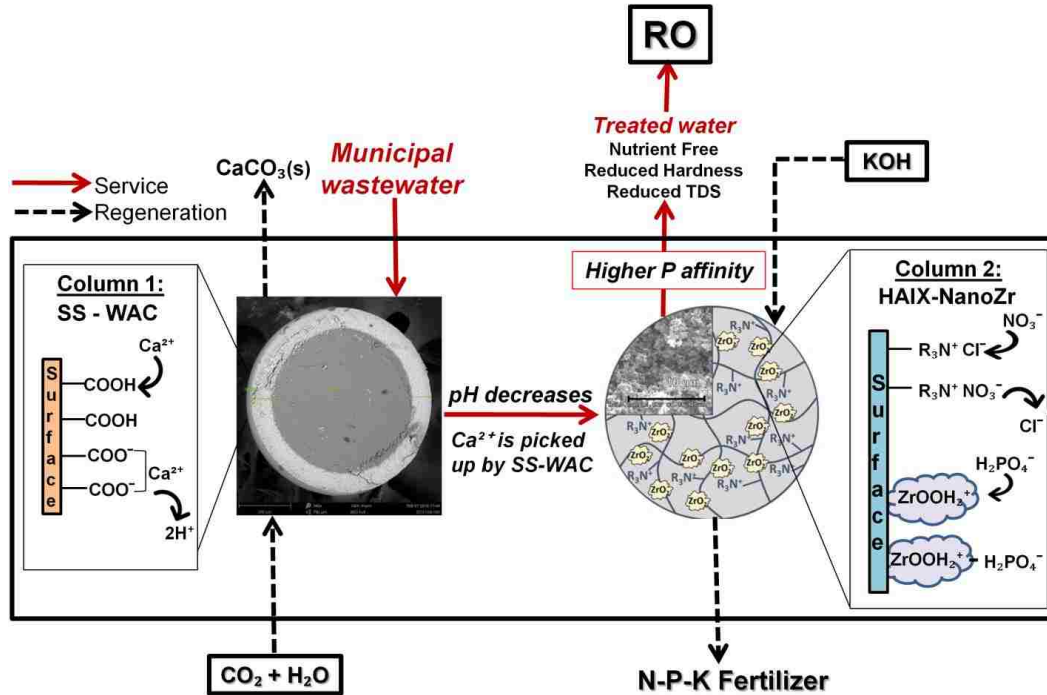


**Figure 2-7.** A schematic depicting the enhancement of phosphate and nitrate removal capacities by the two-bed HIX-NP system with concurrent reduction in hardness aided by  $\text{CO}_2$ .

The first column consists of shallow-shell weak-acid cation (SS-WAC) resin with carboxylate functional groups followed by the second column containing HAIX-NanoZr with dual quaternary ammonium functional groups and zirconium oxide sorption sites. Reactions during the service cycle not only enhance P and N removal capacity, but also achieve hardness removal and partial desalination due to alkalinity reduction. The treated wastewater, thus free of hardness and phosphate, is well suited for desalination by RO and requires no dosing of anti-scaling agents. Use of  $\text{CO}_2$  under pressure is used to regenerate the weak-acid cation exchanger while  $\text{KOH}$  is the preferred regenerant for HAIX-NanoZr. The spent regenerant from HAIX-NanoZr is rich in N, P, K and  $\text{CO}_2$  used for regenerating SS-WAC is sequestered by calcium eluted. Note that  $\text{CO}_2$  is the only chemical used in the

process and KOH used as the regenerant for HAIX-NanoZr is fully recovered as N-P-K fertilizer. No other waste is produced in the process.

## 2.2 BIO-NIX for nitrate removal from groundwater

The BIO-NIX system is comprised of three columns: (i) a citric acid-loaded anion exchanger that slowly releases citric acid as the carbon source for the system; (ii) a fixed-film bed that attaches denitrifiers to a media (in this case Metamateria) for biological denitrification; and (iii) a nitrate-selective anion exchanger that removes any additional nitrate passing through the fixed-film column. The BIO-NIX system is shown in **Figure 2-8** below.

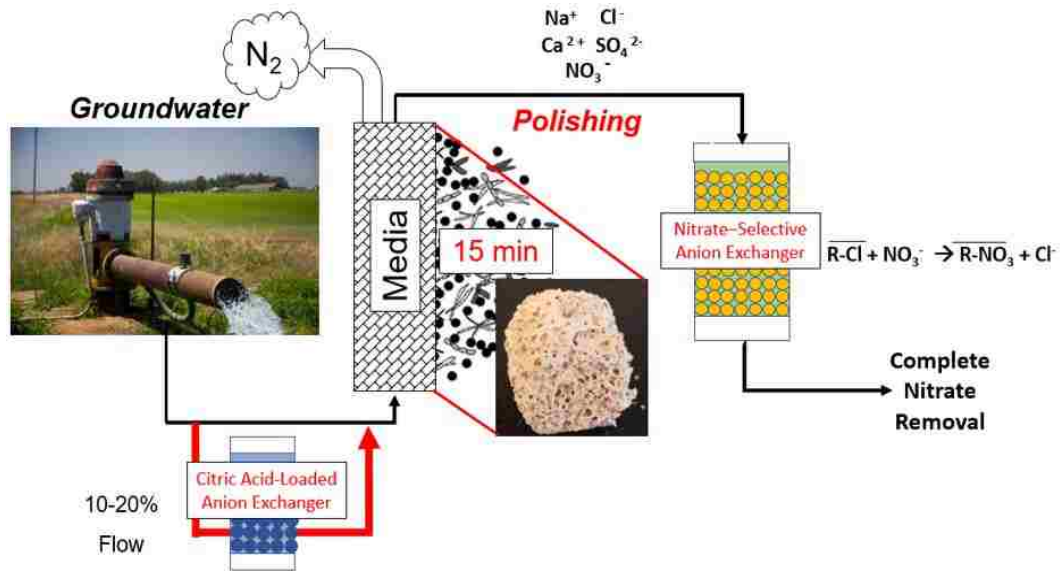


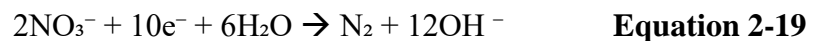
**Figure 2-8.** Schematic of the BIO-NIX system for removal of nitrate.

Note that the citric acid-loaded anion exchange column has a bypass line where 10-20% of the total flow will travel through that column and slowly release citric acid into the main stream line prior to the fixed-film column. As discussed in the previous chapter, selenate acts similarly to nitrate and therefore, selenate removal will also be tested with

this system. However, the main focus will be on nitrate removal so the following sections will discuss the processes role in depth regarding nitrate removal with a brief mention of selenate. During the experiments, selenate removal will only be tested with the system in tandem with nitrate and only to see if the overall process can remove selenate.

### 2.2.1 Fixed-film biological denitrification

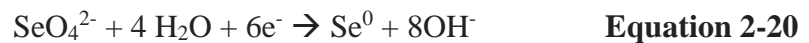
A fixed-film process forms a biofilm (layer(s) of microbial cells that are enclosed in an extracellular polymeric substance matrix) that attaches to a media. In comparison to suspended growth systems, where free-floating microbial cells form flocs and settle at the bottom of a tank, fixed-film processes are advantageous in their stability under shock loads, low energy consumption, and achievement of near-zero concentrations based off the plug flow model.<sup>64,65</sup> The media of the fixed-film processes range from plastic to rocks and bacteria can attach to the surface and within the pores to form a biofilm. Contaminated water flows past the media and the contaminant is biologically degraded as it contacts the biofilm and gets degraded by the cells.<sup>66</sup> The BIO-NIX process utilizes fixed-film as the main treatment for nitrate removal through the biological denitrification process. Bacteria can reduce nitrate to nitrogen gas under anaerobic conditions (i.e. no oxygen is present) as seen in the following half reaction, **Equation 2-19**.



Without oxygen, bacteria cannot use oxygen as the oxidizer ( $E_H$  or redox potential=+0.82 volts) to degrade substrates and turn to nitrate ( $E_H$ =+0.74 volts) as the next favorable electron acceptor.<sup>67</sup> For nitrate to be reduced, another component of the system needs to be oxidized: a carbon source that serves as the electron donor to nitrate. A carbon source

undergoes a half reaction that converts the carbon source to carbon dioxide to represent the fate of that carbon source during biological oxidation-reduction processes.<sup>68</sup> The details of the role of the carbon source in the BIO-NIX process and subsequent reactions will come in the following section.

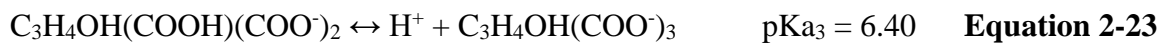
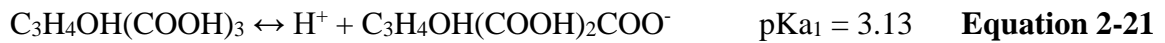
Selenate reduction to elemental selenium can also be biologically mediated under anaerobic conditions as seen in **Equation 2-20**.



The oxidation number of selenium in selenate is +6 and is reduced to 0, similarly to nitrate where N is being reduced from +5 to 0.<sup>67,69</sup> Nitrate reduction is favored more by bacterial degradation than selenate reduction because it takes less energy to go from +5 to 0 than +6 to 0. Therefore, it is predicted that nitrate will be reduced to a greater extent than selenate, but both reductions will occur. Selenate reduction will also produce alkalinity as nitrate reduction does and will be an indicator of removal. Selenate, like nitrate, can produce intermediate compounds between the reduction process to  $\text{Se}^0$ . Selenite ( $\text{SeO}_3^{2-}$  also known as Se(IV)) can occur if selenate reduction is incomplete. Selenite acts as a ligand like phosphate<sup>70</sup>, and in the case that incomplete selenate reduction occurs or selenite is present in the groundwater, a nitrate-selective ion exchange resin can be doped with  $\text{ZrO}_2$  (HAIX-NanoZr) to remove both compounds. Using the same citric acid carbon source, the reduction of selenate will be tested as a co-contaminant to nitrate.

### 2.2.2 Citric acid slow release for carbon dosing

The citric acid-loaded column is designed to release a quantity of carbon source (the electron donor) to completely reduce nitrate to nitrogen gas without excess wasted in the effluent as seen in traditional dosing of carbon sources in wastewater treatment. The following K values can be assigned to the equations representing citric acid chemistry.<sup>71</sup>



Although the ion exchange column is loaded with citric acid in the form of

$\text{C}_3\text{H}_4\text{OH}(\text{COOH})_3$  (where the  $\text{pH} < \text{pKa}_1$ ), the form entering the Metamateria column is

$\text{C}_3\text{H}_4\text{OH}(\text{COO}^-)_3$  because of the 20% dilution of the citric acid stream into the main

stream that has a pH of 7.5. With citrate as the electron donor<sup>72</sup>, the following half

reaction occurs where the carbon atoms in citrate get oxidized to a carbon dioxide form in

**Equation 2-24:**



The combined half reactions for the reduction of nitrate to nitrogen gas (Equation 2-19)

using citric acid as the carbon source (Equation 2-24) is shown in **Equation 2-25:**

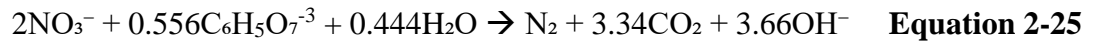


Comparing the nitrate reduction half reaction in Equation 2-19 to the combined half

reaction with citric acid in Equation 2-25, the presence of citric acid as the carbon source

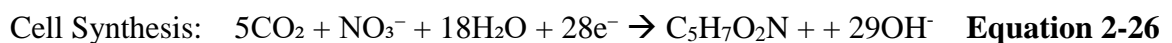
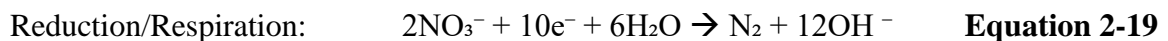
shows another benefit to the system. As Equation 2-19 shows, nitrate reduction to

nitrogen gas will cause an increase in pH due to the alkalinity produced in the process. Normalizing the two equations so they reduce the same amount of nitrate will look as follows:

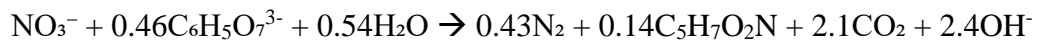


By adding citric acid as the electron donor, the increase in alkalinity is mitigated (i.e. OH<sup>-</sup> mole ratio decreases from 12 to 3.66). The decrease in alkalinity production will allow for a more pH stable system that does not need excessive pH adjustments as biological denitrification in wastewater treatment processes typically do.

Although Equation 2-25 shows a larger picture of nitrate reduction, it is still a simplified reaction without the consideration of microbial cell (C<sub>5</sub>H<sub>7</sub>O<sub>2</sub>N) synthesis.<sup>68,73</sup> For cells to completely reduce a compound, the carbon source generates electrons that are used by respiration (energy production) and cell synthesis reactions. In this case, nitrate is being reduced to nitrogen gas (Equation 2-19), nitrate also provides a nitrogen source for cell composition (**Equation 2-26**), and citric acid is the electron donor (Equation 2-24). These simultaneous occurrences can be demonstrated with the following reactions.



However, the equations are incomplete because the fractions of how much nitrate goes to nitrogen gas ( $F_R$ ) for respiration versus how much nitrate goes to the nitrogen source for cell synthesis ( $F_S$ ) has not been factored into Equation 2-19 and Equation 2-26. From the literature, these values can be roughly estimated as  $F_R = 0.75$  and  $F_S = 0.25$  based on denitrification studies done that capture nitrogen gas formed by nitrate reduction and nitrogen compositions found within bacterial sludge/biofilms.<sup>74-76</sup> By multiplying equation 2-19 by 0.75 and Equation 2-26 by 0.25 and then combining those two equations with Equation 2-24, the final reaction for denitrification with citric acid as a carbon source is shown in **Equation 2-27**:



**Equation 2-27**

With this new defined denitrification reaction, the C:N ratio becomes 2.76:1 for nitrate reduction to nitrogen gas. For design purposes and result analysis, this translates to a requirement of 1.41 mg/L citrate for every 1 mg/L nitrate removed.

Based on the influent nitrate concentration, a citric acid concentration requirement dosed to the system can be generated based on the C:N ratio. However, this system is releasing citric acid by exchanging anions with citric acid loaded onto the exchanger not by dosing the influent. By taking the total anion concentration in the influent water on an equivalents/L basis, we can calculate the total concentration of citric acid being released into solution (with a modest estimate of anions captured by the bed). By taking the concentration of citric acid needed for complete nitrate reduction ( $C_N$ ) and the



concentration of citric acid being released by the ion exchanger ( $C_R$ ), the fraction of the total flow for the bypass flowrate ( $F_{\text{bypass}}$ ) can be determined (**Equation 2-28**).

$$F_{\text{bypass}} = C_N/C_R \quad \text{Equation 2-28}$$

Influent nitrate concentrations will fluctuate at times within the groundwater sources and should be monitored to adjust this bypass flow accordingly.

### 2.2.3 Ion exchange polishing

The purpose of the nitrate-selective ion exchanger is for a polishing step: any nitrate that escapes the fixed-film column will be captured on the ion exchange resin and further decrease the effluent nitrate concentration as discussed in depth in Section 2.1.1. Because of the fast kinetics of ion exchange, the nitrate-selective resins can handle fluctuating parameters, such as concentration, flow, and temperature, as previous studies have already determined.<sup>46,77,78</sup> Biological denitrification is a slower process and changes in these parameters are not as easily mitigated. For example, considering temperature, bacterial growth is optimal between 20°C and 45 °C and freezing temperatures will inhibit growth.<sup>79</sup> Regarding concentration, without the stoichiometric amount of carbon source needed to degrade the compound of interest, bacteria cannot fully degrade the compound. A surge in concentration must be met with a stoichiometric increase in carbon source otherwise some of the compound will pass through. The ion exchange column will aim to mitigate these types of surges that can appear without notice in groundwater.

The purpose of the BIO-NIX system is to combine the kinetics of both processes with the sustainable removal of nitrate to nitrogen gas without use of brine. However, a nitrate-selective anion exchanger is employed in the process and needs to be regenerated

once the bed is exhausted. The BIO-NIX system mitigates the need for brine regeneration as well with the combined columns. **Figure 2-9** below lays out the reason behind the nitrate-selective resin’s ability to regenerate itself safely.

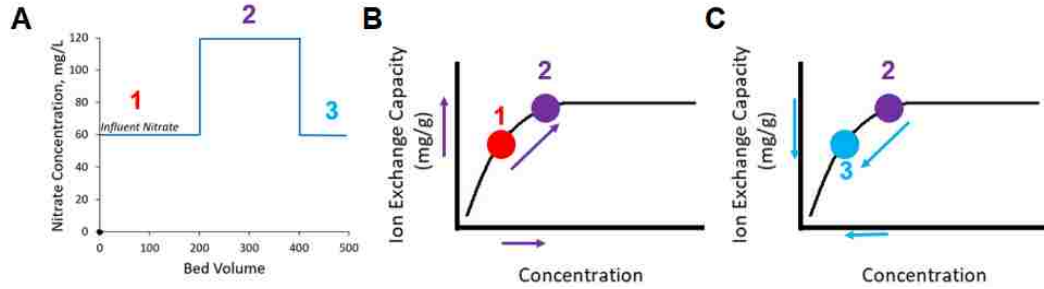
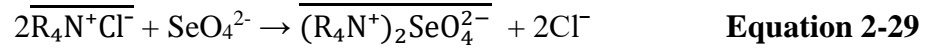


**Figure 2-9.** Steps for self-regeneration of the nitrate-selective ion exchange resin.

Looking to the influent concentration graph in **Figure 2-9A**, the concentration labeled “1” flows into the ion exchange column and has a corresponding capacity (**Figure 2-9B**). The capacity curve shown in Figure 2-9B is standard for a *favorable* capacity curve as a function of concentration that follows a Langmuir isotherm model.<sup>33</sup> As the concentration increases to “2”, following the capacity curve, the ion exchange capacity increases. An increase in capacity means the ion exchange resin can take up more nitrate now. As the concentration then dips back down to concentration “3”, the capacity (**Figure 2-9C**) decreases at the return to a lower concentration. A decrease in capacity will result in a slow release of nitrate from the resin, allowing self-regeneration and still maintaining levels below the MCL. This phenomenon is also significant in that whenever nitrate passes through the fixed-film column without degradation during a surge, the ion exchanger will also increase in capacity and take up more nitrate. Intermittent regeneration with NaCl can be carried out for total regeneration, if necessary.

Selenate also experiences ion exchange,<sup>80</sup> and the SBA's exchange reaction for selenate with a chloride-loaded resin is shown in **Equation 2-29** below:



If the groundwater is simultaneously contaminated with nitrate and selenate, the nitrate-selective resin will favor nitrate and still remove selenate during this polishing step. Note that selenate concentrations found in groundwater are typically much lower than nitrate (i.e. <1 mg/L selenate) so between the fixed-film column and the ion exchange column both compounds can be removed simultaneously.

#### 2.2.4 Modification of BIO-NIX for ion exchange brine regeneration

As previously mentioned, nitrate-selective ion exchangers are the most employed technology for nitrate removal in water treatment facilities and are regenerated with a 10-15% NaCl brine. Another alternative to disposal of brine waste is application of the BIO-NIX fundamentals to treat the highly concentrated nitrate brine waste. The overall process has been modified from the groundwater treatment process and can be seen in **Figure 2-10** below.

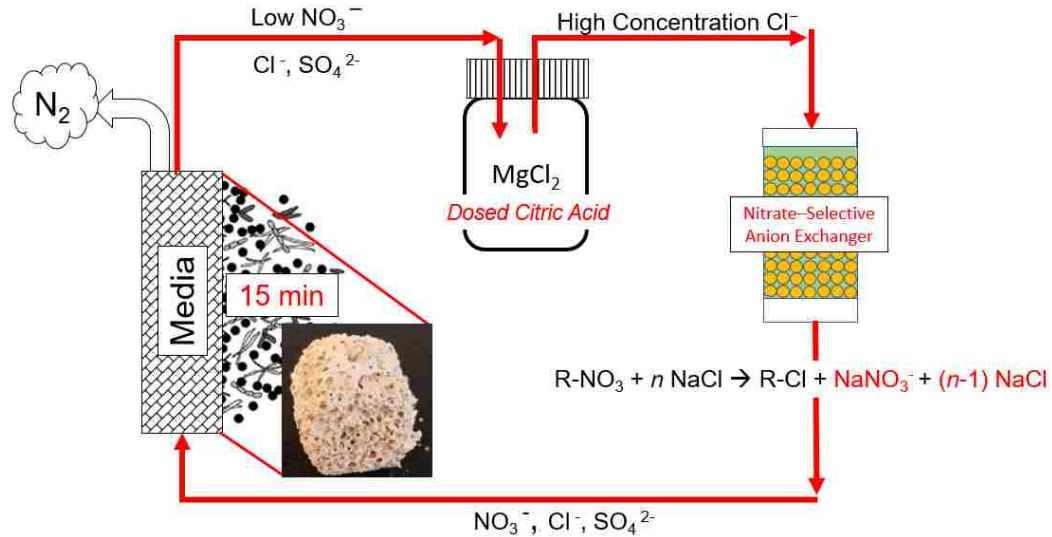


**Figure 2-10.** BIO-RNIX regeneration system schematic.

The BIO-RNIX regeneration system starts with a high concentration brine of  $MgCl_2$  ( $Mg^{2+}$  to further promote bacterial growth<sup>81</sup>) dosed with a carbon source (in this case, citric acid) that has been stoichiometrically (2.76C:1N) added based on the nitrate loaded onto the ion exchanger. The brine is dosed at a higher concentration than the expected nitrate quantity loaded onto the bed to promote expulsion of nitrate from the bed. This follows **Equation 2-30** below that shows a more realistic representation of nitrate regeneration with chloride brine.<sup>18</sup>



Equation 2-30 demonstrates the need for a high concentration brine of 10-15% NaCl typically used to remove nitrate from the bed instead of a 1:1  $Cl^-$  to  $NO_3^-$  ratio.

As the brine is circulated to the exhausted nitrate-selective anion exchanger, nitrate gets expelled from the bed in place of chloride ions. Released nitrate flows from the ion exchanger to the fixed-film bed, where biological denitrification occurs, and

nitrate gets reduced to nitrogen gas. The regenerant solution, now consisting of little to no nitrate, can flow back to the ion exchange column to continue the expulsion of nitrate and its delivery to the fixed-film column to be reduced to nitrogen gas. Once the ion exchanger is regenerated (i.e. effluent nitrate concentration from the ion exchanger is near-zero), the brine that is free of nitrate can be kept for subsequent regenerations. Note that if selenate is present in the feedwater as well and is removed via ion exchanger, this process can also regenerate selenate on the bed and remove selenate from the brine to  $Se^0$ .

## CHAPTER 3: Experimental Materials and Methods

### 3.1 Sources of influent water for column runs

The HIX-NP process is validated in this study using real secondary wastewater to simulate the influent of treated wastewater fed to a water reclamation plant prior to RO. The BIO-NIX process examines contaminated groundwater using a synthesized groundwater influent that was created based on a real nitrate-contaminated groundwater source.

#### 3.1.1 Bethlehem secondary wastewater

The secondary wastewater for the HIX-NP column runs was taken from a 50 L batch sample from the Bethlehem Wastewater Treatment Plant (WWTP) in Bethlehem, PA that was filtered through an 11  $\mu\text{m}$  filter and stored in the refrigerator at 4°C prior to the runs. The Bethlehem WWTP is shown below in **Figure 3-1**.



**Figure 3-1.** Satellite view of the Bethlehem WWTP in Bethlehem, PA (40°37'03.5"N 75°20'00.2"W).<sup>82</sup>

The Bethlehem WWTP is approximately 3 miles from the Lehigh University campus. Note that the plant has a 10 MGD inflow and nitrate, phosphorus, and hardness are not specifically targeted for treatment at this plant, so they are naturally present in the secondary wastewater effluent. Each column run will specify the influent composition used for that run, however, note that the ranges for these elements are as follows: 2-5 mg/L P, 75-120 mg/L NO<sub>3</sub><sup>-</sup>, 43-55 mg/L Ca<sup>2+</sup>.

### 3.1.2 Manheim nitrate-contaminated groundwater

Manheim, Pennsylvania is approximately 79 miles from Lehigh University's campus located in Lancaster County. The Manheim area and its water treatment facility are surrounded by farmland as shown below in **Figure 3-2**.



**Figure 3-2.** A satellite view of the water treatment facility's location in Manheim, Pennsylvania (306 Doe Run Road) surrounded by farmland.<sup>83</sup>

The Manheim area utilizes groundwater as their main source for drinking water. The large presence of farmland surrounding the water treatment facility as well as the larger

Lancaster County attributes to the nitrate contamination of its groundwater source. With a daily influent of approximately 257,000 gallons per day, the water treatment facility has an average influent nitrate concentration of 54 mg/L  $\text{NO}_3^-$  (or 12 mg/L N- $\text{NO}_3^-$ ) which is just above the MCL of 45 mg/L  $\text{NO}_3^-$ . The plant utilizes a nitrate-selective anion exchanger for removal down to 5 mg/L  $\text{NO}_3^-$  and 10% NaCl for regeneration. The average composition of the influent provided by the plant is: 7.4 pH, 370 mg/L TDS, 170 mg/L alkalinity as  $\text{CaCO}_3$ , 92 mg/L  $\text{Ca}^{2+}$ , 54 mg/L  $\text{NO}_3^-$ , 35 mg/L  $\text{Cl}^-$ .

Based on these values provided by the Manheim water treatment facility, we have created synthesized groundwater contaminated with nitrate to simulate the real contaminated groundwater source and applied competing ions for further testing and analysis. A 120 L batch of synthesized groundwater was generated using DI water and the composition is as follows: 60 mg/L  $\text{NO}_3^-$ , 40 mg/L  $\text{Cl}^-$ , 40 mg/L  $\text{SO}_4^{2-}$ , 150 mg/L  $\text{HCO}_3^-$ , 100 mg/L  $\text{Ca}^{2+}$ , and approximately 510 mg/L TDS with a pH of 7.5. Influent samples were taken before each column run to verify these values.

## 3.2 Experimental set-up

### 3.2.1 HIX-NP column runs

Fixed-bed column runs for the HIX-NP system were carried out using a bench-top scaffold manufactured by Swagelok at Allentown, PA with two 300 mL stainless steel columns and one 10 L  $\text{CO}_2$  regeneration tank (designed to withstand pressure up to 20 bar from a high-pressure cylinder of carbon dioxide that was provided by Airgas). A photograph of the schematic of the bench-top system is shown in **Figure 3-3**.



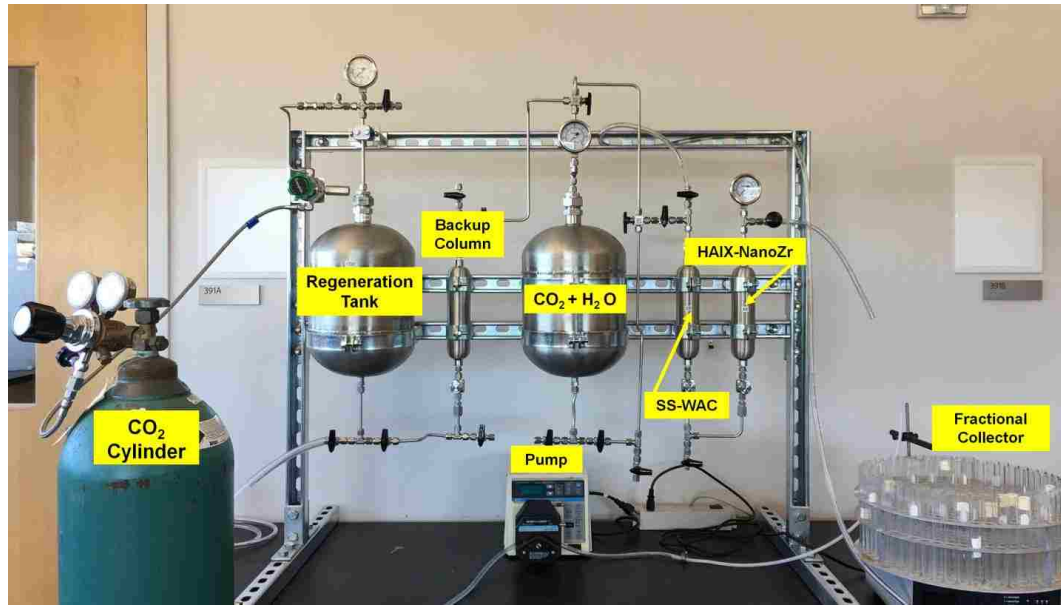


**Figure 3-3.** Two column bench-top stainless-steel setup for the HIX-NP process with a CO<sub>2</sub> regeneration system.

An extra backup column and regeneration tank are also included within the column set-up along with a constant flow rate pump (Masterflex) used to control the flow of the influent stream and a fractional collector (Eldex) used to capture effluent samples. The empty bed contact time and superficial liquid velocity were recorded for each run and remained constant throughout multiple cycles at 5 minutes and 0.60 m/hr respectively. Each column run will be measured in material or resin volume used, which is called one bed volume (BV).

For the WAC regenerant solution, carbon dioxide is sparged in water using a diffuser with micropores placed within the regeneration tank (**Figure 3-4**).



**Figure 3-4.** A diffuser (left) placed within the regeneration tank to sparge carbon dioxide efficiently in water as the regenerant solution.<sup>18</sup>

When the diffuser is connected to the carbon dioxide inlet tube, carbon dioxide turns into microbubbles and as a result increases the carbon dioxide dissolving rate for improved regeneration efficiency. Note that the pressure inside the regeneration tank provides the driving force for the flow. Finally, a 2% KOH solution for runs slowly through the HAIX-NanoZr column only (at a 15 minute empty bed contact time) for regeneration and the regenerant solution is collected for analysis.

### 3.2.2 *BIO-NIX groundwater system*

The BIO-NIX system contains three glass columns: a citric-acid loaded anion exchanger that has a bypass line for reduced flow, a fixed-film media (Metamateria) column for biological denitrification, and a nitrate-selective anion exchanger (Purolite A520E) as shown in **Figure 3-5**.

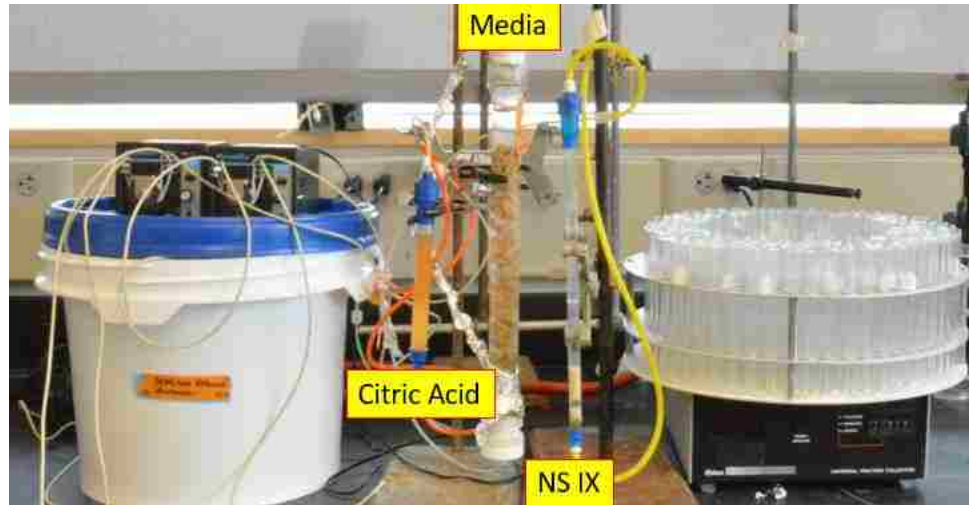


**Figure 3-5.** BIO-NIX system set-up.

The citric acid-loaded column is a Kontes flex column (diameter: 1 cm; length: 15 cm), the Media column consisted is a glass column (ACE Glassware, diameter: 2.5 cm; length: 30 cm) and the NS IX (ion exchange) column is a Kontes flex column (diameter: 0.5 cm; length: 30 cm). A constant flow rate pump (Masterflex) feeds synthetic groundwater to the 20 mL citric acid-loaded anion exchange column at 20% of the total flow rate in the effluent. At the same time, another constant flow rate pump feeds the other 80% of the total flow to a main line, in which the 20% effluent flow from the citric acid column meets up with the 80% of the main line flow to feed influent synthesized groundwater dosed with citric acid to the fixed-film column (20 mL, labeled Media in Figure 3-5). Water flow then proceeds through the Media column and subsequently to the nitrate-selective anion exchanger (5 mL), in which the effluent is then collected by a fractional collector (Eldex). Samples were taken after the citric acid column and following the Media column as well.

The empty bed contact time (EBCT) was recorded for each column for each run and remained constant throughout multiple runs. The EBCT for each column is as

follows: the citric acid-loaded column had an EBCT of 60 minutes at 20% of the total flow rate, the Media column had an EBCT of 15 minutes with total flow running through, and the nitrate-selective ion exchanger had an EBCT of 5 minutes with total flow running through. Citric acid was intermittently reloaded onto the citric-loaded anion exchanger with 1% citric acid for 5 bed volumes. Note that denitrifying bacteria (*Pseudomonas Putida*) were loaded onto the “Media” column prior to any runs. This was completed by taking a 1 mL defrosted sample of bacteria, mixing it with a 400 mL batch of the synthetic wastewater that was dosed with 200 mg/L  $\text{NO}_3^-$  and 300 mg/L citric acid with pH adjustment to pH 7.2 with 1 M NaOH solution, and letting the solution recirculate throughout the Media bed for 48 hours. The Media column was gently rinsed of this solution with tap water prior to the runs.

### *3.2.3 BIO-RNIX brine regeneration runs*

The BIO-RNIX system is comprised of a nitrate-selective anion exchanger (5 mL, Purolite A520E) pre-exhausted by wastewater runs and a Media column (20 mL) as described above. The BIO-RNIX system recirculates 0.8%  $\text{MgCl}_2$  solution (200 mL dosed with 0.2% citric acid for stoichiometric reduction of nitrate) through the ion exchanger, then follows to the Media column, and returns to the batch solution (labeled “Regen Brine”) which can be seen in **Figure 3-6**.

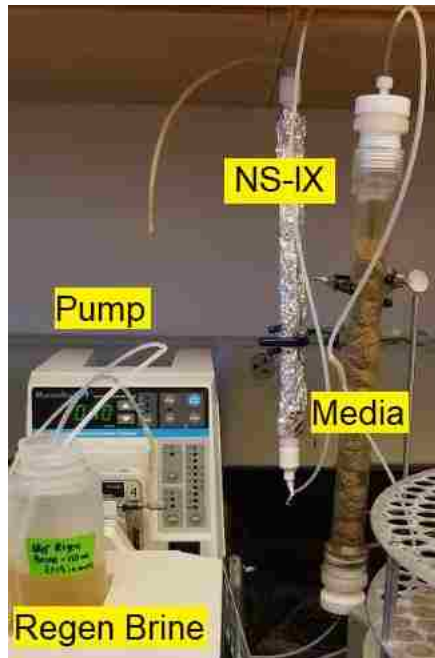


**Figure 3-6.** BIO-RNIX system set-up.

Both columns are glass columns by ACE Glassware (NS-IX column: 1 cm diameter, 30 cm length; Media column: 2.5 cm diameter, 30 cm length). The EBCT for the ion exchange column is 5 minutes and the Media column is 15 minutes, remaining constant throughout each run. Samples were taken following the Media column. Note that the ion exchange column in Figure 3-6 is covered in aluminum foil to negate any algae formation (which is also done for the Media column).

Bacteria was loaded to the Media column prior to the runs with *Pseudomonas Putida*. This was completed by taking a 1 mL defrosted sample of bacteria, mixing it with a 500 mL batch of the  $MgCl_2$  solution to acclimate the bacteria to the high salinity conditions, and dosing that batch with 1000 mg/L  $NO_3^-$  and 1400 mg/L citric acid with pH adjustment to pH 7.2 with 1 M NaOH solution. The higher concentration of nitrate dosed to the batch during bacteria loading reflects the conditions that will ensue during

regeneration of the ion exchange column that enter the Media column. The mixed batch solution recirculates throughout the Media bed for 48 hours.

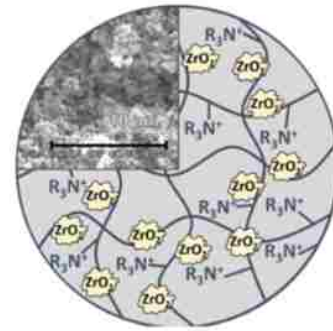
### 3.3 Materials

#### 3.3.1 HAIX-NanoZr synthesis

Purolite Co. provided macroporous strong base A520E that serve as the nitrate-selective anion exchange resin base comprising the HAIX-NanoZr resin, and characteristics are shown below in **Table 3-1**.<sup>84</sup>

**Table 3-1.** Purolite A520E Characteristics

Resin:	Purolite A520E
Manufacturer:	Purolite Co.
Characteristic:	Strong base anion exchanger
Functional Group:	Tributyl quaternary ammonium Type I: $-N^+((CH_2)_3CH_3)_3$
Matrix:	Polystyrene-divinylbenzene, macroporous
Capacity:	0.9 eq/L



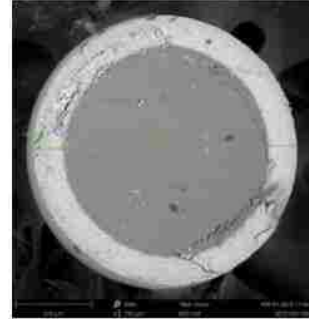
These resins have a diameter range of 300-1200  $\mu\text{m}$ . Purolite A520E was loaded with zirconium oxide in accordance with the following procedure: 1) produce a 15% (w/v)  $\text{ZrO}_2$  solution (using waste zirconium oxide) with either 10% sulfuric acid or 20%  $\text{H}_2\text{SO}_4$  with methanol at a 50:50 ratio (note: methanol decreases the dielectric constant); 2) mix the nitrate selective resin beads in the  $\text{ZrO}_2$  solution for 15 hours; 3) decant and dry the resin; 4) mix the dry resin with equal volume 5%  $\text{NaOH}$ .<sup>50,85</sup>

### 3.3.2 SS-WAC

For the SS-WAC column, SSTC104 resins with carboxylic acid functional groups were used and their characteristics are shown below in **Table 3-2**.<sup>86</sup>

**Table 3-2.** SS-WAC Resin Characteristics

Resin:	Purolite SSTC104
Manufacturer:	Purolite Co.
Characteristic:	Weak acid cation exchanger
Functional Group:	Carboxylic acid: <b>-COOH</b>
Matrix:	Polyacrylic, macroporous
Capacity:	4.7 eq/L



With a spherical shape and a functionalized outer core (designated by the lighter shading of the SS-WAC resin's outer edge in Table 3-2), the resins were manufactured to increase generic regeneration efficiency issues. Note that the outer edge of the resin only had a depth around 100  $\mu\text{m}$  as opposed to the entire cross section of the resin that ranges from 500-1200  $\mu\text{m}$ .

### 3.3.3 Citric acid-loaded resins

The citric acid-loaded resins consist of a regular, macroporous SBA in chloride form, Purolite A400, provided by Purolite. Characteristics of A400 are provided below in **Table 3-3**.<sup>87</sup>



**Table 3-3.** Purolite A400 Characteristics

Resin:	Purolite A400
Manufacturer:	Purolite Co.
Characteristic:	Strong base anion exchanger
Functional Group:	Tributyl quaternary ammonium Type I: $-R_4N^+$
Matrix:	Polystyrene-divinylbenzene, macroporous
Capacity:	1.3 eq/L

A400 resins were placed in a column (Kontes flex column, 1 cm diameter, 15 cm length) and a 100 mL solution of 3% citric acid solution was slowly rinsed through the bed at a 20 min EBCT. The column was then rinsed with 50 mL tap water at a 10 min EBCT.

### 3.3.4 Metamateria for fixed-film media

The material used for the media in the fixed-film column of both the BIO-NIX and BIO-RNIX processes is a ceramic material called Metamateria (and will be referenced as so instead of Media from this point forward). The properties and characteristics that make this material appropriate for denitrifying bacteria attachment are shown below in **Table 3-4**.<sup>88</sup>

**Table 3-4.** Metamateria Properties

Characteristics:	Value:
Diameter (average)	1.6 cm
Bacteria concentration (1-layer)	2 kg microbes per m <sup>3</sup>
Surface area	2,000,000 m <sup>2</sup> /m <sup>3</sup>
Denitrification rate	5 kg NO <sub>3</sub> /m <sup>3</sup> /day
ORP	+50 mV to -100 mV





The Metamateria (specified as Metamateria BIO-DN cubes) was provided by MetaMateria and chosen for its ability to attach denitrifying bacteria specifically. Its high porosity provides a large surface area for a bacterial biofilm to form and its surface allows for high denitrification rates with an oxidation-reduction potential (ORP) within denitrification range. Tests have been conducted by MetaMateria to validate the above characteristics.

### **3.4 Analytical methods**

#### *3.4.1 Influent and effluent composition analysis*

Phosphorus and selenium were analyzed using a Perkin Elmer Optima 2100DV ICP-OES. Calcium, magnesium, and potassium were analyzed by a Perkin Elmer AAnalyst200 Atomic Absorption Spectrometer (AAS). Nitrate, sulfate, and chloride were measured using the Dionex Ion Chromatography (ICS-1000) with an IonPac® AS14 column. Alkalinity was measured by titration with 0.02 N sulfuric acid. Conductivity was measured using a handheld accumet conductivity meter, Model # AP75. pH was measured using accumet XL15 pH meter from Fisher Scientific. ORP was measured with a Hach HQ11d ORP meter. Ibuprofen and citrate were analyzed using a Hach DR 5000 Benchtop UV-VIS Spectrophotometer at 272 nm and 287 nm respectively.

#### *3.4.2 Zeta potential*

Zeta potential and the zero point charge (ZPC) for zirconium oxide precipitates were measured using the Malvern Zetasizer Nano ZS with MPT-2 Titrator using  $\text{NaNO}_3$  at 0.1M ionic strength.<sup>50</sup>

### 3.4.3 Scanning electron microscopy

To characterize the distribution of elements throughout both WAC and HAIX-NanoZr resins between service and regeneration cycles, cross sections of the beads (exhausted and regenerated) were prepared by microtomy and then analyzed by scanning electron microscopy (Model Hitachi JSM-4300) with energy dispersive x-ray (SEM-EDX) spectroscopy.

## CHAPTER 4: Results and Discussion of HIX-NP and its Effectiveness as a Pretreatment to RO

### 4.1 Validation of pH dependency for P removal by HAIX-NanoZr

Figure 4-1A shows pH effects of two separate experimental results superimposed in the same plot: zeta potential of hydrated zirconium oxide (HZrO) particles and phosphate removal capacity of HAIX-NanoZr.

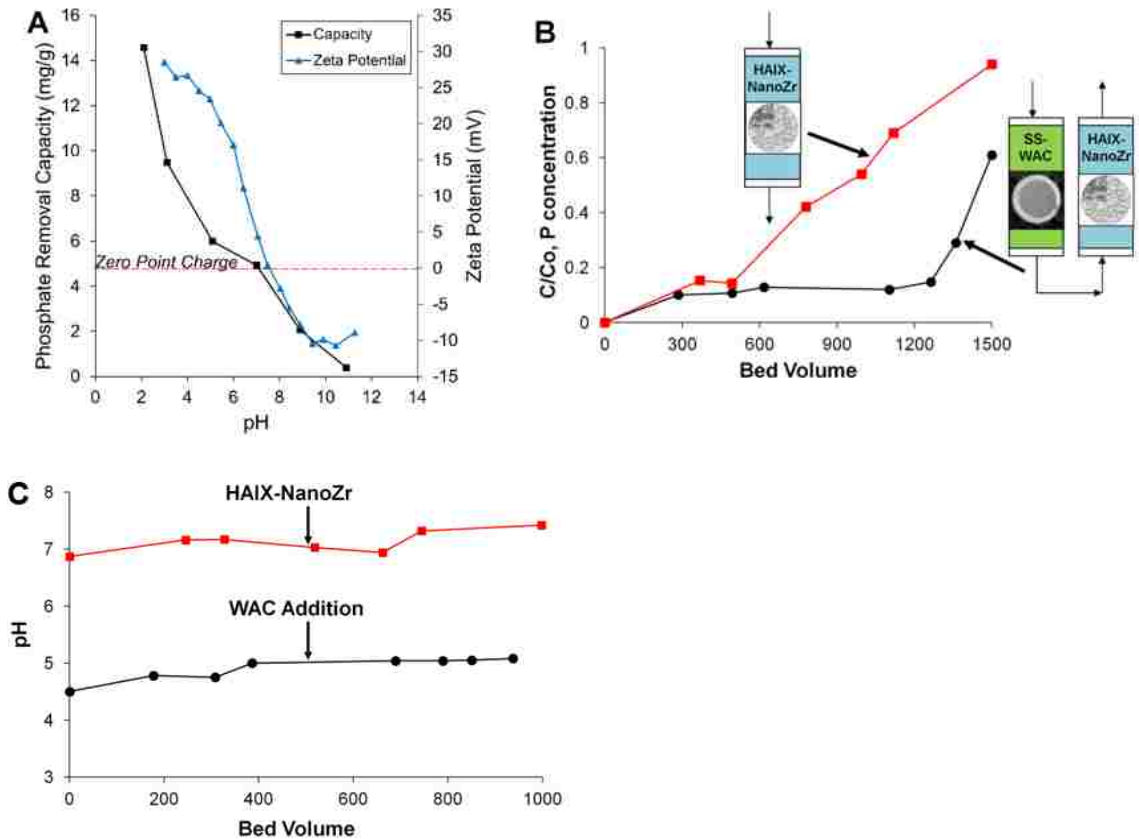


**Figure 4-1.** (A) Phosphorus removal capacity of HAIX-NanoZr and zeta potential of the hydrated zirconium oxide particles as a function of pH; (B) Comparison of phosphate effluent histories and (C) pH effluent values from i) HAIX-NanoZr column alone and ii) SS-WAC column followed by HAIX-NanoZr fed with Bethlehem secondary wastewater. (Influent composition: 5 mg/L P, 65 mg/L  $\text{NO}_3^-$ , 32 mg/L  $\text{SO}_4^{2-}$ , 83 mg/L  $\text{Cl}^-$ , 48 mg/L  $\text{Ca}^{2+}$ , 487 mg/L TDS, pH 7.1)

It is apparent that both zeta potential (positive mV) and P removal capacity exhibited identical effects of pH, i.e., both increased with a decrease in pH. Thus, an engineered process operated at pH around 4.0-4.5 would result in substantially higher P removal capacity. At the same time, an increase in pH, especially at  $\text{pH} \geq 11$ , will completely desorb P in agreement with Figure 4-1A. Note that the pH of the zero point charge lies around 8.0 in agreement with information in the literature.<sup>52</sup>

Two separate column runs were carried out using secondary wastewater from the Bethlehem plant. In one run, a single column with HAIX-NanoZr was used alone and for the other HAIX-NanoZr was preceded by SS-WAC in agreement with the process schematic. **Figure 4-1B** presents a comparison of the performance of the columns under otherwise identical conditions. Note that significantly higher phosphate removal was accomplished by placing a SS-WAC column ahead of HAIX-NanoZr, all other conditions including the feed wastewater composition remaining identical. While 20% phosphate breakthrough (i.e.,  $C/C_0 = 0.2$ ) occurred at approximately 400 bed volumes for HAIX-NanoZr alone, over 1200 bed volumes of wastewater were treated for an identical phosphate breakthrough for the combined SS-WAC and HAIX-NanoZr system. **Figure 4-1C** shows that the pH after the SS-WAC column was consistently between 4.0 and 5.0 resulting in higher phosphate removal capacity by HAIX-NanoZr.

## 4.2 Nutrient removal and recovery by HAIX-NanoZr

### 4.2.1 Multiple runs of HAIX-NanoZr

**Figures 4-2** show effluent histories of P and nitrate for three consecutive column runs using secondary wastewater from the Bethlehem plant, where phosphate and nitrate are simultaneously removed by the HAIX-NanoZr with dual functional groups.

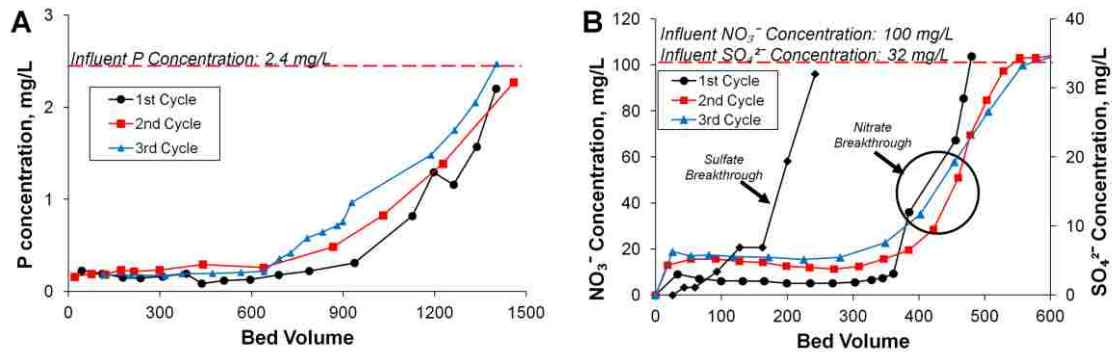


**Figure 4-2.** Three successive effluent history plots of (A) phosphorus and (B) nitrate- with one sulfate effluent history curve for comparison- using secondary wastewater from the Bethlehem Wastewater Treatment Plant in Bethlehem, PA. (Influent composition: 2.4 mg/L P, 100 mg/L NO<sub>3</sub><sup>-</sup>, 32 mg/L SO<sub>4</sub><sup>2-</sup>, 69 mg/L Cl<sup>-</sup>, 50 mg/L Ca<sup>2+</sup>, 466 mg/L TDS, pH 7.0.)

Phosphorus and nitrate effluent histories were nearly the same for three consecutive cycles confirming the long-term sustainability of the process. Even in the presence of much higher concentrations of sulfate and chloride, **Figure 4-2A** demonstrates that phosphate removal was quite selective, and less than 10% P broke through after 800 bed volumes of treatment of the feed wastewater. Suppression of pH in turn enhanced phosphate removal capacity by the WAC. **Figure 4-2B** shows that sulfate broke through before nitrate confirming higher nitrate selectivity over sulfate. Nitrate also achieved >95% removal until breakthrough around 400 BV. Note that more nitrate-selective resins can be added to the column without loading of ZrO<sub>2</sub> to achieve the same breakthrough for P and NO<sub>3</sub><sup>-</sup>. Samples

of wastewater feed and treated water were collected after 200 bed volumes and **Figure 4-3** shows their concentrations.

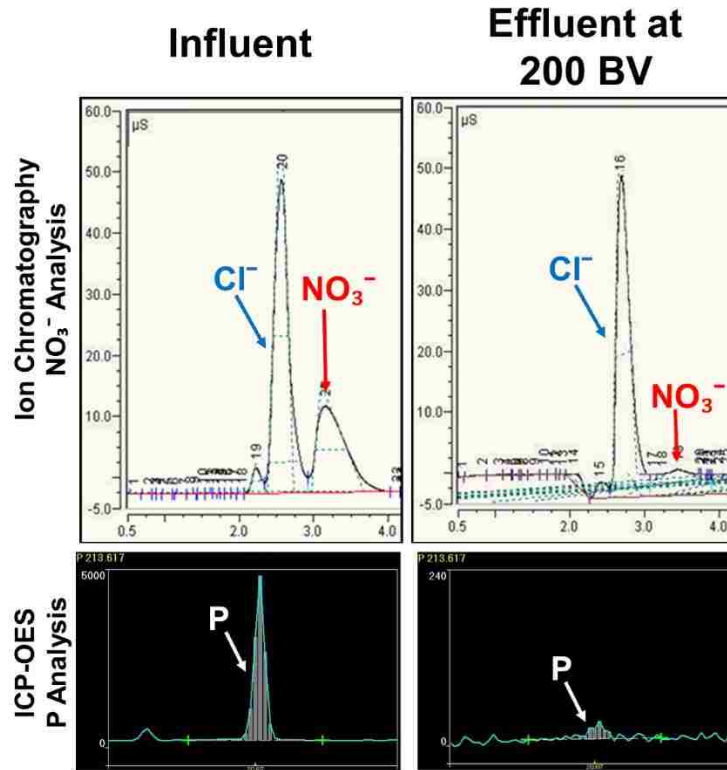


**Figure 4-3.** A comparison of nitrate and phosphorus in the influent (left) to their effluent concentrations at 200 bed volumes (right).

Note that the removal of nutrients namely, phosphate and nitrate, are nearly complete compared to their concentrations in the feed.

Looking back at Figure 4-1A, the phosphate capacity generated at around pH 4.5 is 7.5 mg P/g HAIX-NanoZr. This value can be compared to the phosphate capacity generated from Figure 4-2A from the first run of HIX-NP. The phosphate capacity from the effluent history curve is generated by taking the area between the influent line at 2.4 mg/L P and the effluent history curve, showing how much P was taken up by HAIX-NanoZr during that run. HIX-NP's phosphate capacity is calculated at 6.9 mg P/g HAIX-NanoZr. The two

capacity values generated are very close in value to each other, and the higher capacity found in Figure 4-1A can be explained by the background concentration of the batch tests. The background concentration in Figure 4-1A had a lower total anion concentration and a higher P concentration resulting in an increase in capacity as opposed to Figure 4-2A.

#### 4.2.2 Regeneration and recovery of N and P

After each cycle, the HAIX-NanoZr column was regenerated with 2% KOH and **Figures 4-4A and 4-4B** show phosphate and nitrate elution profiles for three consecutive cycles during regeneration.

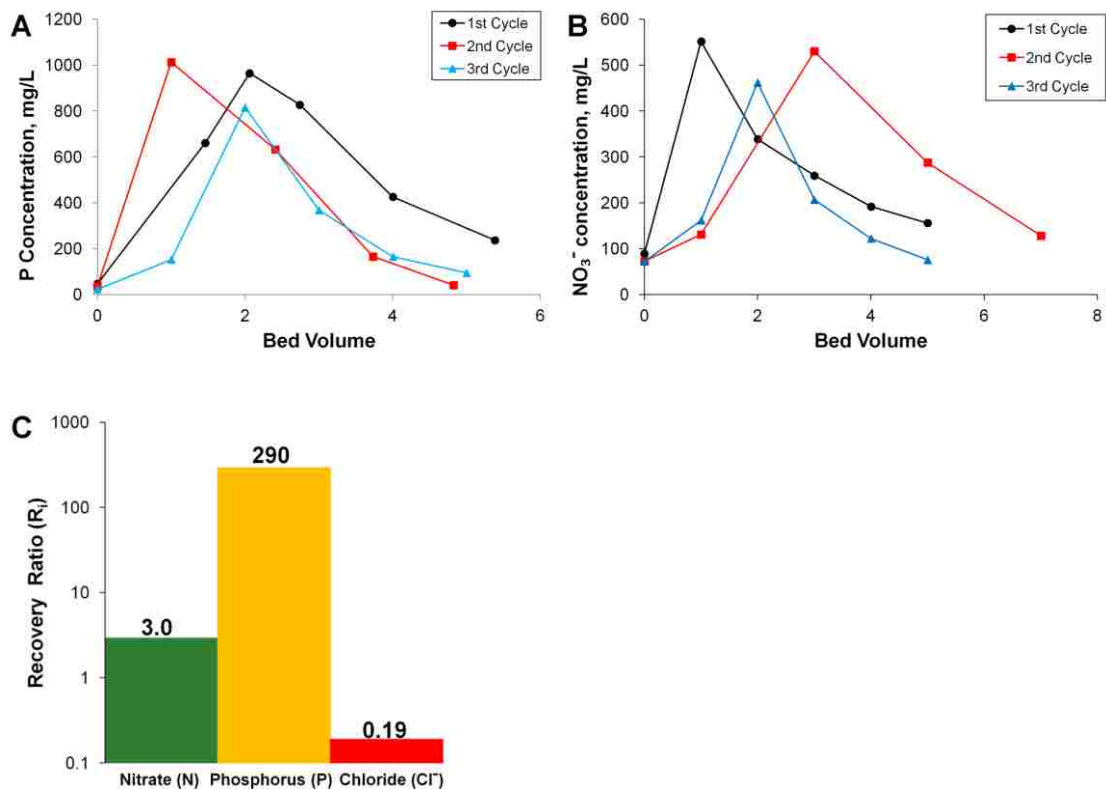


**Figure 4-4.** Three successive regeneration elution curves of (A) phosphorus and (B) nitrate using KOH as the regenerant solution. (C) Recovery factors of N, P and Cl in the spent regenerant.

In less than eight bed volumes, more than 90% recovery of phosphate and nitrate were accomplished; the spent regenerant contained primarily N, P, and K, three critical elements for an efficient fertilizer. The observation that phosphate and nitrate effluent histories remained nearly identical for three successive column runs as shown in Figures 4-4A and 4-4B demonstrates that the sorption-desorption cycle of HAIX-NanoZr is sustainable for long-term application.

In order to further assess the effectiveness of N and P recovery, a recovery factor,  $R_i$ , was calculated for anions of interest shown in **Equation 4-1**;  $R_i$  is the dimensionless ratio of concentrations of N, P or chloride (Cl) in the concentrated regenerant over their concentrations in the secondary wastewater from the Bethlehem plant i.e.,

$$R_i = \frac{C_i^R}{C_i^F} \quad \text{Equation 4-1}$$

where  $C_i^R$  and  $C_i^F$  are the concentrations of element “i” in the regenerant solution and the feed water respectively. **Figure 4-4C** shows  $R_N$  and  $R_P$  values for three consecutive cycles along with  $R_{Cl}$ . Significantly greater than unity values for  $R_N$  and  $R_P$  demonstrate that they are well concentrated in the recovered regenerant. In contrast,  $R_{Cl}$  values are much lower than unity signifying P and N are the most predominant species in the recovered regenerant.

In an attempt to reconcile the experimental data with the scientific hypothesis of phosphate sorption, slices of both parent and exhausted HAIX-NanoZr were characterized as shown in **Figure 4-5** by SEM-EDX mapping which shows i) Zr in the parent bead; ii) P in the exhausted bead and iii) chloride in the exhausted bead.



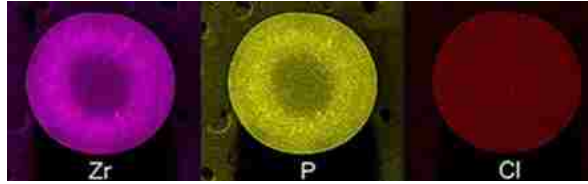


**Figure 4-5.** SEM-EDX maps of Zr from a parent HAIX-NanoZr resin bead and of P and Cl from an exhausted bead.

Note that the presence of Zr in the parent resin and P in the exhausted resin merge with each other implying phosphate is adsorbed almost solely by zirconium oxide nanoparticles irreversibly dispersed within the anion exchange resin. On the contrary, chloride is distributed throughout the bead, thus confirming that quaternary ammonium groups of the parent anion exchanger are the primary sorption sites for chloride anions. Throughout all service and regeneration runs, no Zr leakage was detected.

#### 4.2.3 Precipitation of N-P-K regenerant

The concentrated N-P-K regenerant described in Figure 4-4C can be tailored to the N:P:K ratios needed for a specific fertilizer. Most wastewater treatment technologies for phosphate recovery focus on precipitation as struvite ( $\text{NH}_4\text{MgPO}_4$ ). **Figure 4-6A** below shows an Imhoff cone containing the successive addition of  $\text{MgCl}_2$  to the concentrated regenerant to form a precipitated fertilizer.

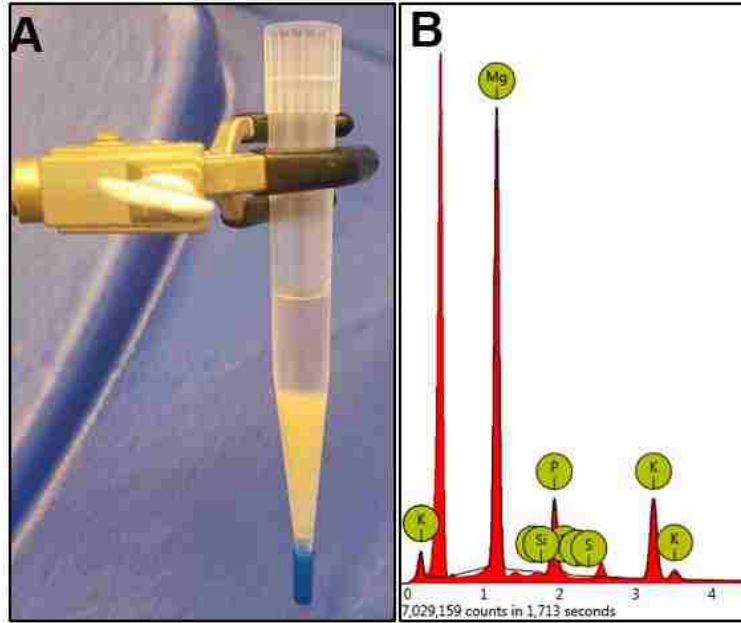


**Figure 4-6.** (A) Imhoff cone of precipitated N-P-K fertilizer by  $MgCl_2$  addition. (B) SEM-EDX analysis of the solid formed in the Imhoff cone (SEM conditions: FOV at 153  $\mu m$ , 15kV Point, BSD Full detector).

Through SEM-EDX, the x-ray analysis in **Figure 4-6B** shows that the precipitate is concentrated in Mg, P, and K. N is not present due to restrictions on EDX mapping capabilities of the SEM. Note that S was also analyzed, and no significant peak was found, again showing the selectivity of N and P over sulfate. Further analysis was conducted on the precipitated regenerant through EDX mapping and the result is shown below in **Figure 4-7A**.

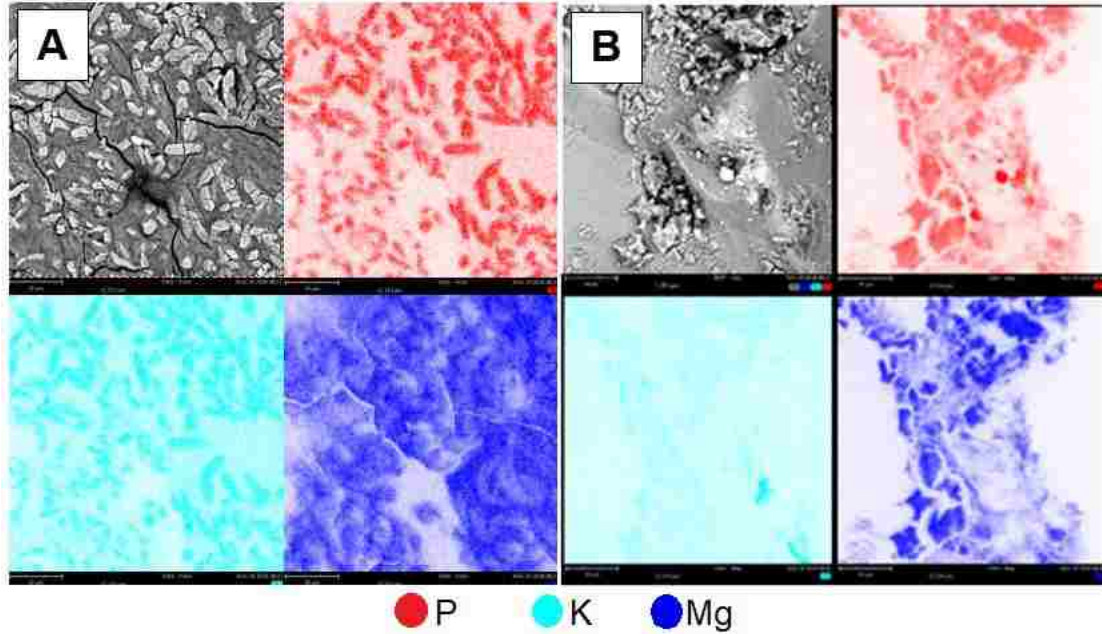


**Figure 4-7.** (A) SEM-EDX mapping of the solid formed in the Imhoff cone at (A) pH 9 and (B) pH 6.5. (SEM conditions: FOV at 153  $\mu\text{m}$ , 15kV Point, BSD Full detector)

The precipitate formed in Figure 4-7A concluded successive addition of  $\text{MgCl}_2$  at pH 9. The EDX map of this precipitate shows that at pH 9, the N-P-K-Mg precipitate forms a base of MgO while P and K are linked. **Figure 4-7B** shows the same regenerant solution precipitated at pH 6.5. The main bond is now between P and Mg, now that the pH is too low for MgO formation.<sup>89</sup> Based on the nutrient requirements for specific fertilizers needed by agriculture, the concentrated regenerant solution can precipitate as a solid fertilizer and can be tailored to P-K fertilizer versus P-Mg fertilizer with pH considerations.

### 4.3 SS-WAC performance

#### 4.3.1 Hardness removal by SS-WAC

Calcium is removed in the first SS-WAC column and the calcium effluent histories are shown in **Figure 4-8A** below.

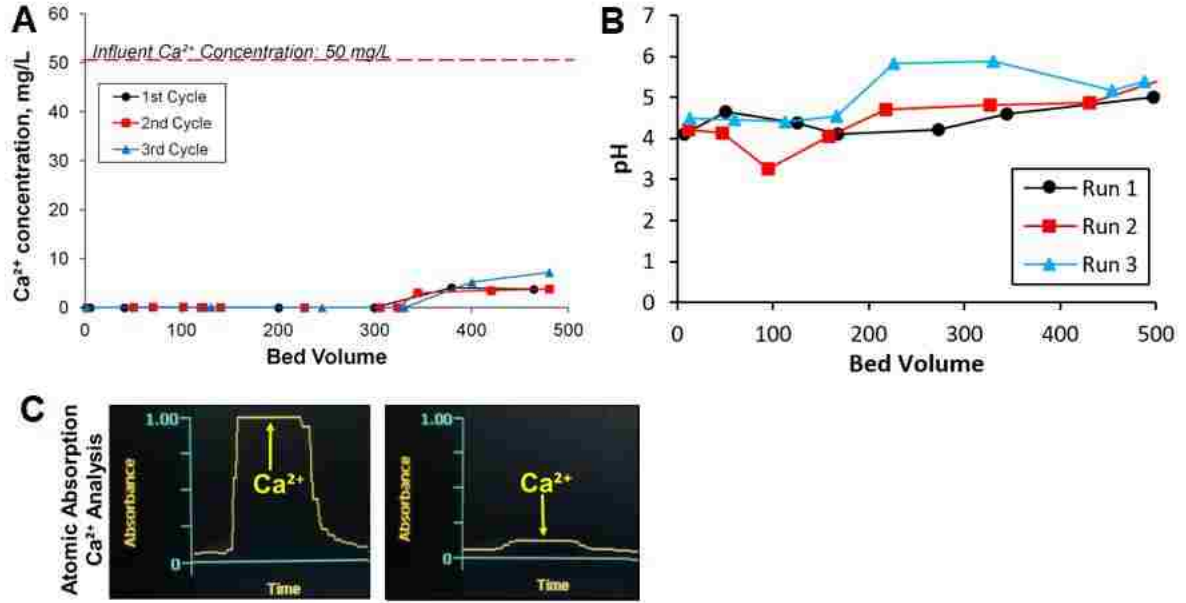
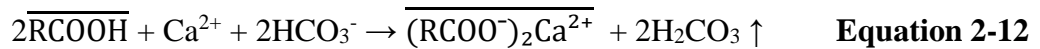


**Figure 4-8.** Three successive effluent history plots of (A) calcium and (B) pH using secondary wastewater from the Bethlehem Wastewater Treatment Plant in Bethlehem, PA. (C) Calcium in the influent (left) compared to the effluent concentrations at 200 bed volumes (right). (Influent composition: 2.4 mg/L P, 100 mg/L NO<sub>3</sub><sup>-</sup>, 32 mg/L SO<sub>4</sub><sup>2-</sup>, 69 mg/L Cl<sup>-</sup>, 50 mg/L Ca<sup>2+</sup>, 466 mg/L TDS, pH 7.0.)

Calcium effluent histories were nearly the same for three consecutive cycles to near-zero levels. As calcium was removed by the SS-WAC column, **Figure 4-8B** shows that the pH dropped moderately due to the concurrent production of carbonic acid according to Equation 2-12:



Suppression of pH as a result of  $H^+$  exchange with  $Ca^{2+}$  on the SS-WAC bed enhanced phosphate removal capacity. Samples of wastewater feed and treated water were collected after 200 bed volumes and **Figure 4-8C** shows their calcium concentrations. Note that the removal of hardness is nearly complete compared to their concentrations in the feed.

#### 4.3.2 $CO_2$ regeneration of SS-WAC

Calcium loaded SS-WAC was regenerated at three different  $CO_2$  pressures and calcium recoveries were recorded. **Figure 4-9A** demonstrates how the efficiency of regeneration or calcium desorption consistently improved with an increase in partial pressure of  $CO_2$  from 3.4 atm to 6.8 atm and then to 10.2 atm.<sup>18</sup>

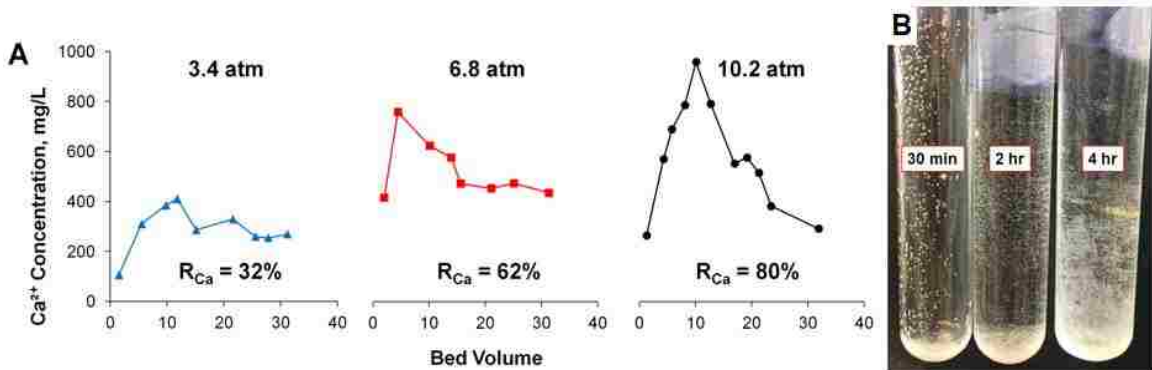


**Figure 4-9.** (A) Calcium recovery ( $R_{Ca}$ ) during regeneration with  $CO_2$  as the sole regenerant at 3.4 atm, 6.8 atm, and 10.2 atm; (B) Delayed precipitation of  $CaCO_3$  in the SS-WAC spent regenerant over time.

Furthermore, calcium desorbed was stoichiometrically sequestered by  $CO_2$  and the bulk of calcium precipitated as  $CaCO_3(s)$  outside the column as shown in **Figure 4-9B**. No  $CaCO_3$  precipitate was observed within the SS-WAC column during regeneration and it took nearly 30 minutes before the precipitation was initiated in the spent regenerant. Slices of both exhausted and regenerated SS-WAC were characterized as shown in **Figure 4-10** by SEM-EDX analysis showing Ca x-ray analysis across the diameters of the cross sections.

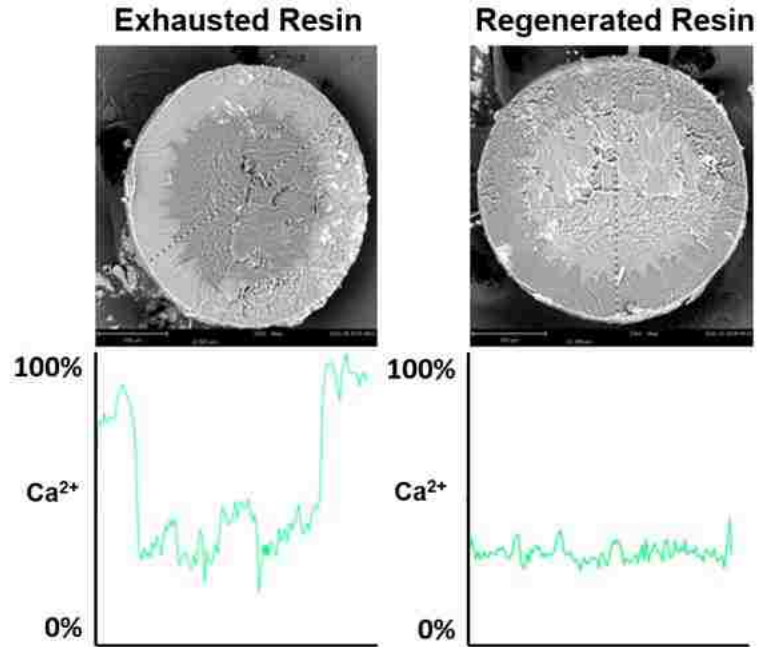


**Figure 4-10.** SEM-EDX analysis of Ca from an exhausted SS-WAC resin bead (left) and from a regenerated bead (right)

Due to the shell core of the SS-WAC, the exhausted SS-WAC shows a spike in calcium on the outer edges of the cross section as expected. After regeneration, the SS-WAC resin shows no spikes of calcium on the outer edges and maintains a flat calcium line throughout the cross-section, showing efficient regeneration by 10.2 atm CO<sub>2</sub>.

One distinctive feature of the proposed process is the use of CO<sub>2</sub> as a viable regenerant for the weak acid cation exchanger (SS-WAC) instead of mineral acid. As a result, the regenerant wastewater generated in the HIX-NP process does not contain any additional mineral salts. Furthermore, calcium regeneration is concurrently accompanied by sequestration of two moles of CO<sub>2</sub> for every mole of Ca<sup>2+</sup> according to the following stoichiometry as shown previously in Equation 2-17:

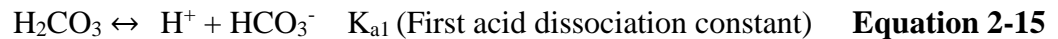


Using this stoichiometry and considering BWWP capacity of 10 MGD, Equation 2-17 represents sequestration over 1.5 million kg of carbon dioxide annually which otherwise was not possible if a mineral acid were used instead for the regeneration of the SS-WAC resin.

The role of CO<sub>2</sub> pressure on the efficiency of regeneration of the HIX-NP process is an important process variable that needs to be quantified for scale-up. The equilibrium constant for CO<sub>2</sub> regeneration in Equation 2-17 may be written as:

$$K_{\text{overall}} = \frac{[\overline{(\text{RCOOH})}]^2 [\text{Ca}^{2+}] [\text{HCO}_3^-]^2}{[\overline{(\text{RCOO}^-)}]_2 \text{Ca}^{2+} P_{\text{CO}_2}^2} \quad \text{Equation 4-2}$$

Upon dissolution in water, carbon dioxide or CO<sub>2</sub> produces carbonic acid (H<sub>2</sub>CO<sub>3</sub>) which further dissociates into H<sup>+</sup> and bicarbonate (HCO<sub>3</sub><sup>-</sup>), often referred to as alkalinity. The equilibrium relationships can be presented as previously shown:



Also, the core ion-exchange reaction for regeneration essentially involves replacing calcium with hydrogen ions i.e.,



where K<sub>IX</sub> is the ion exchange equilibrium constant. The overall regeneration reaction in Equation 2-17 essentially involves Equation 4-2, Equation 2-14, and Equation 2-15 and K<sub>overall</sub> can be presented as



$$K_{\text{overall}} = K_{\text{H}}^2 K_{\text{a1}}^2 K_{\text{IX}} \quad \text{Equation 4-3}$$

Where  $K_{\text{H}}$ ,  $K_{\text{a1}}$ , and  $K_{\text{IX}}$  are Henry's constant for carbon dioxide dissolution in water, the first dissociation constant of carbonic acid, and the equilibrium constant for the ion exchange between hydrogen and calcium ions respectively. Combining Equations 4-2 and 4-3, now we get

$$[\text{Ca}^{2+}][\text{HCO}_3^-]^2 = K_{\text{H}}^2 K_{\text{a1}}^2 K_{\text{IX}} \frac{[(\text{RCOO}^-)_2\text{Ca}^{2+}]}{[(\text{RCOOH})]^2} P_{\text{CO}_2}^2 \quad \text{Equation 4-4}$$

Under the condition of electroneutrality considering ideality,

$$2[\text{Ca}^{2+}] \approx [\text{HCO}_3^-] \quad \text{Equation 4-5}$$

and for any given percentage regeneration efficiency, the calcium and hydrogen loading on the resin is constant, and Equation 4-4 can be simplified as

$$[\text{Ca}^{2+}] = \text{constant} P_{\text{CO}_2}^{2/3} \quad \text{Equation 4-6}$$

Converting to log form,

$$\log[\text{Ca}^{2+}] = 0.67 \log P_{\text{CO}_2} + \log \text{constant} \quad \text{Equation 4-7}$$

**Equations 4-6 and 4-7** depict enhancement of calcium concentration with an increase in carbon dioxide partial pressure during regeneration, and their relationship is linear in a log-log plot with a slope of 0.67. From the experimental regeneration data in Figure 4-9 for three different  $\text{CO}_2$  pressures (3.4, 6.8 and 10.2 atmosphere), moles of calcium eluted were determined. **Figure 4-11** shows the plot of calcium eluted versus corresponding  $\text{CO}_2$  partial pressure during regeneration runs.



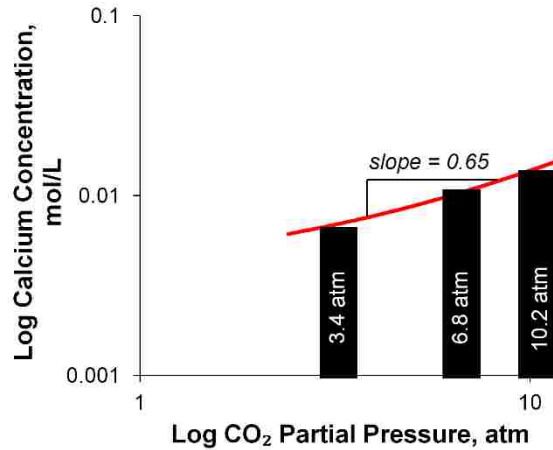


**Figure 4-11.** Log-log plot of eluted calcium concentrations versus partial pressures of CO<sub>2</sub> from the experimental data.

Note that the plot of  $\log Ca^{2+}$ -  $\log P_{CO_2}$  in Figure 4-11 has a slope of 0.65, which is quite close to the predicted value of 0.67 in Equation 4-7. Equation 4-7 can thus be used as a rational design basis for scale-up of the CO<sub>2</sub> regeneration system. A more in-depth account of the research and calculations behind energy requirements for this type of system have already been completed in the literature.<sup>18</sup>

#### 4.4 Potential for co-contaminant removal

It is increasingly well recognized that specific applications of recovered water may warrant removal of trace pharmaceutical products often present in municipal wastewater. Table 2-2 includes the names and formulae of commonly encountered pharmaceutical products most of which are essentially hydrophobic ionizable organic compounds (HIOCs).<sup>19,46</sup> **Figure 4-12A** demonstrates how an anion exchange resin with polystyrene matrix selectively removes ibuprofen from spiked Bethlehem secondary wastewater.

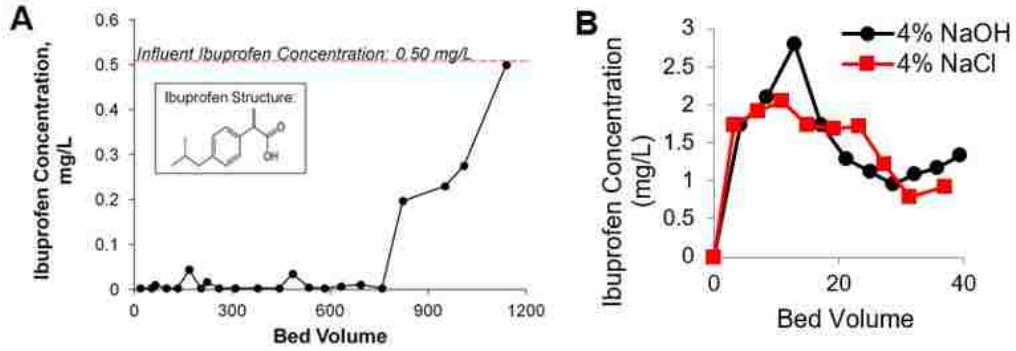


**Figure 4-12.** (A) Ibuprofen effluent history plots using secondary wastewater from the Bethlehem Wastewater Treatment Plant in Bethlehem, PA. (B) Regeneration effluent curves of ibuprofen using 4% NaOH versus 4% NaCl. (Influent composition: 2.4 mg/L P, 100 mg/L  $\text{NO}_3^-$ , 32 mg/L  $\text{SO}_4^{2-}$ , 69 mg/L  $\text{Cl}^-$ , 50 mg/L  $\text{Ca}^{2+}$ , 466 mg/L TDS, pH 7.0.)

HIX-NP is also able to remove ibuprofen to near-zero levels (>95% removal) for 800 bed volumes. Note that the low concentrations of such HIOCs warrant longer time to exhaustion. Removal of diclofenac by strong-base anion resins has also been recorded previously.<sup>19</sup> Thus, the HIX-NP process may be amended and adapted to address removals of trace pharmaceutical products, if needed. **Figure 4-12B** shows that regeneration with just NaCl or NaOH is not efficient for elution because the elution curves show a small peak and 40 BV of regeneration as opposed to the large concentration peaks and 8 BV for nitrate and phosphate. This regeneration process can be used to keep N-P-K fertilizer high quality and then proceed with a methanol-NaCl solution to remove any HIOCs subsequently, which has proven successful in the literature.<sup>62,63</sup>

# CHAPTER 5 BIO-NIX and its Effectiveness for Groundwater Remediation

## Remediation

### 5.1 Validation of the complete BIO-NIX system

With synthetic groundwater contaminated with nitrate, the BIO-NIX system was tested for efficient removal of nitrate to below the maximum contaminant level (MCL) of 45 mg/L  $\text{NO}_3^-$ . The results are shown below in **Figure 5-1**.

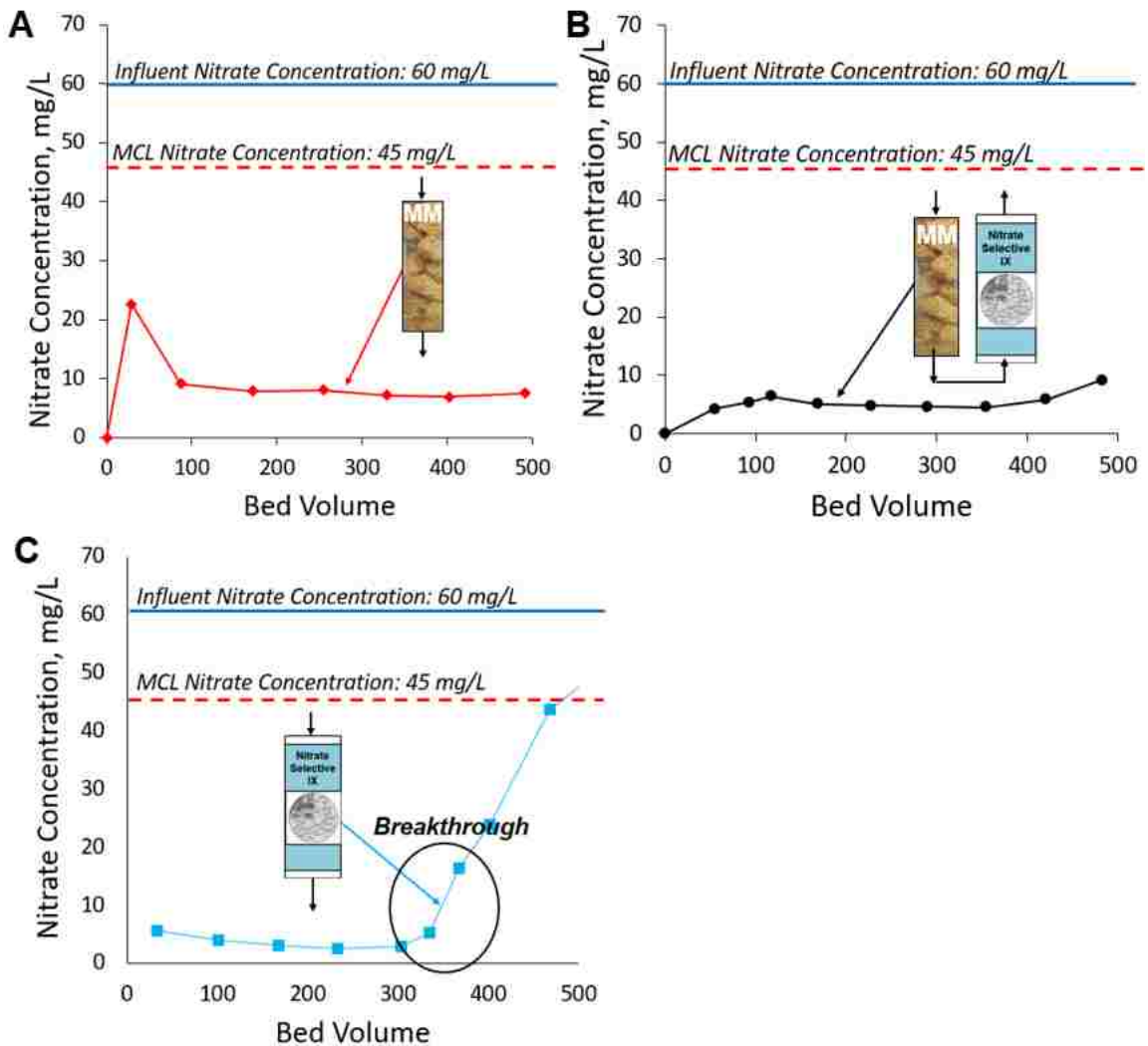


**Figure 5-1.** Nitrate effluent results of the BIO-NIX system through 500 BV (A) after the Metamateria column and (B) after the entire BIO-NIX system. (C) Nitrate effluent results from a nitrate-selective ion exchange column only run.

**Figure 5-1A** shows the nitrate effluent history after the Metamateria column and prior to entering the ion exchange column (i.e. nitrate results due to biological denitrification). Throughout the 500 BV shown, the nitrate effluent concentration did not exceed the MCL. **Figure 5-1B** shows the nitrate effluent history following the entire BIO-NIX system run (i.e. leaving the ion exchange column). The nitrate concentrations following the ion exchange column also did not exceed the MCL and pushed the concentrations even lower than the values following the Metamateria column shown in Figure 5-1A. The fixed-film column performed majority of the nitrate removal and the ion exchange column polished the removal efficiency. The ion exchange column also acted as a buffer against a fluctuation in the nitrate concentration leaving the Metamateria column at 30 BV in Figure 5-1A. The fluctuation occurred early on due to a lag time by bacteria while adjusting to the new water flow. Even though this fluctuation was approximately 23 mg/L  $\text{NO}_3^-$ , the ion exchange column was able to keep the total effluent value at 6 mg/L  $\text{NO}_3^-$ .

**Figure 5-1C** shows the nitrate effluent concentrations from a run using the same synthetic groundwater influent flowing only to a nitrate-selective ion exchange column (no citric acid column or Metamateria column were present). The nitrate-selective ion exchanger shows the nitrate effluent concentrations remaining below the MCL (on average 5 mg/L  $\text{NO}_3^-$ ) for approximately 350 bed volumes. Although the nitrate-selective ion exchanger can provide high removal efficiency on its own, the BIO-NIX system outlasts the ion exchange column and provides the same removal efficiency (approximately 90% removal). Ion exchangers alone will always have a finite capacity until regeneration with a brine is necessary. However, the BIO-NIX can run continually with the proper carbon source supply and maintaining a functional environment (neutral

pH, sufficient colonies, etc.) for the bacteria. **Figure 5-2** shows the results of the ion chromatograph of the influent and the effluent samples from this run.

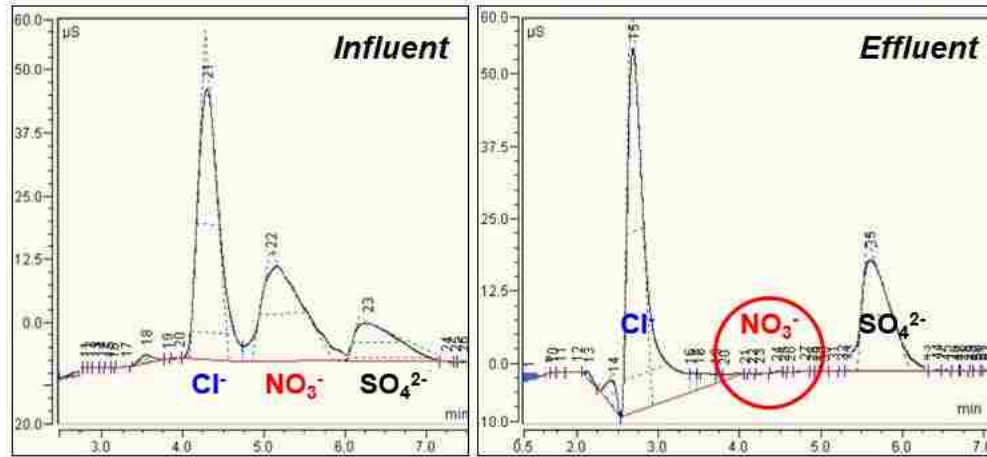


**Figure 5-2.** Ion chromatograph of the influent samples (left) and effluent samples (right) after 200 BV of service during the BIO-NIX run.

The ion chromatographs show the large reduction in nitrate with the effluent sample containing no nitrate peak at all. Sulfate and chloride remain the same throughout both samples, further validating nitrate's selectivity in BIO-NIX over competing ions. No nitrite peak was observed in the effluent showing complete reduction of nitrate.

During the BIO-NIX runs, pH, oxidation-reduction potential (ORP), and agar plates were measured to further validate bacterial existence within the Metamateria column. **Figure 5-3** below shows the effluent pH values and ORP values (measured in mV and converted to pE) from the samples exiting the Metamateria column.

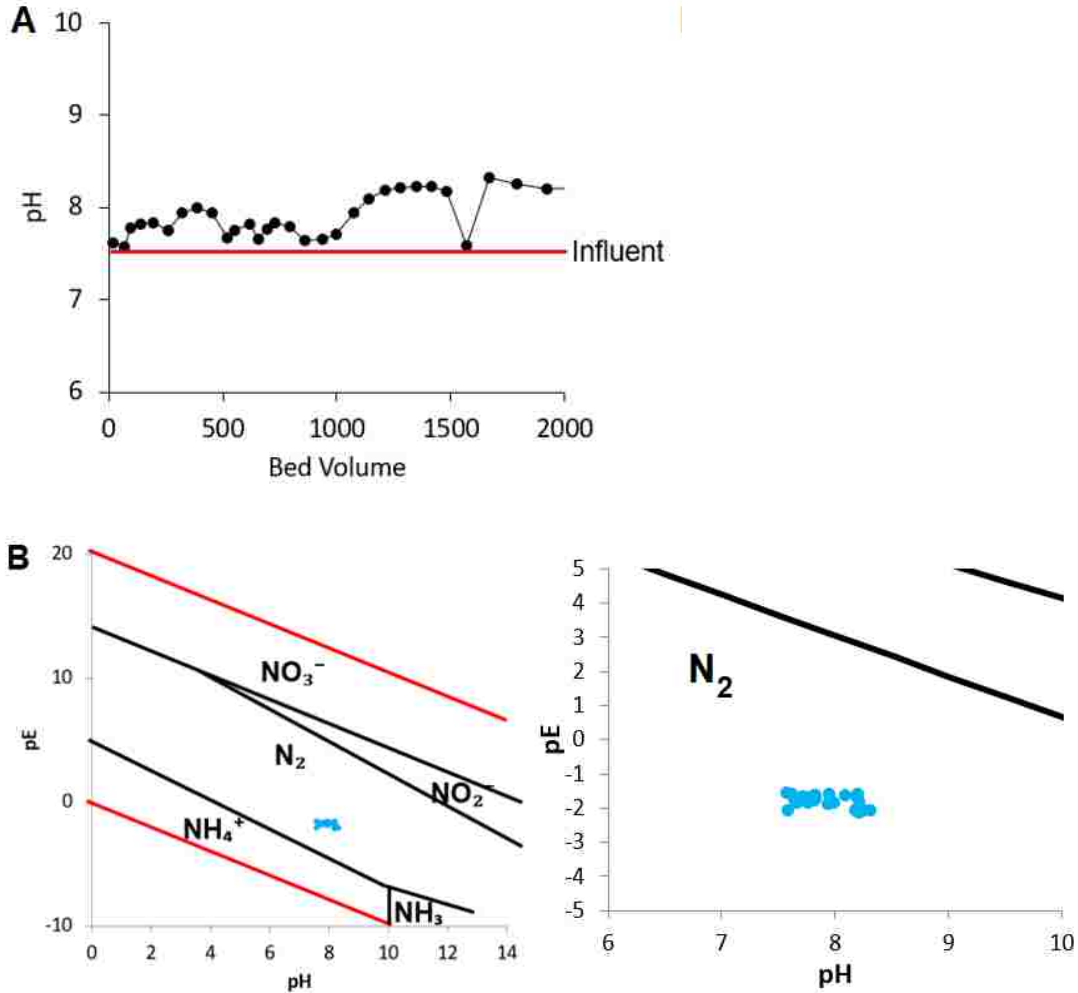


**Figure 5-3.** (A) pH values exiting the Metamateria column during the run shown in Figures 5-1A,B. (B) pE-pH diagram of nitrogen species in aqueous solution overlaid with ORP values during the BIO-NIX run and a close-up of the pe points plotted.

**Figure 5-3A** shows pH values always exceeding the influent during every sample between the range of 7.5 and 8.5. As shown previously in Equation 2-19, biological reduction of nitrate to nitrogen gas will produce alkalinity and raises pH. The pH increasing from the influent is a direct result of the fixed-film column because ion exchange does not change the pH (unless in the form of  $\text{OH}^-$  which is not the case for the nitrate-selective ion exchanger loaded with  $\text{Cl}^-$ ) and citric acid release would only provide a decrease in pH. Note that the pH does not increase excessively and remains below 8.5.

A drastic increase in pH to 10 or above could damage the bacteria growth because the optimal pH for denitrifiers is around 8.3.<sup>90</sup> A pH increase above 8.3 has not adversely impacted bacterial growth which can be confirmed with a nitrate decrease following the MetaMateria column throughout the entire run.

**Figure 5-3B** shows the pE-pH diagram of nitrogen species in aqueous solution. The pE-pH diagram separates species present in water at a specific pH and ORP value. The blue dots represented in Figure 5-3B are the ORP values measured at each of the pH values determined during the nitrate runs in Figure 5-3A. Incomplete biological denitrification can lead to harmful byproducts such as nitrite ( $\text{NO}_2^-$ )<sup>91</sup> shown on the pE-pH diagram. All blue dots fall within the realm of  $\text{N}_2(\text{g})$ , showing that nitrate has been biologically reduced to nitrogen gas, and no intermediates such as nitrite have formed. This is an extremely significant finding for the BIO-NIX system because drinking water standards (U.S. EPA) designate nitrite with a MCL of 1 mg/L  $\text{N-NO}_2^-$ .

Based on pH and ORP values, it has been shown that nitrate is being biologically reduced to nitrogen gas. Petri dishes loaded with agar were used to visually show any bacteria present on the Metamateria and the ion exchangers as seen in **Figure 5-4**.



**Figure 5-4.** Agar-loaded petri dishes to show bacterial presence on the Metamateria (left) and ion exchangers (right) after 24 hours.

After 24 hours, bacteria colonies formed around every piece of Metamateria placed on the agar, showing a visual representation of the density of bacteria located on and within the Metamateria pieces. Comparatively, the ion exchangers that were placed on a separate dish did not show any signs of bacteria colony formation after 24 hours. This result demonstrates that bacteria are not passing from the Metamateria column and infiltrating the ion exchange column and effluent. Because the Metamateria column is a fixed-film process, bacteria are not suspended in solution which is why there is no presence on the of bacteria on the petri dish with resin beads. However, bacteria form a biofilm that will grow accordingly to bacterial growth rates, EPS production, and substrate concentrations. When a biofilm becomes too large for attachment, the biofilm will break off the attachment at some point within the thickness (a process known as sloughing).<sup>92,93</sup> Because of the large surface area and pore density of Metamateria, no visually significant biofilm has formed on the pieces and no sloughing has been detected (which would manifest in chunks of EPS, like a white mucus, in the effluent).

## **5.2 Resiliency tests**

Now that the BIO-NIX system has been validated to remove nitrate from contaminated groundwater with high efficiency and sustainably, the resiliency of the BIO-NIX system will be analyzed. Groundwater sources will fluctuate regarding flow, compositions, etc. as they are a product of human behavior and the surrounding environment. The BIO-NIX system must be able to handle sudden changes in a range of parameters to consistently remove nitrate from variable influent streams, i.e. groundwater from any location globally to below the MCL.



### 5.2.1 Carbon source interruption

Because a carbon source is necessary to biologically reduce nitrate to nitrogen gas and to maintain cell synthesis, the carbon dosing provided by the citric acid-loaded anion exchanger was interrupted to see the effects of the entire system without a carbon source. After the 500 BV of service already passed through the BIO-NIX system in Figure 5-1, the bypass line to the citric acid column was shut off and the nitrate effluent results are shown in **Figure 5-5**.

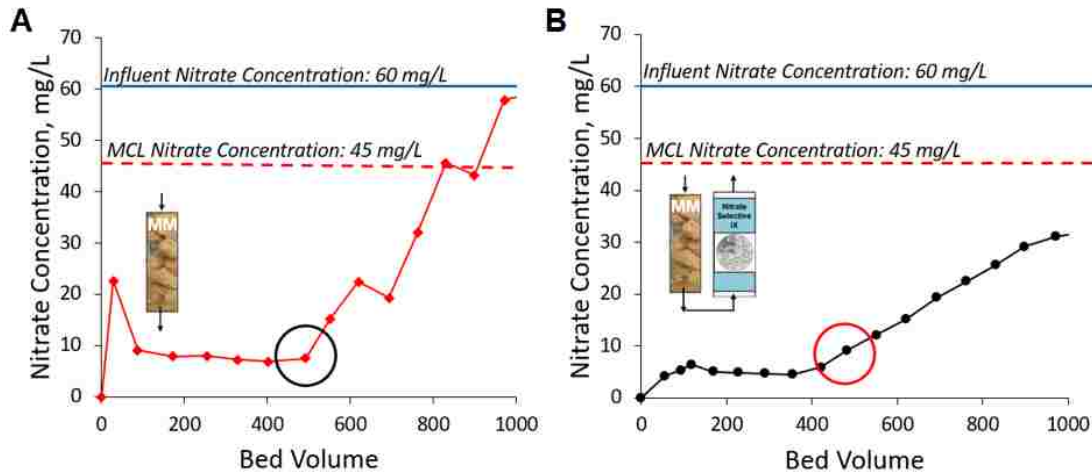


**Figure 5-5.** Nitrate effluent history following a shut-down of the citric acid bypass line at 500 BV (designated by circles) (A) after the Metamateria column and (B) after the ion exchange column.

**Figure 5-5A** shows that the nitrate effluent concentration following the Metamateria column increases rapidly to the MCL by 800 BV. The Metamateria column failed during the break in carbon dosing overall but had a buffer of 300 BV before meeting the MCL for corrections to be made to the system. **Figure 5-5B** illustrates the nitrate effluent history following the BIO-NIX system (minus the citric acid column) which is sampled after the ion exchanger. Compared to the Metamateria column effluent, the ion exchanger's effluent concentration slowly increases towards the MCL and after 300 BV the concentration is only 25 mg/L  $\text{NO}_3^-$  as opposed to Metamateria that reaches the MCL

at that point. The ion exchanger provides a dampening effect that keeps nitrate below the MCL longer than biological denitrification alone to provide time for troubleshooting if the citric acid-loaded anion exchanger was to get knocked offline or became exhausted without notice.

After interrupting the carbon dosing, the citric acid bypass line was then added back into the BIO-NIX system to determine its ability to rebound from this type of failure. **Figure 5-6** below shows the nitrate effluent concentrations between and after the two columns from the citric acid interruption and citric acid reintroduction.

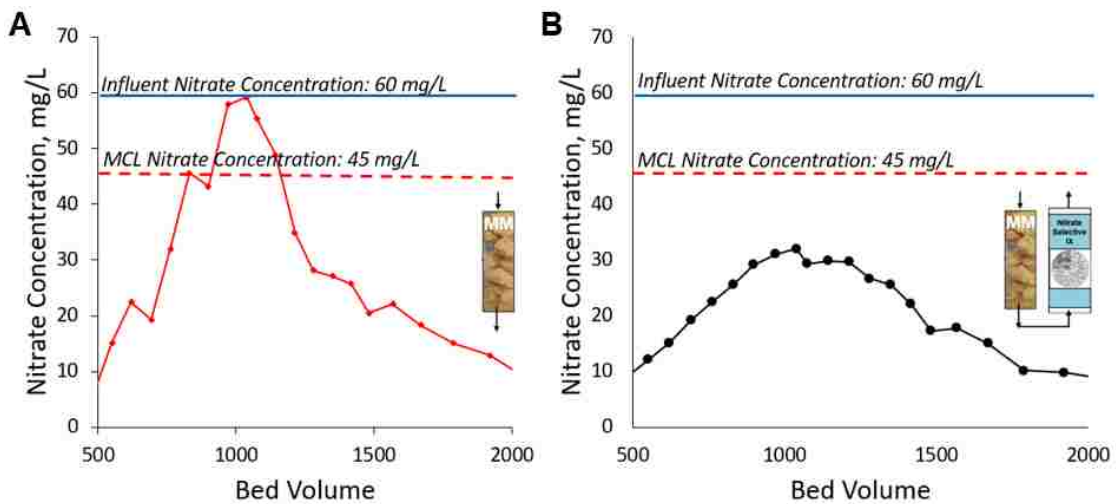


**Figure 5-6.** Nitrate effluent histories (A) between and (B) after the two columns from the time citric acid was interrupted (500BV) and after citric acid was reintroduced (1000 BV).

Between the Metamateria and ion exchange columns, **Figure 5-6A** demonstrates that the nitrate effluent concentration immediately began to decrease as citric acid was added back into the system and remained under the MCL after 200 BV. The Metamateria column eventually rebounds completely and arrives at the levels of nitrate removal achieved at the beginning run (approximately 6 mg/L  $\text{NO}_3^-$ ). After both columns (**Figure**

**5-6B**), the nitrate effluent concentrations also begin to immediately decrease, and stayed below the MCL throughout the entire run. The total effluent also attains the consistent nitrate levels found during the first 500 BV. Note that the decrease in the total effluent stream is not as sharp as the decrease following the Metamateria column. This is due to small self-elution being performed by the ion exchangers themselves due to the change in concentration and a resulting change in capacity which will be discussed further in Section 5.5. The BIO-NIX system can handle an interruption of carbon dosing for over 500 BV and rebounds back to complete removal when initial conditions have been reaffirmed without damage to the system.

#### *5.2.2 Influent nitrate surge*

Nitrate concentrations will vary in the groundwater composition based on over utilization of fertilizer, runoff, and other discharges.<sup>94</sup> To further test the resiliency of BIO-NIX, the nitrate concentration was spiked to 120 mg/l NO<sub>3</sub><sup>-</sup>, double the original influent amount. **Figure 5-7** indicates the nitrate effluent concentrations between and after the two columns before, during, and after a nitrate spike to 120 mg/l NO<sub>3</sub><sup>-</sup>.

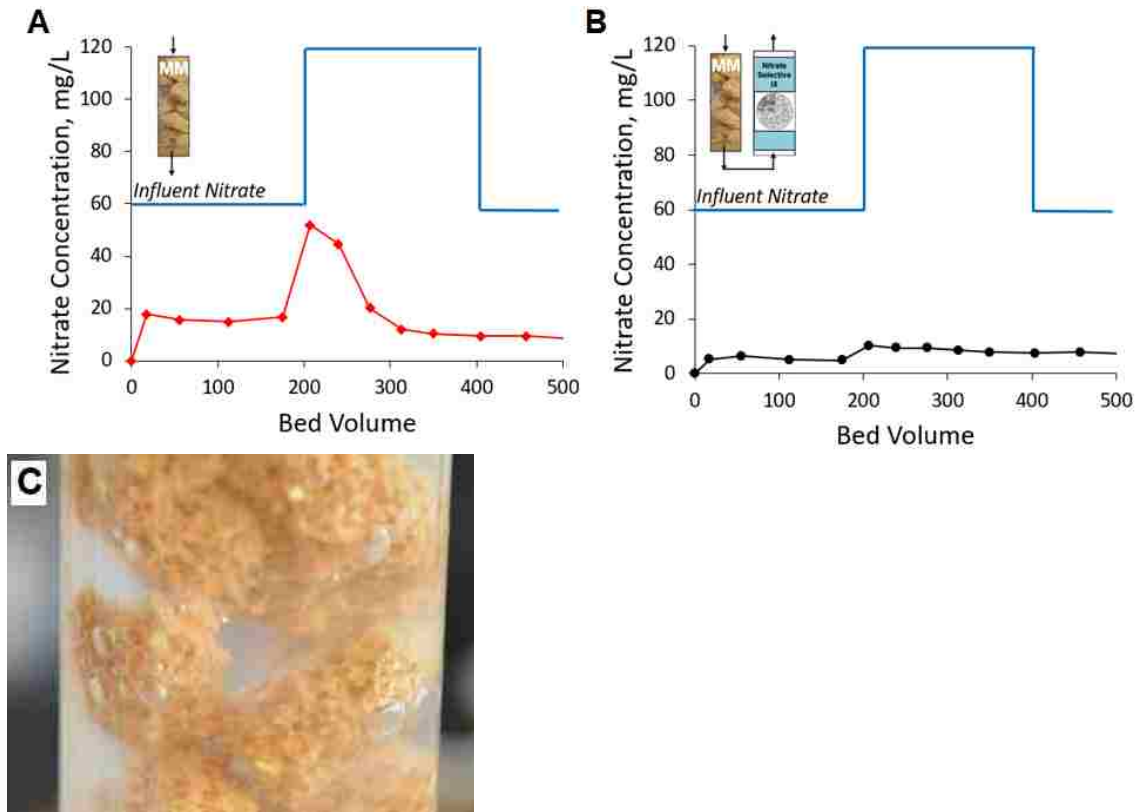


**Figure 5-7.** Nitrate effluent histories (A) between and (B) after the two columns during the transition to a sudden spike of influent nitrate to 120 mg/L  $\text{NO}_3^-$ . (C) Image of the Metamateria column that highlights bubbles trapped within the column during the nitrate spike.

**Figure 5-7A** shows that the bacteria cannot maintain a low nitrate effluent concentration when the spike immediately hits at 200 BV and exceeds the MCL concentration at approximately 52 mg/L  $\text{NO}_3^-$ . However, within the next 100 BV, the bacteria adjust their substrate utilization rates to the higher nitrate influent concentration and effluent levels are back to 8 mg/L  $\text{NO}_3^-$ . **Figure 5-7B** shows a smaller increase of effluent nitrate concentrations from 5 mg/L  $\text{NO}_3^-$  to 11 mg/L  $\text{NO}_3^-$  when the nitrate spike occurs and maintains a nitrate concentration well below the MCL during the entire length of the spike. Again, the ion exchange column provides a buffer to an increase in nitrate coming out of the Metamateria column, maintaining concentrations below the MCL during the variant nitrate influent. **Figure 5-7C** shows a close-up of the Metamateria column, where

bubbles have visually formed during the 120 mg/L  $\text{NO}_3^-$  spike. Bubble formation occurs because a greater amount of nitrate provided for the bacteria to degrade results in a greater amount of nitrogen gas formed. Bubbles can be released from the column by maintaining upward flow in that column or temporarily opening the column for release.

### 5.2.3 Flow increase

If the BIO-NIX system is to be applied for any groundwater sources, water demand of the city, town, village, etc. will fluctuate based on population and affect the flow rate entering the BIO-NIX system. Therefore, the BIO-NIX system was tested for its resiliency to an increase in flow rate, also known as a decrease in detention time (how long it takes water to travel throughout the column). **Figure 5-8** shows the results of the nitrate effluent concentrations from the BIO-NIX system during a period of increased flow rate, measured in a decrease in detention time from 15 minutes to 10 minutes.

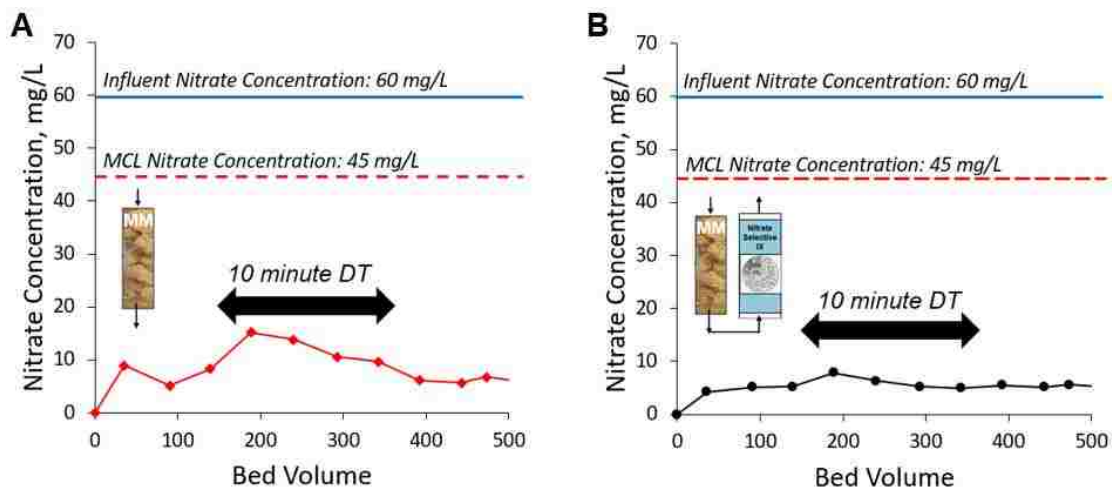


**Figure 5-8.** Nitrate effluent history as a result of a decreased detention time from 15 minutes to 10 minutes from 150 BV to 350 BV (A) after the Metamateria column and (B) after the ion exchange column.

**Figure 5-8A** shows that the Metamateria column experienced a small spike from approximately 7 mg/L  $\text{NO}_3^-$  to about 18 mg/L  $\text{NO}_3^-$ . The increase in nitrate concentration

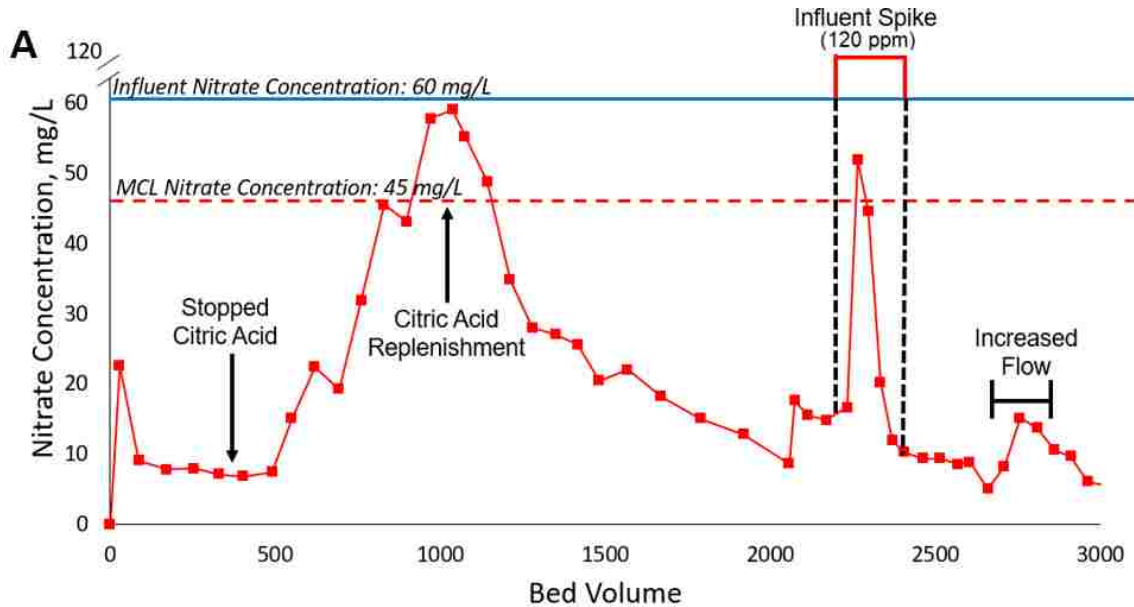
was attributed to the shorter contact time that bacteria take to metabolize nitrate and the carbon source when they were adjusted to a specific contact time for over 2000 BV of previous runs. The fixed-film adapted to the change by a decreasing nitrate effluent concentration back towards the 7 mg/L  $\text{NO}_3^-$  over the 200 BV. Because of the EPS material that mostly comprises the biofilm<sup>92,95</sup>, the effect of the decreased contact time of nitrate and citric acid is lessened because the biofilm can catch the compounds within the biofilm structure and allow time for bacteria within the biofilm to degrade the compounds later. Therefore, an effluent nitrate spike occurred after the Metamateria column, but it did not exceed the MCL during the 200 BV of increased flow.

**Figure 5-8B** shows the nitrate effluent concentrations of the entire BIO-NIX system resulting from the decreased detention time and the dampening effect of the ion exchange column that follows the Metamateria column. At around 180 BV, the ion exchange column incurs a small increase in effluent nitrate concentration from approximately 5 mg/L  $\text{NO}_3^-$  to about 8 mg/L  $\text{NO}_3^-$ . This spike occurred because the ion exchange capacity was adjusting from a low influent nitrate concentration prior to the decreased detention time to a higher influent nitrate concentration leaving the Metamateria column. The ion exchange column adjusts capacity within 50 bed volumes to maintain about 5 mg/L  $\text{NO}_3^-$  in the effluent and staying under the MCL during the entire 200 BV of increased flow. Although a change in detention time of 5 minutes seems like a small change, this resulted in a 33.3% increase in flow, which is a significant change for a laboratory-scale experiment. A scale-up of the BIO-NIX system would increase according to the dimensions of the new fixed-film column.

#### 5.2.4 Summary of resiliency

The BIO-NIX system was tested for various interruptions that can occur during groundwater treatment including an interruption in carbon source dosing, influent nitrate concentration fluctuations, and an increase in flow rate. Even though each interruption was noted separately, the BIO-NIX system continuously ran during each interruption.

The summary of the effluent nitrate history in between the Metamateria and ion exchange column as well as the final effluent leaving the ion exchange column is shown in **Figure 5-9**.





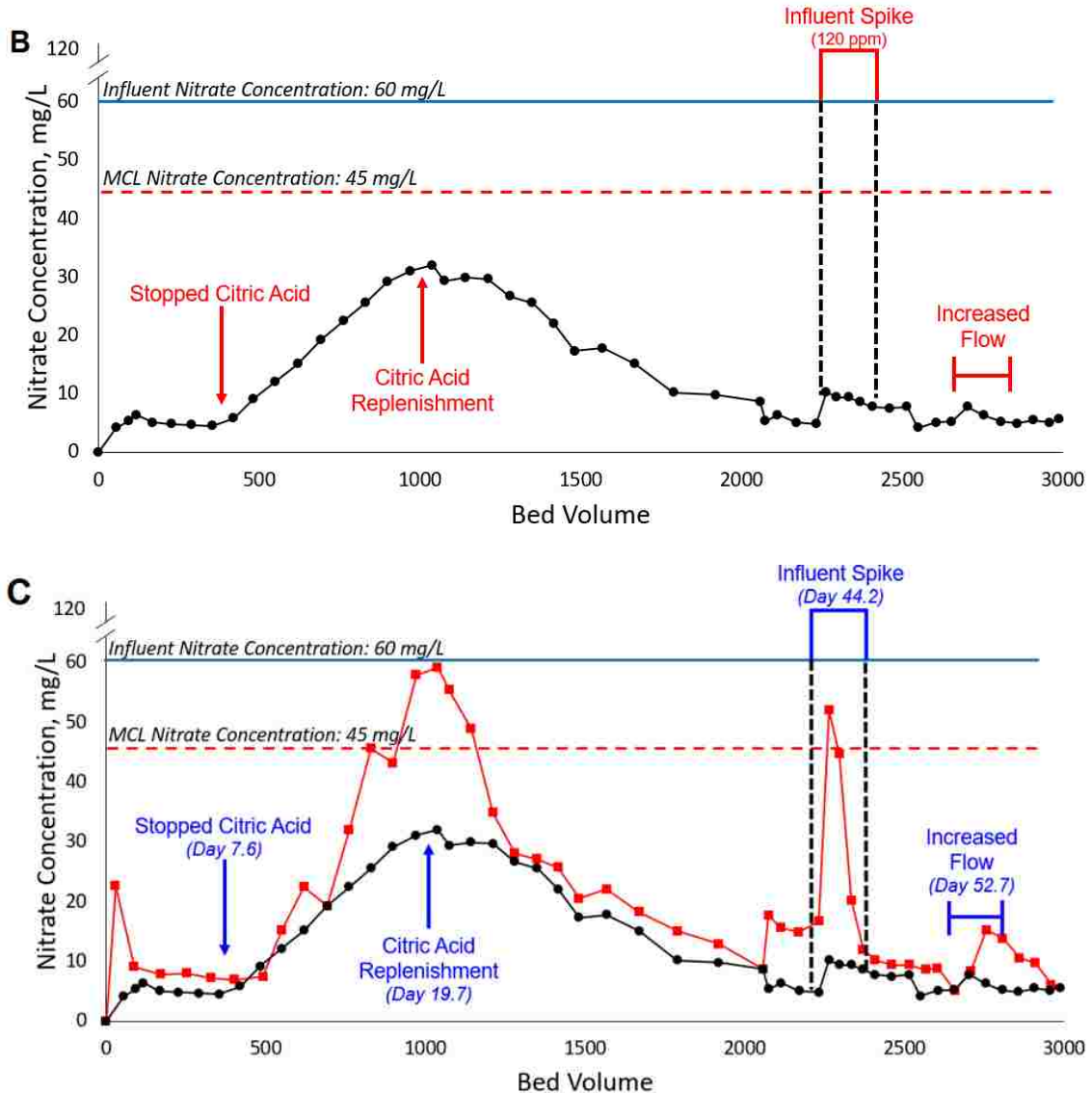


**Figure 5-9.** A summary of the nitrate effluent histories (A) leaving the Metamateria column (red line) and (B) leaving the ion exchange column (black line) as a result of various interruptions of the BIO-NIX system. (C) A comparison of both effluent histories overlapped.

**Figure 5-9A** shows that the Metamateria column was affected by each interruption and was able to rebound after each interruption back to its stable effluent concentrations. Even though there were two points in which the effluent concentrations exceeded the MCL following the Metamateria column, the total effluent leaving the ion exchange column in **Figure 5-9B** represented by the black line had not reached the MCL in 3000



BV of service. The overlapping of the entire effluent history in **Figure 5-9C** shows that after adaptation to the interruptions, the Metamateria column performed most of the nitrate removal and the ion exchange column served as a polishing step during those periods and as a dampener during interruption periods. The effluent nitrate concentrations following the ion exchange column did not mirror the effluent nitrate concentrations following the Metamateria column, showing that ion exchange capacity can change based on the influent concentration leading into the ion exchange column. Note that the ion exchange bed had not been regenerated at all during the 3000 BV run and no chemicals were used in the process.

### **5.3 Selenate removal using BIO-NIX**

Following the 3000 BV of service, selenate was introduced into the same feed water at 1 mg/L Se as  $\text{SeO}_4^{2-}$  for 500 BV. BIO-NIX performance for selenate removal is shown below in **Figure 5-10**.

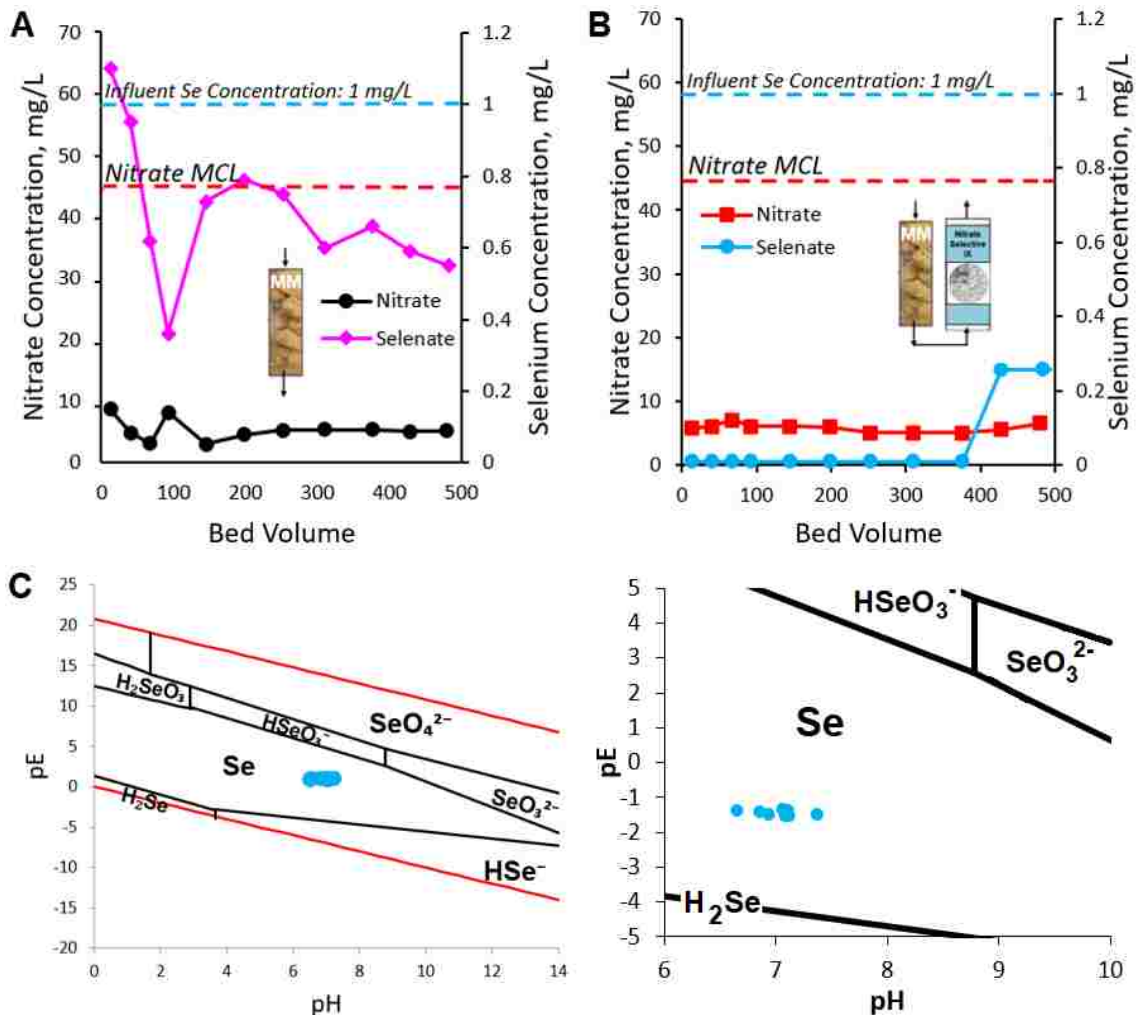


**Figure 5-10.** Nitrate and selenate effluent results of the BIO-NIX system through 500 BV (A) after the Metamateria column and before the ion exchange column and (B) after the entire BIO-NIX system. (C) pE-pH diagram of selenium species in aqueous solution overlaid with ORP values during the BIO-NIX run with a close-up of the plotted pe-pH points on the right.

Note that selenate concentrations are represented by total selenium values. After the Metamateria column in **Figure 5-10A**, selenate concentrations fluctuate throughout the 500 BV run and on average biological processes degraded 40% of the influent selenate. During that time, nitrate reduction remained constant at >90% removal throughout

biological denitrification and remained below the MCL throughout the entire run in the presence of selenium.

**Figure 5-10B** shows that the ion exchange column was the most effective selenate removal process as selenium effluent concentrations remained below 0.05 mg/L Se through 400 BV. The ion exchanger also dampened any selenium concentration variations leaving the Metamateria column. Effluent selenium concentrations from the ion exchange column begin to increase at 400 BV showing a decrease in selenate capacity of the ion exchanger and the Metamateria column stepping in to decrease selenate at that time. Nitrate remains constant around 6 mg/L  $\text{NO}_3^-$ , below the MCL and at >90% removal. To increase reduction of selenate to selenium in the Metamateria column, the bacteria could be acclimated to selenium species prior to the run by recirculating a solution with high selenium, carbon source, and the background feedwater. This would allow the bacteria to adjust to selenate presence and begin selenate degradation faster as the bacteria were beginning to do towards the end of the run.

**Figure 5-10C** shows the selenium species redox potential of each sample as a function of pH. Each sample value fell within the  $\text{Se}^0$  regions showing further proof of selenate reduction to selenium within the Metamateria column. Additional validation is the reduction in total selenium concentrations in Figure 5-10A. If selenate were to be reduced to selenite or intermediate species, there would be no reduction in total aqueous selenium concentration. However, because selenate is reduced to  $\text{Se}^0$ , a precipitate of Se forms, and there is a reduction in total selenium aqueous concentrations.<sup>69,96</sup> The BIO-NIX system is able to remove selenate to near-zero levels and has potential for high reduction of selenate to  $\text{Se}^0$ .

## 5.4 Citric acid-loaded anion exchanger design

The BIO-NIX system has proven to operate so that the Metamateria column performs majority of the nitrate removal. This can only result if carbon dosing is appropriate from the citric acid-loaded column and citric acid utilization is performed during the Metamateria column without excess leaving to the ion exchange column.

**Figure 5-11A** below shows the effluent citric acid, nitrate, and sulfate concentrations leaving the citric acid-loaded ion exchanger during 2000 BV of the total run (starts at the citric acid replenishment period through the decreased detention time period).

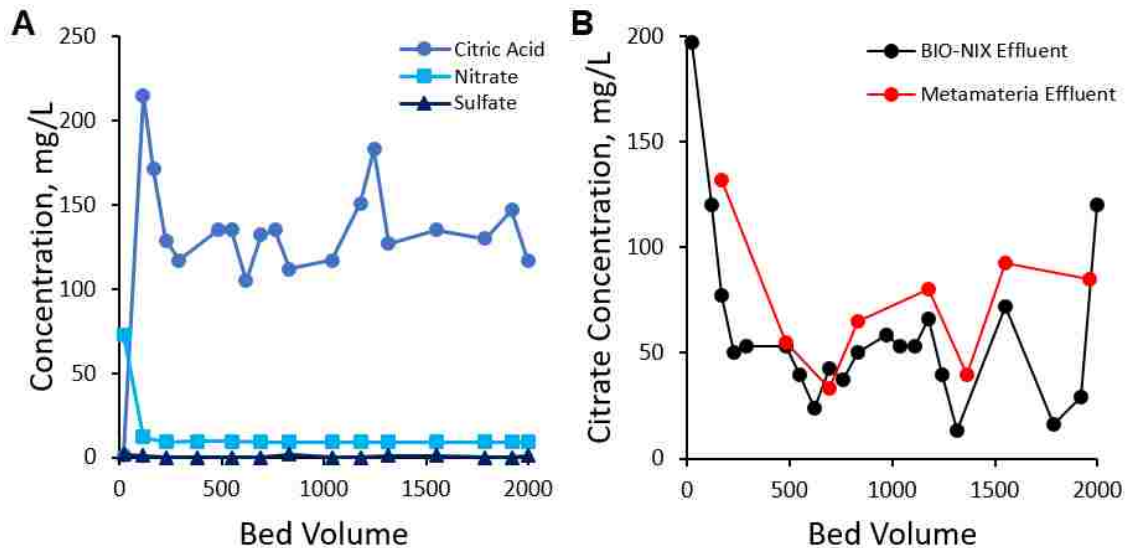


**Figure 5-11.** (A) Effluent history of citric acid (diluted to 20%), nitrate, and sulfate leaving the citric acid-loaded column. (B) Comparison of citrate effluent histories between the Metamateria column and the BIO-NIX effluent.

Please note that the citric acid concentrations in Figure 5-11A were diluted to 20% to show what concentrations would be continuing to the Metamateria column after leaving the ion exchange column and meeting up with the main flow line. Nitrate and sulfate are presented as the actual concentrations directly leaving the citric acid-loaded column prior to joining the main stream. Figure 5-11A demonstrates that citric acid is being released from the citric acid-loaded column and is being exchanged with nitrate, sulfate, and other

anions present in solution.<sup>46</sup> **Equation 5-1** is shown below to calculate the theoretical citric acid concentration leaving the citric acid-loaded anion exchanger and validate these release values with the design:

$$C_C = \Sigma[\text{Anion}(\text{meq/L})] \times N \times \text{MM} \quad \text{Equation 5-1}$$

where  $C_C$  is the citric acid concentration,  $\Sigma$  means summation,  $N$  is the normality of citric acid, and  $\text{MM}$  is the molar mass of citrate. By taking the sum of the total anion concentration in the influent in meq/L, it can be assumed that at a maximum every meq of total anions entering the system will be exchanged with one meq of citric acid. With a total anion concentration of 5.47 meq/L and taking the valence of citric acid to be -1, the citric acid concentration leaving the citric acid-loaded column at ideal exchange is 1050 mg/L citric acid. Factoring in dilution by 20% of the bypass flow meeting the main flow, the citrate concentration entering the Metamateria column would be 210 mg/L. Figure 5-11A shows an average value of 131 mg/L citrate entering the Metamateria column, which validates the calculation in Equation 5-1 and taking into consideration that not every meq of anion will directly be exchanged with 1 meq of citric acid. This assumption that not every meq will be exchanged can also be seen by the fact that nitrate effluent concentrations are not zero out of the citric acid-loaded anion exchanger, but 9 mg/L  $\text{NO}_3^-$ . Note that effluent sulfate concentrations were near-zero.

**Figure 5-11B** shows the citrate concentrations leaving the Metamateria column during the 2000 BV were 63 mg/L on average. With an average effluent value of citrate at 131 mg/L entering the Metamateria column, the citrate being taken up was 68 mg/L. Taking the equilibrium concentration of effluent nitrate from the 2000 BV leaving the Metamateria column only to be approximately 8 mg/L  $\text{NO}_3^-$  and the influent

concentration to be 60 mg/L  $\text{NO}_3^-$ , 52 mg/L  $\text{NO}_3^-$  is degraded throughout the run at a maximum. With a 2.76:1 C to N ratio necessary to degrade nitrate, 74 mg/L citrate is needed as an electron donor for nitrate reduction, which is close to the calculations of citrate utilization of 68 mg/L on average. Figure 5-11B effluent results leaving the ion exchange column show a slight decrease in citric acid concentration in comparison to citric acid leaving the Metamateria column, which can be attributed to minor uptake by the ion exchanger.

### **5.5 Regeneration of the nitrate-selective ion exchange column**

Throughout the entire BIO-NIX runs, the ion exchange column was not regenerated and there was no need for high concentration NaCl brine. This result was predicted in Figure 2-9 that shows the ion exchange capacity increases with an increase in influent nitrate concentration and the BIO-NIX system validated this phenomenon. First, Figure 5-1C shows the ion exchange column performance alone, in which a sharp increase occurs starting at 350 BV and hits the influent concentration by 450 BV once the resin bed has been exhausted. Ion exchangers perform to near-zero levels for targeted contaminants and incur a sharp increase to the influent once exhaustion ensues, as shown with the nitrate-selective anion exchanger alone. In contradiction to that notion, Figure 5-9C (the summary of effluent nitrate history as a result of all interruptions during the resiliency tests) shows a steady nitrate effluent increase towards the influent from 500 BV to 1000 BV leaving the ion exchanger column. The Metamateria column performance for denitrification failed at this point due to a lack of carbon source, and the concentration leaving the Metamateria column increased as it entered the ion exchange

column. With ion exchange as the only process removing nitrate because the Metamateria column fails at that point, a sharp increase in nitrate effluent concentration should ensue for typical exchanger exhaustion behavior but a steady increase occurs instead. This is due to a sudden increase in capacity that results from a higher influent nitrate concentration. The nitrate-selective ion exchanger is removing nitrate at a greater rate than previously (i.e. the area between ion exchange column curve and the Metamateria is greater at this point) so the concentration is not as close to the influent as it would be with just the ion exchanger even though the anion exchanger shows nitrate effluent increasing.

Nitrate bleeding is also present in Figure 5-9C between 1300 BV to 2000 BV and 2400 BV to 2700 BV. During these time periods, the Metamateria effluent history almost lays on top of the ion exchange effluent history as opposed to the effluent histories that are spaced apart from 500 BV to 1000 BV. This decrease in spacing shows that the nitrate removal capacity of the ion exchanger has decreased and is now slowly eluting nitrate.

## **5.6 Cost comparison to Manheim's water treatment facility**

The feed water of the BIO-NIX system mirrored the Manheim, PA water treatment facility's influent composition. Because Manheim utilizes ion exchange only for nitrate removal, they need to regenerate their columns periodically, which adds material cost and wastewater to be disposed. Once per day, the plant regenerates the resins with 10% NaCl, which uses over 500 lbs (0.55 tons) of NaCl and generates over 2000 gallons of wastewater from the regenerant each day. If NaCl prices are approximately \$80 per ton (prices range based on the source of NaCl)<sup>97</sup>, the annual cost

of brine for Manheim, PA is \$16,000. Note that transportation and discharge of the brine reject solution would incur additional costs. This plant is a smaller-scale water treatment facility with a flow rate of 0.25 MGD. For small cities like Bethlehem, PA for example that produce approximately 15 MGD on average from their drinking water facility and assuming the same level of nitrate contamination, the number of ion exchange vessels would need to increase and regeneration periods would also be more frequent leading to a significant increase in salt consumption, wastewater generated, and costs associated with both that would amount to approximately \$1 million per year. BIO-NIX does not need any regeneration and therefore would not incur such costs.

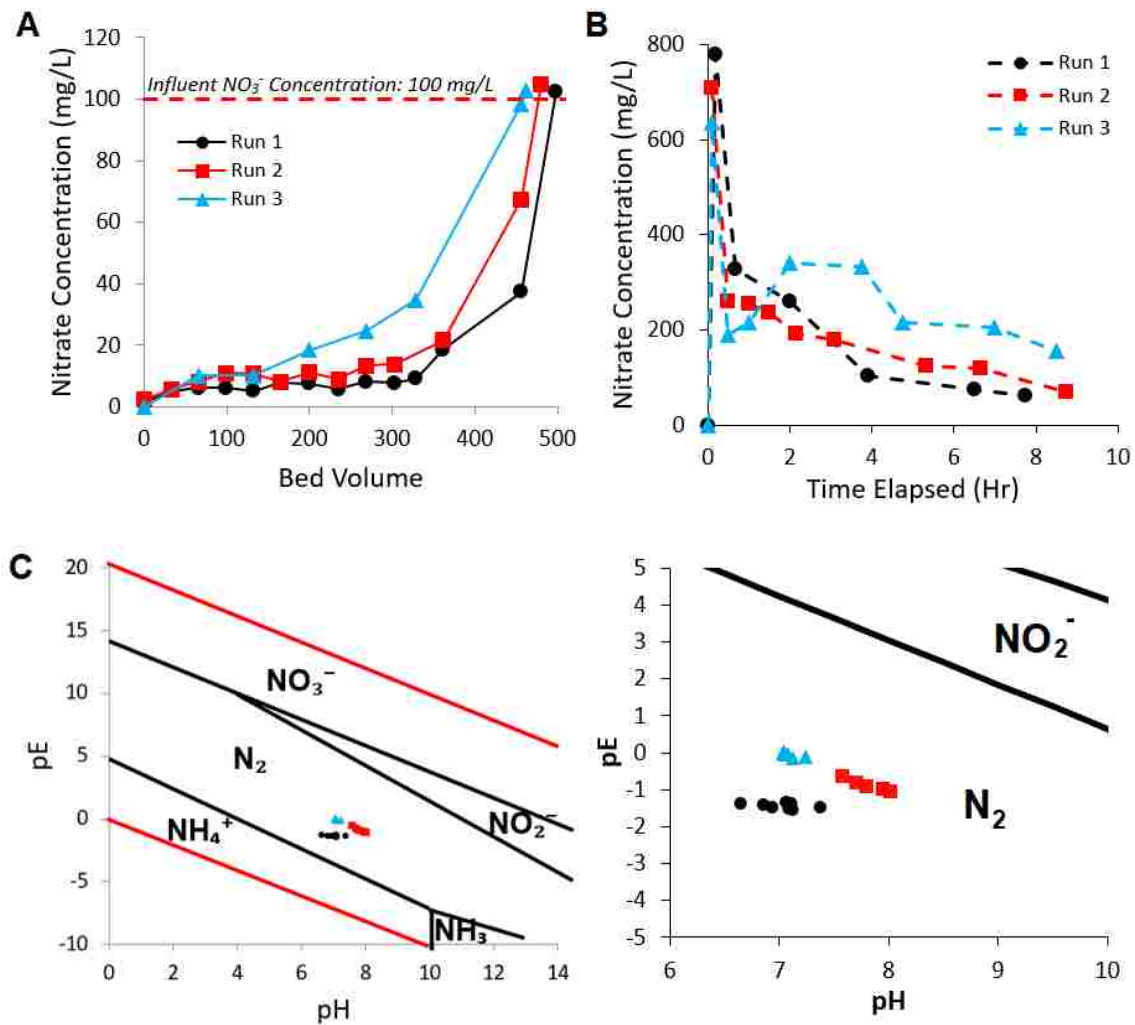
## **5.7 BIO-RNIX, modification for ion exchange regeneration from wastewater removal**

The BIO-NIX system was modified to perform regeneration of nitrate and selenate-loaded brine forming the BIO-RNIX process. The results below focus on nitrate and selenate regeneration from ion exchange runs using nitrate-selective SBA and a BWWP wastewater influent composition.

### *5.7.1 Nitrate analysis of the regeneration process*

The nitrate removal performance of the nitrate-selective anion exchanger with wastewater feed is shown below in **Figure 5-12A**.





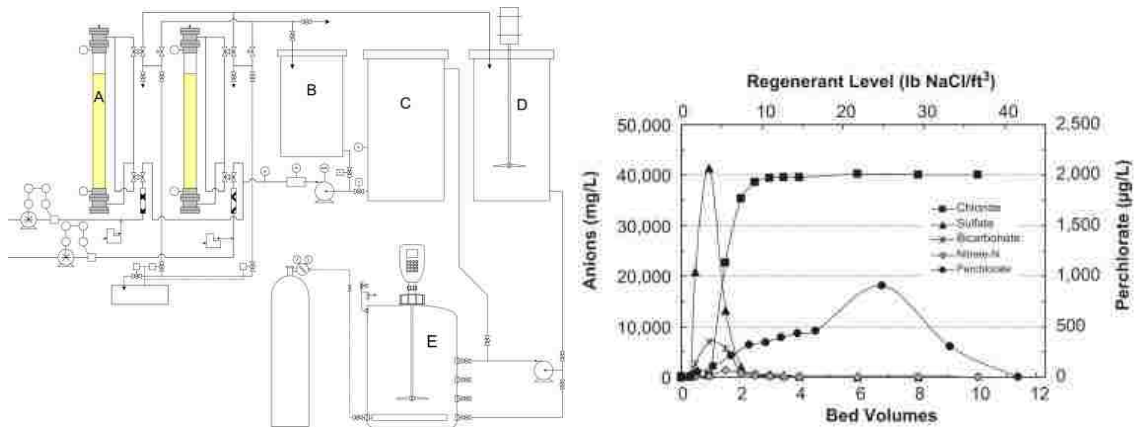
**Figure 5-12.** (A) Three successive effluent history plots of nitrate using secondary wastewater from the Bethlehem Wastewater Treatment Plant in Bethlehem, PA. (B) Three successive regeneration effluent history plots of nitrate using the BIO-RNIX process. (C) pE-pH diagram of aqueous nitrogen species with overlapping plotted pE points during each regeneration run and a close-up of the plotted pe-pH points on the right. (Influent composition: 1 mg/L Se as  $\text{SeO}_4^{2-}$ , 2.4 mg/L P, 100 mg/L  $\text{NO}_3^-$ , 32 mg/L  $\text{SO}_4^{2-}$ , 69 mg/L  $\text{Cl}^-$ , 50 mg/L  $\text{Ca}^{2+}$ , 466 mg/L TDS, pH 7.0.).

Figure 5-12A is consistent with the nitrate effluent history from the HAIX-NanoZr results in Chapter 4 also completed with a wastewater feed. Nitrate removal is >95% for all three runs and exhaustion occurs between 350 BV and 450 BV. Significant removal provides a concentrated nitrate regenerant solution that is fed to the Metamateria column during BIO-RNIX regeneration.

**Figure 5-12B** shows the nitrate effluent history leaving the Metamateria column during the BIO-RNIX regeneration process as a function of time elapsed. Using a 0.8%  $MgCl_2$  brine, within 0.5 hours of the recirculation process, all three regeneration runs show a tall spike in nitrate leaving the Metamateria column. The large peak indicates that the chloride brine has a high enough concentration to efficiently kick nitrate off the bed as planned and these peaks are comparable to the peaks found in regeneration of nitrate from HIX-NP using NaOH in Figure 4-4B. Each successive run has a smaller peak than the previous run in congruent with the nitrate removal results (i.e. the first run has the largest capacity). It is important to appropriately choose a salt concentration high enough to effectively remove nitrate from the bed while maintaining low salinity to avoid inhibition of bacterial growth and degradation.<sup>98</sup> Throughout the remaining 8 hours at a 15-minute EBCT, the first and second runs show a constant decrease in nitrate concentration leaving the Metamateria column to below 50 mg/L  $NO_3^-$ . The third run also consistently removes nitrate, but not as efficiently as the first and second runs most likely due to a declining citric acid quantity. Overall, removal efficiency for all the runs was greater than 75%. By placing more Metamateria in the column and maintaining sufficient carbon source, these nitrate effluent concentrations can be brought down even further within the same time frame. **Figure 5-12C** shows all data points from the regeneration runs falling within the nitrogen gas species on the aqueous nitrogen species pE-pH diagram. By falling within this range on the pE-pH diagram, nitrate has been reduced to nitrogen gas during regeneration of all three runs.

### 5.7.2 BIO-RNIX comparison to other brine reuse processes

Similar technologies to the BIO-RNIX systems have been studied in the literature (specifically Lehman et al., 2008) where regeneration of a nitrate-loaded ion exchange resin is achieved through recirculation of a reusable brine solution. The process by Lehman et al. is outlined in their schematic shown in **Figure 5-13A** as an example.



**Figure 5-13.** (A) Schematic of the SBR regeneration system by Lehman et al., 2008. (B) Regeneration effluent profiles of nitrate (among perchlorate as well) in the SBR following the draw stage.<sup>99</sup>

The schematic can be explained as the following process: brine rinses through the ion exchange column, continues to a spent regenerant tank that then mixes with a clean regenerant tank line, and proceeds to the biological SBR that undergoes fill, mix and react, settle, and draw steps. On the other hand, the BIO-RNIX system starts with the brine flowing to the ion exchange column and continues straight to the biological process/the fixed-film column, continuing that two-column recirculation process. There is no need for additional tanks between the ion exchange column and the fixed-film column in the BIO-RNIX process as opposed to the SBR process. Another key difference is that the fixed-film column of BIO-RNIX only requires flow through of the column, whereas the SBR requires full mixing and settling of sludge before it is reused due to suspended growth.

With similar parameters of the BIO-RNIX process present in the SBR process (7 min EBCT, acetic acid stoichiometric dosing, influent nitrate at approximately 60 mg/L  $\text{NO}_3^-$  with sulfate present as a competing ion), the SBR process was able to achieve in the first regeneration less than 0.5 mg/L  $\text{NO}_3^-$ -N within 24 h in 6% NaCl solution with acetate and magnesium as the only amendments as shown in **Figure 5-13B**. Comparatively, the BIO-RNIX system achieved approximately 5 mg/L  $\text{NO}_3^-$ -N within 8 hours of recirculation with 0.8%  $\text{MgCl}_2$  solution. The performance of BIO-RNIX achieved comparatively low nitrate effluent concentrations to the SBR process within a smaller time frame, with a lower brine concentration, and without magnesium addition to the brine (as it is already present). Noting that direct comparison can only be made with the same parameters and the same run being performed through both systems in parallel, the BIO-RNIX system provides comparative nitrate removal to processes in the literature such as the SBR process by using a simpler system consisting of two columns in series with brine recirculation and a reduced chemical addition.<sup>99</sup>

### *5.7.3 Application for selenate regeneration*

Selenate performance was simultaneously analyzed during nitrate analysis of the BIO-NIX system and results are shown below in **Figure 5-14**.

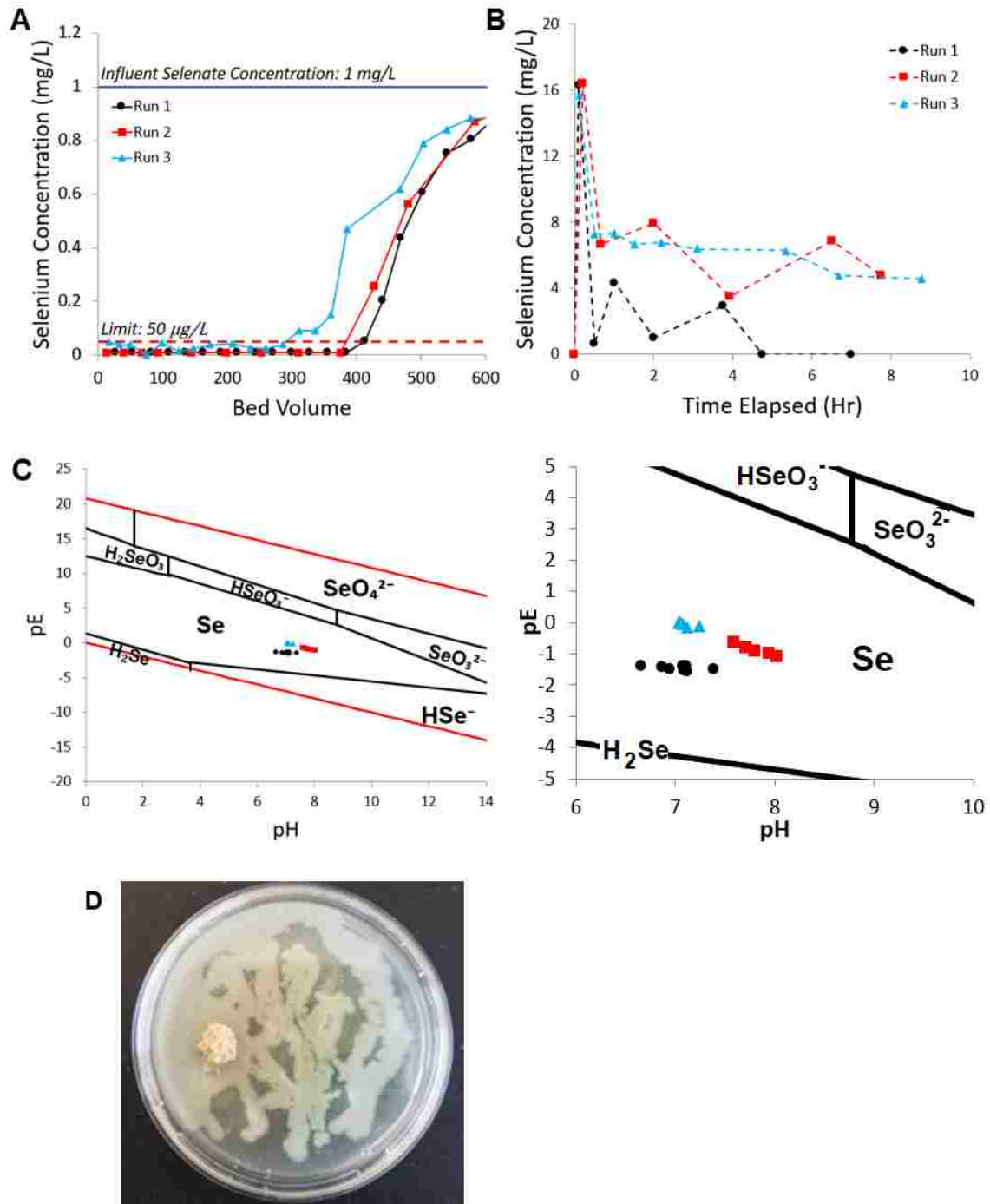


**Figure 5-14.** (A) Three successive effluent history plots of selenate using secondary wastewater from the Bethlehem Wastewater Treatment Plant in Bethlehem, PA. (B) Three successive regeneration effluent history plots of selenate using the BIO-RNIX process. (C) pE-pH diagram of aqueous selenium species with overlapping plotted pE points during each regeneration run and a close-up of the plotted pe-pH points on the right. (D) Visual representation of the bacteria present on the Metamateria pieces after three runs. (Influent composition: 1 mg/L Se as  $SeO_4^{2-}$ , 2.4 mg/L P, 100 mg/L  $NO_3^-$ , 32 mg/L  $SO_4^{2-}$ , 69 mg/L  $Cl^-$ , 50 mg/L  $Ca^{2+}$ , 466 mg/L TDS, pH 7.0.).

**Figure 5-14A** shows consistent selenate removal across all three runs with >90% removal and breakthrough occurring around 400 BV (similar to nitrate breakthrough). During removal, selenate remained below the 50 µg/L limit until breakthrough. **Figure 5-14B** shows the effluent selenate concentration leaving the Metamateria column during regeneration simultaneously with nitrate. The selenate regeneration performance emits a large effluent selenate peak within the first half hour of regeneration for all three runs, consistent with the nitrate removal performance. The BIO-RNIX system is efficient at kicking selenate off the bed and removing selenate in the brine with a consistent decrease in selenium concentration for all three runs. Specifically, in the first recirculation, selenate reaches near zero-levels. All three regeneration runs decreased selenate concentrations in the brine to over 75% from the first peak.

**Figure 5-14C** shows that every data point taken during all three regeneration runs fall into the  $Se^0$  region of the pE-pH diagram. By seeing a total selenium concentration decrease in the regeneration effluent (since total selenium is measured instead of selenate directly), it can be concluded that  $Se^0$  is formed as a solid during regeneration. To validate bacterial presence on the Metamateria pieces, an agar-loaded petri dish was swabbed with the Metamateria surface and **Figure 5-14D** shows the results after 24 hours. This image is comparable to the petri dish in Figure 5-4, but Figure 5-14D shows a slightly heavier growth within the same time frame. This observation is congruent with the fact that a higher nitrate concentration being degraded in the BIO-RNIX process will result in a greater quantity of bacterial cells present.

## CHAPTER 6: Conclusions

### 6.1 Process summary conclusions

Impaired secondary wastewater in large metropolises is a reliable water resource that is large and insulated from global warming. Transforming, recovering and reusing this large water body poses some insurmountable problems especially for inland applications regarding RO reject disposal. The HIX-NP process was conceived as a holistic pretreatment prior to RO and investigated to study its attributes using secondary wastewater from Bethlehem, Pennsylvania. Key findings of the process can be summarized as follows:

- For the first time, one hybrid anion exchanger (HAIX-NanoZr) was synthesized to simultaneously exhibit high sorption affinity for both nitrate and phosphate. Both nitrate and phosphate can be selectively removed and recovered. Consequently, the reject from the downstream RO will be free of nitrate and phosphate for inland disposal.
- Besides nitrate and phosphate removal, the HIX-NP process also removes hardness eliminating any need for anti-scaling chemical dosing to protect RO membranes from fouling. Furthermore, no salt or acid is needed for regeneration; CO<sub>2</sub> is the sole regenerant for the process. The CO<sub>2</sub> regeneration process can be easily scaled up for large scale implementation.
- The HIX-NP process can extend to PPCP co-contaminant removal prior to RO without interference with N-P-K recovery.

From a sustainability viewpoint, the HIX-NP process does not produce any disposable stream of environmental concern including nitrogen, phosphate, added salt or acid and anti-scaling chemicals.

Nitrate-contaminated groundwater treated by ion exchange processes alone is efficient but elicits brine disposal problems both sustainably and costly during regeneration. Biological denitrification is efficient in terms of removal rates and sustainability but provides slow kinetics and instability with sudden changes in the feedwater. The BIO-NIX process was conceived as a combination of these two technologies: fast kinetics of ion exchange with the sustainability of no material addition or brine waste. BIO-NIX was tested for its resiliency and high nitrate removal from groundwater and was investigated to study its attributes using synthetic wastewater designed from Manheim, Pennsylvania's nitrate-contaminated groundwater. Key findings of the process can be summarized as follows:

- The BIO-NIX process removed nitrate consistently below the MCL for over 3000 bed volumes and continuing. The citric acid-loaded column consistently provided appropriate quantities of carbon source to the fixed-film column, which provided the main treatment for nitrate removal. The ion exchange column provided additional removal following the Metamateria column for >90% removal and the column did not need to be regenerated throughout the entire run.
- BIO-NIX was tested for its resiliency against varying feedwater parameters including carbon source interruption, influent nitrate spike, and increased flow rate and remained below the MCL throughout these interruptions. The ion



exchange column served as the buffer during each interruption to keep nitrate below the MCL and the Metamateria column rebounded after each interruption.

- Selenate removal was also tested using the BIO-NIX process, in which removal was achieved by both biological degradation and ion exchange, and effluent concentrations were kept below the influent concentration throughout the entire run.

The BIO-NIX process proved efficient and sustainable through the 3000 BV run with the added benefit of co-contaminant removal of selenate. Compared to the Manheim, PA water filtration plant that utilizes nitrate-selective ion exchange resins to treat their nitrate-contaminated groundwater, this process does not contain any material addition to the system negating costs upwards of \$16,000 plus that Manheim spends on material addition costs for the ion exchange column annually.

For treatment plants that utilize ion exchange for nitrate removal, a 10-15% brine is used for regeneration that is unsustainably disposed. The BIO-NIX system was modified to treat brine generated from nitrate-selective anion exchange removal of nitrate and selenate for continuous brine reuse, known as the BIO-RNIX system. BIO-RNIX was tested for its nitrate and selenate removal efficiency of a low concentration  $MgCl_2$  brine waste regenerating an exhausted anion exchanger loaded during wastewater treatment. The process was investigated to study its attributes using secondary wastewater from Bethlehem, Pennsylvania to load the ion exchanger. Key findings of the process can be summarized as follows:

- BIO-RNIX provided removal of nitrate and selenate from the ion exchanger and reduced brine concentrations over 75% for multiple runs within hours. Nitrate and

selenate were reduced to their sustainable and innocuous counterparts, N<sub>2</sub> and Se<sub>(s)</sub>.

BIO-RNIX provided an alternative to high concentration brine regeneration and reuse to mitigate continuous chemical addition and associated costs.

## 6.2 Future work and potential for scale-up

### 6.2.1 HIX-NP scale-up

The HIX-NP system has been applied to real water systems contaminated with phosphorus as part of the George Barley Water Prize, an Everglades Foundation competition designed to inspire innovation to remove excess phosphorus from freshwater sources.<sup>100</sup> One of the stages of the competition was treating a lake in Ontario, Canada with influent P in the µg/L levels. Water was pumped out of the lake with a flow of 2000 to 3000 gallons per day using the two column HIX-NP process and the results for P treatment are shown below in **Table 6-1**.

**Table 6-1.** Phosphorus Data from the George Barley Water Prize

Days of Operation	Influent P (ppb)	Effluent P (ppb)	P Removal (%)
Day 1	605	90.0	85.1%
Day 2	520	84.0	83.8%
Day 3	520	95.5	81.6%
Day 4	370	91.0	75.4%
Day 5	580	11.0	98.1%
Day 6	350	75.0	78.6%
Day 7	370	73.0	80.3%
Day 8	300	65.5	78.2%
Day 9	325	71.0	78.2%
Day 10	280	51.0	81.8%
Day 11	290	59.0	79.7%
Day 12	0	0.0	N/A
Day 13	240	79.0	67.1%
Day 14	320	62.0	80.6%
Day 15	270	51.0	81.1%
Day 16	320	50.5	84.2%
Day 17	295	54.0	81.7%
Day 18	270	44.5	83.5%

For 18 days, the HIX-NP system was able to remove >80% phosphorus from the system, negating harmful effects of eutrophication of the lake. Full-scale applications continue for the HIX-NP ranging from lake water treatment to dairy farm wastewater treatment, and more thought will be put to recovery of N and P post-treatment at full-scale.

### *6.2.2 BIO-NIX future work*

Although the BIO-NIX process has been thoroughly tested in the lab, continued work remains on co-contaminant removal, modeling, and pilot testing. One area of co-contaminant removal that the BIO-NIX process can be applied is PPCPs. Many of these compounds can be biologically degraded (as discussed in the Introduction) as well as picked up by ion exchangers. Testing of the BIO-NIX system will continue with ibuprofen and diclofenac dosing of the feed water and seeing if the process is viable for biological degradation by the Metamateria column.

Modeling of the system is important for full-scale application of the process to real groundwater and water filtration systems. This can include determining biological parameters of the system based on influent composition and flow: denitrification rates, bacterial cell yield and decay, sloughing potential, etc. Pilot tests have been initiated in China to examine the BIO-NIX system against real groundwater contaminated with nitrate and real distribution flow rates as shown in **Figure 6-1**.



**Figure 6-1.** A collection of photos from the BIO-NIX pilot tests conducted in China. Bacteria growth is very prevalent on the scaled-up Metamateria column seen in the top left corner of Figure 6-1. Work in China will be ongoing to test their 20 mg/L  $\text{NO}_3^-$ -N groundwater influent with the BIO-NIX system at the same EBCT of 15 minutes.

## References

<sup>1</sup> Davis, J. R., Chen, Y., Baygents, J. C., & Farrell, J., 2015. Production of acids and bases for ion exchange regeneration from dilute salt solutions using bipolar membrane electro dialysis. *ACS Sustainable Chemistry & Engineering* 3(9), 2337-2342.

<https://doi.org/10.1021/acssuschemeng.5b00654>.

<sup>2</sup> Areas of Physical and Economic Water Scarcity, 2007. Food and Agricultural Organization of the United Nations. <http://www.fao.org/land-water/outreach/graphs-and-maps/details/en/c/237285/> (accessed January 2019).

<sup>3</sup> Walha, K., Amar, R. B., Firdaous, L., Quéméneur, F., Jaouen, P., 2007. Brackish groundwater treatment by nanofiltration, reverse osmosis and electro dialysis in Tunisia: performance and cost comparison. *Desalination* 207(1-3), 95-106.

<https://doi.org/10.1016/j.desal.2006.03.583>.

<sup>4</sup> McFarland, P.H., Lewis, S., (2012). The Top 10 Biggest Wastewater Treatment Plants.

<https://www.enr.com/articles/3571-the-top-10-biggest-wastewater-treatment-plants?v=preview> (accessed October 2018).

<sup>5</sup> Alexandratos, S. D., Barak, N., Bauer, D., Davidson, F. T., Gibney, B. R., Hubbard, S. S., Taft, H. L., Westerhof, P., 2019. Sustaining water resources: environmental and economic impact. *ACS Sustainable Chemistry & Engineering* 7(3), 2879–2888.

<https://doi.org/10.1021/acssuschemeng.8b05859>.

<sup>6</sup> City of San Diego Water Reuse Study 2005, 2004.

<https://www.sandiego.gov/sites/default/files/legacy/water/pdf/purewater/aa1wp.pdf>

(accessed November 2018).

<sup>7</sup> Ocean County's Groundwater Authority, 2018. Orange County Water District Study.

<https://www.ocwd.com/about/my-water-bill-and-service/> (accessed November 2018).

<sup>8</sup> Singapore Reclamation Study: Expert Panel Review and Findings, 2002.

<http://uwatech.com/wp-content/uploads/2015/11/newwater-study-report.pdf> (accessed

December 2018).

<sup>9</sup> Deaton, J., 2018. If we don't want to run out of water, we should look to the sun.

<https://www.popsci.com/thermal-water-desalination> (accessed February 2019).

<sup>10</sup> Ahmed, M., Shayya, W. H., Hoey, D., Mahendran, A., Morris, R., Al-Handaly, J.,

2000. Use of evaporation ponds for brine disposal in desalination

plants. Desalination 130(2), 155-168. [https://doi.org/10.1016/S0011-9164\(00\)00083-7](https://doi.org/10.1016/S0011-9164(00)00083-7)

<sup>11</sup> Zhang, Y., Ma, H., Lin, L., Cao, W., Ouyang, T., Li, Y. Y., 2018. Enhanced

simultaneous nitrogen and phosphorus removal performance by anammox–HAP

symbiotic granules in the attached film expanded bed reactor. ACS Sustainable

Chemistry & Engineering 6(8), 10989-10998.

<https://doi.org/10.1021/acssuschemeng.8b02414>.

<sup>12</sup> Lalley, J., Han, C., Li, X., Dionysiou, D. D., & Nadagouda, M. N. (2016). Phosphate

adsorption using modified iron oxide-based sorbents in lake water: kinetics, equilibrium,

and column tests. Chemical Engineering Journal 284, 1386-1396.

<https://doi.org/10.1016/j.cej.2015.08.114>.

<sup>13</sup> Mayer, B. K., Baker, L. A., Boyer, T. H., Drechsel, P., Gifford, M., Hanjra, M. A., Parameswaran, P., Stoltzfus, J., Westhoff, P., Rittmann, B. E., 2016. Total value of phosphorus recovery. Environmental Science & Technology 50 (13), 6606-6620.

<https://doi.org/10.1021/acs.est.6b01239>.

<sup>14</sup> Cordell, D., Rosemarin, A., Schröder, J. J., Smit, A. L., 2011. Towards global phosphorus security: a systems framework for phosphorus recovery and reuse options.

Chemosphere 84(6), 747-758. <https://doi.org/10.1016/j.chemosphere.2011.02.032>.

<sup>15</sup> Cumbal, L., SenGupta, A. K., 2005. Arsenic removal using polymer-supported hydrated iron (III) oxide nanoparticles: Role of donnan membrane effect. Environmental Science & Technology 39(17), 6508-6515. <https://doi.org/10.1021/es050175e>.

<sup>16</sup> Rahardianto, A., Gao, J., Gabelich, C. J., Williams, M. D., Cohen, Y., 2007. High recovery membrane desalting of low-salinity brackish water: integration of accelerated precipitation softening with membrane RO. Journal of Membrane Science 289(1-2), 123-137.

<sup>17</sup> Smith, R. C., 2015. Integrating tunable anion exchange with reverse osmosis for enhanced recovery during inland brackish water desalination. Ph.D. Dissertation, Lehigh University.

<sup>18</sup> Dong, H., Shepsko, C. S., German, M., SenGupta, A. K., 2018. Hybrid ion exchange desalination (HIX-Desal) of impaired brackish water using pressurized carbon dioxide

(CO<sub>2</sub>) as the source of energy and regenerant. Environmental Science & Technology Letters 5(11), 701-706. <https://doi.org/10.1021/acs.estlett.8b00487>.

<sup>19</sup> Sahar, E., David, I., Gelman, Y., Chikurel, H., Aharoni, A., Messalem, R., & Brenner, A., 2011. The use of RO to remove emerging micropollutants following CAS/UF or MBR treatment of municipal wastewater. Desalination 273(1), 142-147.

<https://doi.org/10.1016/j.desal.2010.11.004>.

<sup>20</sup> New Hampshire Department of Environmental Services, 2010. Pharmaceuticals and Personal Care Products in Drinking Water and Aquatic Environments.

<https://www.des.nh.gov/organization/commissioner/pip/factsheets/dwgb/documents/dwgb-22-28.pdf> (accessed March 2019).

<sup>21</sup> Fewtrell, L., 2004. Drinking-water nitrate, methemoglobinemia, and global burden of disease: a discussion. Environmental Health Perspectives 112(14), 1371-1374.

<https://doi.org/10.1289/ehp.7216>.

<sup>22</sup> Power, J., Schepers, J. S., 1989. Nitrate contamination of groundwater in North America. Agriculture, Ecosystems & Environment 26(3-4), 165-187.

[https://doi.org/10.1016/0167-8809\(89\)90012-1](https://doi.org/10.1016/0167-8809(89)90012-1).

<sup>23</sup> US Geological Survey, 1999. Areas at high risk of nitrogen contamination of groundwater. <https://www.usgs.gov/media/images/areas-high-risk-nitrogen-contamination-groundwater>

(accessed January 2019).

<sup>24</sup> Tredoux, G., Engelbrecht, P., Israel, S., 2009. Nitrate in Groundwater. CSIR, Natural Resources and the Environment, Stellenbosch.



<http://citeseerx.ist.psu.edu/viewdoc/download?doi=10.1.1.600.4781&rep=rep1&type=pdf>

(accessed on January 2019).

<sup>25</sup> Zhang, L. M., Offre, P. R., He, J. Z., Verhamme, D. T., Nicol, G. W., Prosser, J. I., 2010. Autotrophic ammonia oxidation by soil thaumarchaea. Proceedings of the National Academy of Sciences 107(40), 17240-17245. <https://doi.org/10.1073/pnas.1004947107>.

<sup>26</sup> Nolan, J., Weber, K. A., 2015. Natural uranium contamination in major US aquifers linked to nitrate. Environmental Science & Technology Letters 2(8), 215-220. <https://doi.org/10.1021/acs.estlett.5b00174>.

<sup>27</sup> Bleiman, N., Mishaal, Y. G., 2010. Selenium removal from drinking water by adsorption to chitosan-clay composites and oxides: batch and columns tests. Journal of Hazardous Materials 183(1-3), 590-595. <https://doi.org/10.1016/j.jhazmat.2010.07.065>.

<sup>28</sup> Global Energy World, 2018. Flue Gas Desulfurization (FGD) System Market Worth 21.00 Bn USD by 2022. <http://www.globalenergyworld.com/news/traditional-energy/2018/01/15/flue-gas-desulfurization-fgd-system-market-worth-2100-bn-usd-2022> (accessed November 2018).

<sup>29</sup> Li, H. F., McGrath, S. P., Zhao, F. J., 2008. Selenium uptake, translocation and speciation in wheat supplied with selenate or selenite. New Phytologist 178(1), 92-102. <https://doi.org/10.1111/j.1469-8137.2007.02343.x>.

<sup>30</sup> Tan, T. P., & Rawat, S., 2018. NEWater in Singapore. <http://www.globalwaterforum.org/2018/01/15/newater-in-singapore/> (accessed February 2019).

- <sup>31</sup> Li, J., Koner, S., German, M., SenGupta, A. K., 2016. Aluminum-cycle ion exchange process for hardness removal: a new approach for sustainable softening. *Environmental Science & Technology* 50(21), 11943-11950. <https://doi.org/10.1021/acs.est.6b03021>.
- <sup>32</sup> Obaja, D., Mace, S., Mata-Alvarez, J., 2005. Biological nutrient removal by a sequencing batch reactor (SBR) using an internal organic carbon source in digested piggery wastewater. *Bioresource Technology* 96(1), 7-14. <https://doi.org/10.1016/j.biortech.2004.03.002>.
- <sup>33</sup> Blaney, L. M., Cinar, S., SenGupta, A. K., 2007. Hybrid anion exchanger for trace phosphate removal from water and wastewater. *Water Research* 41(7), 1603-1613. <https://doi.org/10.1016/j.watres.2007.01.008>.
- <sup>34</sup> Chakraborty, T., Gabriel, M., Amiri, A. S., Santoro, D., Walton, J., Smith, S., Ray, M. B., Nakhla, G., 2017. Carbon and phosphorus removal from primary municipal wastewater using recovered aluminum. *Environmental Science & Technology* 51(21), 12302-12309. <https://doi.org/10.1021/acs.est.7b03405>.
- <sup>35</sup> Huang, Y., Yang, J., Keller, A. A., 2014. Removal of arsenic and phosphate from aqueous solution by metal (hydr-)oxide coated cand. *ACS Sustainable Chemistry & Engineering* 2(5), 1128-1138. <https://doi.org/10.1021/sc400484s>.
- <sup>36</sup> Kirinovic, E., Leichtfuss, A. R., Navizaga, C., Zhang, H., Schuttlefield Christus, J. D., Baltrusaitis, J., 2017. Spectroscopic and microscopic identification of the reaction products and intermediates during the struvite ( $MgNH_4PO_4 \cdot 6H_2O$ ) formation from magnesium oxide (MgO) and magnesium carbonate ( $MgCO_3$ ) microparticles. *ACS*

Sustainable Chemistry & Engineering 5 (2), 1567-1577.

<https://doi.org/10.1021/acssuschemeng.6b02327>.

<sup>37</sup> Li, H., Yao, Q. Z., Dong, Z. M., Zhao, T. L., Zhou, G. T., Fu, S. Q., 2018. Controlled synthesis of struvite nanowires in synthetic wastewater. ACS Sustainable Chemistry & Engineering 7(2), 2035-2043. <https://doi.org/10.1021/acssuschemeng.8b04393>.

<sup>38</sup> Rabinovich, A., Rouff, A. A., Lew B., Ramlogan, M. V., 2018. Aerated fluidized bed treatment for phosphate recovery from dairy and swine wastewater. ACS Sustainable Chemistry & Engineering 6 (1), 652-659.

<https://doi.org/10.1021/acssuschemeng.7b02990>.

<sup>39</sup> Sengupta, S., Pandit, A., 2011. Selective removal of phosphorus from wastewater combined with its recovery as a solid-phase fertilizer. Water Research 45(11), 3318-3330. <https://doi.org/10.1016/j.watres.2011.03.044>.

<sup>40</sup> Huang, H., Liu, G., Lv, W., Yao, K., Kang, Y., Li, F., Lin, L., 2015. Ozone-oxidation products of ibuprofen and toxicity analysis in simulated drinking water. Journal of Drug Metabolism & Toxicology 6(3).

<sup>41</sup> Liang, S., Mann, M. A., Guter, G. A., Kim, P. H. S., Hardan, D. L., 1999. Nitrate removal from contaminated groundwater. Journal-American Water Works Association 91(2), 79-91. <https://doi.org/10.1002/j.1551-8833.1999.tb08587.x>.

<sup>42</sup> Kartal, B., Kuenen, J. V., Van Loosdrecht, M. C. M., 2010. Sewage treatment with anammox. Science 328(5979), 702-703. <https://doi.org/10.1126/science.118594>.

<sup>43</sup> Hallin, S., Rothman, M., Pell, M., 1996. Adaptation of denitrifying bacteria to acetate and methanol in activated sludge. *Water Research* 30(6), 1445-1450.

[https://doi.org/10.1016/0043-1354\(96\)00033-4](https://doi.org/10.1016/0043-1354(96)00033-4).

<sup>44</sup> Dinh, Q. T., Wang, M., Tran, T. A. T., Zhou, F., Wang, D., Zhai, H., ..., Lin, Z. Q., 2018. Bioavailability of selenium in soil-plant system and a regulatory approach. *Critical Reviews in Environmental Science and Technology*, 1-75.

<https://doi.org/10.1080/10643389.2018.1550987>.

<sup>45</sup> Oremland, R. S., Blum, J. S., Bindi, A. B., Dowdle, P. R., Herbel, M., & Stolz, J. F. (1999). Simultaneous reduction of nitrate and selenate by cell suspensions of selenium-respiring bacteria. *Applied Environmental Microbiology* 65(10), 4385-4392.

<sup>46</sup> SenGupta, A. K., 2017. *Ion Exchange in Environmental Processes: Fundamentals, Applications and Sustainable Technology*. John Wiley & Sons, Hoboken, New Jersey.

<sup>47</sup> Samatya, S., Kabay, N., Yüksel, Ü., Arda, M., Yüksel, M., 2006. Removal of nitrate from aqueous solution by nitrate selective ion exchange resins. *Reactive and Functional Polymers* 66(11), 1206-1214. <https://doi.org/10.1016/j.reactfunctpolym.2006.03.009>.

<sup>48</sup> Padungthon, S., German, M., Wiriathamcharoen, S., SenGupta, A. K., 2015. Polymeric anion exchanger supported hydrated Zr (IV) oxide nanoparticles: a reusable hybrid sorbent for selective trace arsenic removal. *Reactive and Functional Polymers* 93, 84-94. <https://doi.org/10.1016/j.reactfunctpolym.2015.06.002>.

<sup>49</sup> Pan, B., Wu, J., Pan, B., Lv, L., Zhang, W., Xiao, L., Wang, X., Tao, X., Zheng, S., 2009. Development of polymer-based nanosized hydrated ferric oxides (HFOs) for

enhanced phosphate removal from waste effluents. *Water Research* 43(17), 4421-4429.  
<https://doi.org/10.1016/j.watres.2009.06.055>.

<sup>50</sup> German, M. S., 2017. Hybrid anion exchange nanotechnology (HAIX-NanoZr) for concurrent trace contaminant removal with partial desalination laboratory and field-scale investigations. Ph.D. Dissertation, Lehigh University.

<sup>51</sup> Sengupta, A. K., Padungthon, S., 2015. Hybrid anion exchanger impregnated with hydrated zirconium oxide for selective removal of contaminating ligand and methods of manufacture and use thereof. U.S. Patent No. 9,120,093.

<sup>52</sup> Padungthon, S., Li, J., German, M., SenGupta, A. K., 2014. Hybrid anion exchanger with dispersed zirconium oxide nanoparticles: a durable and reusable fluoride-selective sorbent. *Environmental Engineering Science* 31(7), 360-372.  
<https://doi.org/10.1089/ees.2013.0412>.

<sup>53</sup> Sarkar, S., SenGupta, A. K., Prakash, P., 2010. The donnan membrane principle: opportunities for sustainable engineered processes and materials. *Environmental Science & Technology* 44, 1161-1166. <https://doi.org/10.1021/es9024029>.

<sup>54</sup> Tomaszewska, M., Jarosiewicz, A., 2002. Use of polysulfone in controlled-release NPK fertilizer formulations. *Journal of Agricultural and Food Chemistry* 50(16), 4634-4639. <https://doi.org/10.1021/jf0116808>.

<sup>55</sup> Höll, W., Sontheimer, H., 1977. Ion exchange kinetics of the protonation of weak acid ion exchange resins. *Chemical Engineering Science* 32(7), 755-762.  
[https://doi.org/10.1016/0009-2509\(77\)80125-5](https://doi.org/10.1016/0009-2509(77)80125-5).

- <sup>56</sup> Pabst, T. M., Carta, G., 2007. pH transitions in cation exchange chromatographic columns containing weak acid groups. *Journal of Chromatography A* 1142(1), 19-31. <https://doi.org/10.1016/j.chroma.2006.08.066>.
- <sup>57</sup> Andersen, C. B., 2002. Understanding carbonate equilibria by measuring alkalinity in experimental and natural systems. *Journal of Geoscience Education* 50(4), 389-403. <https://doi.org/10.5408/1089-9995-50.4.389>.
- <sup>58</sup> Schmuckler, G., 1984. Kinetics of moving-boundary ion-exchange processes. *Reactive Polymers, Ion Exchangers, Sorbents* 2(1-2), 103-110. [https://doi.org/10.1016/0167-6989\(84\)90013-8](https://doi.org/10.1016/0167-6989(84)90013-8)
- <sup>59</sup> Greenleaf, J. E., Lin, J. C., Sengupta, A. K., 2006. Two novel applications of ion exchange fibers: Arsenic removal and chemical-free softening of hard water. *Environmental Progress* 25(4), 300-311. <https://doi.org/10.1002/ep.10163>
- <sup>60</sup> Hoell, W. H., Feuerstein, W., 1986. Partial demineralization of water by ion exchange using carbon dioxide as regenerant part iii field tests for drinking water treatment. *Reactive Polymers, Ion Exchangers, Sorbents* 4(2), 147-153. [https://doi.org/10.1016/0167-6989\(86\)90009-7](https://doi.org/10.1016/0167-6989(86)90009-7).
- <sup>61</sup> Choi, K. J., Son, H. J., Kim, S. H., 2007. Ionic treatment for removal of sulfonamide and tetracycline classes of antibiotic. *Science of the Total Environment* 387(1-3), 247-256. <https://doi.org/10.1016/j.scitotenv.2007.07.024>.

- <sup>62</sup> Landry, K. A., Sun, P., Huang, C. H., Boyer, T. H., 2015. Ion-exchange selectivity of diclofenac, ibuprofen, ketoprofen, and naproxen in ureolyzed human urine. *Water Research* 68, 510-521. <https://doi.org/10.1016/j.watres.2014.09.056>.
- <sup>63</sup> Wang, J., Li, H., Shuang, C., Li, A., Wang, C., Huang, Y., 2015. Effect of pore structure on adsorption behavior of ibuprofen by magnetic anion exchange resins. *Microporous and Mesoporous Materials* 210, 94-100. <https://doi.org/10.1016/j.micromeso.2015.02.026>.
- <sup>64</sup> Characklis, W. G., 1973. Attached microbial growths-I. Attachment and growth. *Water Research* 7(8), 1113-1127.
- <sup>65</sup> Jou, C. J. G., Huang, G. C., 2003. A pilot study for oil refinery wastewater treatment using a fixed-film bioreactor. *Advances in Environmental Research* 7(2), 463-469. [https://doi.org/10.1016/S1093-0191\(02\)00016-3](https://doi.org/10.1016/S1093-0191(02)00016-3).
- <sup>66</sup> Kim, H. S., Gellner, J. W., Boltz, J. P., Freudenberg, R. G., Gunsch, C. K., Schuler, A. J. 2010. Effects of integrated fixed film activated sludge media on activated sludge settling in biological nutrient removal systems. *Water Research* 44(5), 1553-1561. <https://doi.org/10.1016/j.watres.2009.11.001>.
- <sup>67</sup> LaGrega, M. D., Buckingham, P. L., Evans, J. C., 2010. *Hazardous Waste Management*. Waveland Press.
- <sup>68</sup> Rittmann, B. E., McCarty, P. L., 2012. *Environmental Biotechnology: Principles and Applications*. Tata McGraw-Hill Education.

- <sup>69</sup> Oremland, R. S., Hollibaugh, J. T., Maest, A. S., Presser, T. S., Miller, L. G., Culbertson, C. W., 1989. Selenate reduction to elemental selenium by anaerobic bacteria in sediments and culture: biogeochemical significance of a novel, sulfate-independent respiration. *Applied and Environmental Microbiology* 55(9), 2333-2343.
- <sup>70</sup> Hingston, F. J., Posner, A. M., Quirk, J. P., 1971. Competitive adsorption of negatively charged ligands on oxide surfaces. *Discussions of the Faraday Society* 52, 334-342.  
<https://doi.org/10.1039/DF9715200334>.
- <sup>71</sup> Darvell, B. W., 2018. *Materials Science for Dentistry*. Woodhead publishing.  
<https://doi.org/10.1016/B978-0-08-101035-8.50030-4>.
- <sup>72</sup> Mielcarek, A., Rodziewicz, J., Janczukowicz, W., Thornton, A., 2015. The feasibility of citric acid as external carbon source for biological phosphorus removal in a sequencing batch biofilm reactor (SBBR). *Biochemical Engineering Journal* 93, 102-107.  
<https://doi.org/10.1016/j.bej.2014.10.001>.
- <sup>73</sup> Rittmann, B. E., Langeland, W. E., 1985. Simultaneous denitrification with nitrification in single-channel oxidation ditches. *Journal of Water Pollution Control Federation*, 300-308.
- <sup>74</sup> Moura, I., Moura, J. J., Pauleta, S. R., Maia, L. B. (Eds.), 2016. *Metalloenzymes in Denitrification: Applications and Environmental Impacts*. Royal Society of Chemistry.
- <sup>75</sup> Strohm, T. O., Griffin, B., Zumft, W. G., Schink, B., 2007. Growth yields in bacterial denitrification and nitrate ammonification. *Applied and Environmental Microbiology*, 73(5), 1420-1424. <https://doi.org/10.1128/AEM.02508-06>.



- <sup>76</sup> Koike, I., Hattori, A., 1975. Growth yield of a denitrifying bacterium, *Pseudomonas denitrificans*, under aerobic and denitrifying conditions. *Microbiology* 88(1), 1-10.  
<https://doi.org/10.1099/00221287-88-1-1>.
- <sup>77</sup> Hunt, H. R., Taube, H., 1958. Effect of temperature, pressure, acidity and solvent on an aquo ion exchange reaction. *Journal of the American Chemical Society* 80(11), 2642-2646.
- <sup>78</sup> Marinsky, J. A., Marcus, Y. (Eds.), 1981. *Ion Exchange and Solvent Extraction: a Series of Advances* (8). CRC Press.
- <sup>79</sup> Ratkowsky, D. A., Olley, J., McMeekin, T. A., Ball, A., 1982. Relationship between temperature and growth rate of bacterial cultures. *Journal of Bacteriology* 149(1), 1-5.
- <sup>80</sup> Nishimura, T., Hashimoto, H., Nakayama, M., 2007. Removal of Selenium (VI) from Aqueous Solution with Polyamine-type Weakly Basic Ion Exchange Resin. *Separation Science and Technology* 42(14), 3155-3167.  
<https://doi.org/10.1080/01496390701513107>
- <sup>81</sup> Chen, H., He, L. L., Liu, A. N., Guo, Q., Zhang, Z. Z., Jin, R. C., 2015. Start-up of granule-based denitrifying reactors with multiple magnesium supplementation strategies. *Journal of Environmental Management* 155, 204-211.  
<https://doi.org/10.1016/j.jenvman.2015.03.036>
- <sup>82</sup> Google. (n.d.). *Bethlehem Wastewater Treatment Plant*. Retrieved from  
<https://www.google.com/maps/place/Bethlehem+Wastewater+Treatment+Plant/@40.6173726,->

[75.3360692,552m/data=!3m1!1e3!4m5!3m4!1s0x89c4158404e8a70d:0xad8235d8b4ac2c30!8m2!3d40.6173726!4d-75.3338805](https://www.google.com/maps/place/306+Doe+Run+Rd,+Manheim,+PA+17545/@40.172206,-76.371649,556m/data=!3m1!1e3!4m5!3m4!1s0x89c4158404e8a70d:0xad8235d8b4ac2c30!8m2!3d40.6173726!4d-75.3338805) (accessed on February 2019).

<sup>83</sup> Google. (n.d.). *Doe Run Road*. Retrieved from <https://www.google.com/maps/place/306+Doe+Run+Rd,+Manheim,+PA+17545/@40.172206,-76.371649,556m/data=!3m2!1e3!4b1!4m5!3m4!1s0x89c61f35d7c4f567:0xa843ceb344a6a374!8m2!3d40.172206!4d-76.3694603> (accessed on February 2019).

<sup>84</sup> Purolite, 2019. Purolite A520E. <https://www.purolite.com/product-pdf/A520E.pdf> (accessed on October 2018).

<sup>85</sup> SenGupta, A., Cumbal, L., 2005. *U.S. Patent Application No. 10/925,600*.

<sup>86</sup> Purolite, 2019. Purolite C104Plus. <https://www.purolite.com/product/c104plus> (accessed on October 2018).

<sup>87</sup> Purolite, 2019. Purolite A400. <https://www.purolite.com/product/a400> (accessed on March 2019).

<sup>88</sup> MetaMateria, 2018. Products for Denitrification. <http://metamateria.com/public/uploaded/media/PDFs/Denitrification%20Technology.pdf> (accessed on January 2019).

<sup>89</sup> Li, R., Wang, J. J., Zhou, B., Awasthi, M. K., Ali, A., Zhang, Z., Lahori, A. H., Mahar,

A., 2016. Recovery of phosphate from aqueous solution by magnesium oxide decorated

magnetic biochar and its potential as phosphate-based fertilizer substitute. *Bioresource Technology* 215, 209-214. <https://doi.org/10.1016/j.biortech.2016.02.125>.

<sup>90</sup> Timmermans, P., Van Haute, A., 1983. Denitrification with methanol: fundamental study of the growth and denitrification capacity of *Hyphomicrobium* sp. *Water Research* 17(10), 1249-1255. [https://doi.org/10.1016/0043-1354\(83\)90249-X](https://doi.org/10.1016/0043-1354(83)90249-X).

<sup>91</sup> Kaspar, H. F., Tiedje, J. M., 1981. Dissimilatory reduction of nitrate and nitrite in the bovine rumen: nitrous oxide production and effect of acetylene. *Applied and Environmental Microbiology* 41(3), 705-709.

<sup>92</sup> Olson, M. E., Ceri, H., Morck, D. W., Buret, A. G., Read, R. R., 2002. Biofilm bacteria: formation and comparative susceptibility to antibiotics. *Canadian Journal of Veterinary Research* 66(2), 86.

<sup>93</sup> Applegate, D. H., Bryers, J. D., 1991. Effects of carbon and oxygen limitations and calcium concentrations on biofilm removal processes. *Biotechnology and Bioengineering* 37(1), 17-25. <https://doi.org/10.1002/bit.260370105>.

<sup>94</sup> Canter, L. W., 2019. *Nitrates in Groundwater*. Routledge.

<sup>95</sup> Garrett, T. R., Bhakoo, M., Zhang, Z., 2008. Bacterial adhesion and biofilms on surfaces. *Progress in Natural Science* 18(9), 1049-1056. <https://doi.org/10.1016/j.pnsc.2008.04.001>.

<sup>96</sup> Hockin, S. L., Gadd, G. M., 2003. Linked redox precipitation of sulfur and selenium under anaerobic conditions by sulfate-reducing bacterial biofilms. *Applied and*

Environmental Microbiology 69(12), 7063-7072.

<https://doi.org/10.1128/AEM.69.12.7063-7072.2003>.

<sup>97</sup> Maul, G., 2013. Sustainability of Ion Exchange Regeneration with Sodium, Potassium, Chloride, and Bicarbonate Salts. Ph.D. Dissertation, University of Florida.

<sup>98</sup> Cole, M. B., Jones, M. V., Holyoak, C., 1990. The effect of pH, salt concentration and temperature on the survival and growth of *Listeria monocytogenes*. Journal of Applied Bacteriology 69(1), 63-72. <https://doi.org/10.1111/j.1365-2672.1990.tb02912.x>

<sup>99</sup> Lehman, S. G., Badruzzaman, M., Adham, S., Roberts, D. J., Clifford, D. A., 2008. Perchlorate and nitrate treatment by ion exchange integrated with biological brine treatment. Water Research 42(4-5), 969-976.

<https://doi.org/10.1016/j.watres.2007.09.011>.

<sup>100</sup> Everglades Foundation, 2018. George Barley Water Prize.

<https://www.barleyprize.org/> (accessed on March 2019).

## Vita

Chelsey Shepsko was born on October 6, 1991 in Englishtown, New Jersey to Susan and William Shepsko. She has received all three of her degrees from Lehigh University which include a B.S. in Environmental Engineering (May 19, 2014 with High Honors), a M.S. in Environmental Engineering (May 18, 2015), and a Ph.D. in Environmental Engineering (May 19, 2019). Her first co-authored paper is “Hybrid Ion Exchange Desalination (HIX-Desal) of Impaired Brackish Water Using Pressurized Carbon Dioxide (CO<sub>2</sub>) as the Source of Energy and Regenerant” published in *Environmental Science & Technology: Letters* on October 5, 2018. Her first author paper has been recently accepted to the *Sustainable Chemistry & Engineering* journal called “Treated Municipal Wastewater Reuse: A Holistic Approach Using Hybrid Ion Exchange (HIX) with Concurrent Nutrient Recovery and CO<sub>2</sub> Sequestration”. She is also co-inventor of a patent labeled “Contaminants Removal with Simultaneous Desalination Using Carbon Dioxide Regenerated Hybrid Ion Exchanger Nanomaterials” (U.S. Patent Application No. 15/934,548) and is completing a patent application for her work on nitrate-contaminated groundwater using the BIO-NIX system. She has presented at various conferences including but not limited to New Jersey Water Environment Association’s (NJWEA) Annual Conference, Pennsylvania Water Environment Association’s (PWEA) Technical Conference, American Water Works Association’s (AWWA) ACE, and Association of Environmental Engineering and Science Professors (AEESP) Conferences. She has won the 2017 Student Research Podium Award from PWEA’s 89<sup>th</sup> Annual Technical Conference as well as the 2018 David A. Long Scholarship Award by the Pennsylvania Section of AWWA. During her tenure at Lehigh University, she has received the

Presidential Scholar award in 2014, the Glenn J. Gibson Fellowship in 2015, and P.C. Rossin Doctoral Fellow award in 2017.